Quantum state engineering with Josephson-junction devices

Yuriy Makhlin[1,2], Gerd Schön[1,3], and Alexander Shnirman[1]

[1] *Institut für Theoretische Festkörperphysik, Universität Karlsruhe, D-76128 Karlsruhe, Germany*
[2] *Landau Institute for Theoretical Physics, Kosygin st. 2, 117940 Moscow, Russia*
[3] *Forschungszentrum Karlsruhe, Institut für Nanotechnologie, D-76021 Karlsruhe, Germany*

Quantum state engineering, i.e., active control over the coherent dynamics of suitable quantum mechanical systems, has become a fascinating prospect of modern physics. With concepts developed in atomic and molecular physics and in the context of NMR, the field has been stimulated further by the perspectives of quantum computation and communication. For this purpose a number of individual two-state quantum systems (qubits) should be manipulated and coupled in a controlled way. Several physical realizations of qubits have been considered, incl. trapped ions, NMR, and quantum optical systems. For potential applications such as logic operations, nano-electronic devices appear particularly promising because they can be embedded in electronic circuits and scaled up to large numbers of qubits. Here we review the quantum properties of low-capacitance Josephson junction devices. The relevant quantum degrees of freedom are either Cooper pair charges on small islands or fluxes in ring geometries, both in the vicinity of degeneracy points. The coherence of the superconducting state is exploited to achieve long phase coherence times. Single- and two-qubit quantum manipulations can be controlled by gate voltages or magnetic fields, by methods established for single-charge systems or the SQUID technology. Several of the interesting single-qubit properties, incl. coherent oscillations have been observed in recent experiments, thus demonstrating in a spectacular way the laws of quantum mechanics in solid state devices. Further experiments, such as entanglement of qubit states, should be within reach. They are crucial steps towards a realization of logic elements. In addition to manipulations of qubits a measurement of the resulting quantum state should be performed. For a Josephson charge qubit this can be accomplished by coupling it capacitively to a single-electron transistor (SET). To describe the quantum measurement process we analyze the time evolution of the density matrix of the coupled system. As long as the transport voltage is turned off, the transistor has only a weak influence on the qubit. When the voltage is switched on, the dissipative current through the SET destroys the phase coherence of the qubit within a short time. The measurement is accomplished only after a longer time, when the macroscopic signal, i.e., the current through the SET, resolves different quantum states. At still longer times the measurement process itself destroys the information about the initial state. Similar scenarios are found when the quantum state of a flux qubit is measured by a dc-SQUID, coupled to it inductively.

CONTENTS

I. INTRODUCTION

The interest in 'macroscopic' quantum effects in low-capacitance Josephson junction circuits has persisted for many years. One of the motivations was to test whether the laws of quantum mechanics apply in macroscopic systems, in a Hilbert space spanned by macroscopically distinct states (Leggett 1987). The degrees of freedom studied were the phase difference of the superconducting order parameter across a junction, or the flux in a superconducting ring (SQUID) geometry. Various quantum phenomena, such as macroscopic quantum tunneling (MQT) and resonance tunneling were demonstrated (see e.g. Voss & Webb 1981, Martinis et al. 1987, Rouse et al. 1995). On the other hand, despite experimental efforts (e.g. Tesche 1990) coherent oscillations of the flux between two macroscopically distinct states (macroscopic quantum coherence, MQC) had not been observed.

The field received new attention recently, after it was recognized that suitable Josephson devices may serve as quantum bits (qubits) in quantum information devices, and that quantum logic operations [1] can be performed by controlling gate voltages or magnetic fields (e.g. Bouchiat 1997, Shnirman et al. 1997, Averin 1998, Makhlin et al. 1999, Nakamura et al. 1999, Mooij et al. 1999, Ioffe et al. 1999). In this context, as well as for other conceivable applications of quantum state engineering, the experimental milestones are the observation of quantum superpositions of macroscopically distinct states, of coherent oscillations, and of entangled quantum states of several qubits. For Josephson devices first successful experiments have been performed. These systems can be fabricated by established lithographic methods, and the control and measurement techniques are quite advanced. They further exploit the coherence of the superconducting state, which helps achieving sufficiently long phase coherence times.

Two alternative realizations of quantum bits have been proposed, based on either charge or phase (flux) degrees of freedom. In the former the charge in low-capacitance Josephson junctions is used as quantum degree of freedom, with basis states differing by the number of Cooper pair charges on an island. These devices combine the coherence of Cooper pair tunneling with the control mechanisms developed for single-charge systems and Coulomb-blockade phenomena. The manipulations can be accomplished by switching gate voltages (Shnirman et al. 1997); designs with controlled inter-qubit couplings were proposed (Averin 1998, Makhlin et al. 1999). Experimentally, the coherent tunneling of Cooper pairs and the related properties of quantum mechanical superpositions of charge states has been demonstrated (Bouchiat 1997, Nakamura et al. 1997). Most spectacular are recent experiments of Nakamura et al. (1999), where the quantum coherent oscillations of a Josephson charge qubit prepared in a superposition of eigenstates were observed in the time domain. We describe these systems, concepts and results in Section II.

The alternative realization is based on the phase of a Josephson junction or the flux in a ring geometry near a degeneracy point as quantum degree of freedom (see e.g. Mooij et al. 1999, Ioffe et al. 1999). In addition to the earlier experiments, where macroscopic quantum tunneling had been observed (Voss & Webb 1981, Martinis et al. 1987, Rouse et al. 1995), the groups in Delft and Stony Brook (van der Wal et al. 2000, Friedman et al. 2000) demonstrated recently by spectroscopic measurements the flux qubit's eigenenergies, they observed eigenstates which are superpositions of different flux states, and new efforts are made to observe the coherent oscillation of the flux between degenerate states (Mooij et al. 1999, Friedman et al. 2000, Cosmelli et al. 1998). We will discuss the quantum properties of flux qubits in Section III.

To make use of the quantum coherent time evolution it is crucial to find systems with intrinsically long phase coherence times and to minimize external sources of dephasing. The latter can never be avoided completely since, in order to perform the necessary manipulations, one has to couple to the qubits, e.g., by attaching external leads. Along the same channels as the signal (e.g., gate voltages) also the noise enters the system. However, by operating at low temperatures and choosing suitable coupling parameters, these dephasing effects can be kept at an acceptable level. We provide estimates of the phase coherence time in Section IV.

In addition to controlled manipulations of qubits, quantum measurement processes are needed, e.g., to read out the final state of the system. In our quantum mechanics courses we learned to express the measurement process as a "wave function collapse", i.e., as a non-unitary projection, which reduces the quantum state of the qubit to one of the possible eigenstates of the observed quantity with state-dependent probabilities. However, in reality any measurement is performed by a device which itself is realized by a physical system, suitably coupled to the measured quantum system and with a macroscopic read-out variable. Its presence, in general, disturbs the quantum manipulations. Therefore the dissipative processes which accompany the measurement should be switched on only when needed.

An example is provided by a normal-state single-electron transistor (SET) coupled capacitively to a single-Cooper pair box. This system is widely used as an electro-meter in classical single-charge systems. We describe in Section V how a SET can also be used to read out the quantum state of a charge qubit. For this purpose we study the time evolution of the density matrix of the coupled system (Shnirman & Schön 1998). During quantum manipulations of the qubit the transport voltage of the SET is turned off, in which case it acts only as an extra capacitor. To perform the measurement the transport voltage is turned on. In this stage the dissipative current through the transistor dephases the the state of the qubit rapidly. This current also provides the macroscopic read-out signal for the quantum state of the qubit. However, it requires a longer 'measurement time' until the noisy signal resolves different qubit states. Finally, on the still longer 'mixing time' scale, the measurement process itself destroys the information about the initial quantum state.

Many results and observations made in the context of the normal state single-electron transistor apply also to other physical systems, e.g., a superconducting SET

[1] Since computational applications are widely discussed, we employ here and below frequently the terminology of quantum information theory, referring to a two-state quantum system as qubit and denoting unitary manipulations of its quantum state as quantum logic operations or gates.

(SSET) coupled to a charge qubit (Averin 2000*b*, Cottet et al. 2000) or a dc-SQUID monitoring as a quantum magneto-meter the state of a flux qubit (see e.g. Mooij et al. 1999, Friedman et al. 2000, Averin 2000*b*). The results can also be compared to the nonequilibrium dephasing processes discussed theoretically (Levinson 1997, Aleiner et al. 1997, Gurvitz 1997) and demonstrated experimentally by Buks et al. (1998).

One of the motivations for quantum state engineering with Josephson devices is their potential application as logic devices and quantum computing. By exploiting the massive parallelism of the coherent evolution of superpositions of states quantum computers could perform certain tasks which no classical computer can do in acceptable times (Bennett 1995, Barenco 1996, DiVincenzo 1995, Aharonov 1998). In contrast to the development of physical realizations of qubits and gates, i.e., the "hardware", the theoretical concepts of quantum computing, the "software", are already rather advanced. As an introduction, and in order to clearly define the goals, we present in Appendix A an ideal model Hamiltonian with sufficient control to perform all the needed manipulations. (We can mention that the Josephson junction devices come rather close to this ideal model.) Then in Appendix B we show by a few representative examples how these manipulations can be combined for useful computations.

Various other physical systems have been suggested as possible realizations of qubits and gates. They are discussed in much detail, e.g., in a recent Fortschritte der Physik special issue on *Experimental Proposals for Quantum Computation* (Braunstein & Lo 2000). In some systems quantum manipulations of a few qubits have already been demonstrated experimentally. These include ions in electro-magnetic traps manipulated by laser irradiation (Cirac & Zoller 1995, Monroe et al. 1995), NMR on ensembles of molecules in liquids (Gershenfeld & Chuang 1997, Cory et al. 1997), and cavity QED systems (Turchette et al. 1995). In comparison, solid-state devices, including the mentioned Josephson systems, are more easily embedded in electronic circuits and scaled up to large registers. Ultra-small quantum dots with discrete levels, and in particular, spin degrees of freedom embedded in nano-structured materials are candidates as well. They can be manipulated by tuning potentials and barriers (Loss & DiVincenzo 1998, Kane 1998). Because of the difficulties of controlled fabrication their experimental realization is still at a very early stage.

II. JOSEPHSON CHARGE QUBIT

A. Superconducting charge box as a quantum bit

In this section we describe the properties of low-capacitance Josephson junctions, where the charging energy dominates over the Josephson coupling energy, and discuss how they can be manipulated in a quantum coherent fashion. Under suitable conditions they provide physical realizations of qubits with two states differing by one Cooper pair charge on a small island. The necessary one-bit and two-bit gates can be performed by controlling applied gate voltages and magnetic fields. Different designs will be presented which differ in complexity, but also in the accuracy and flexibility of the manipulations.

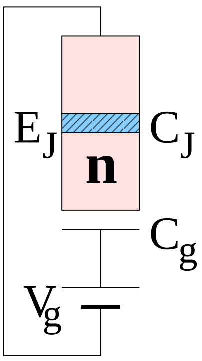

FIG. 1. A Josephson charge qubit in its simplest design formed by a superconducting single-charge box.

The simplest Josephson junction qubit is shown in Fig. 1. It consists of a small superconducting island ("box") with n excess Cooper pair charges (relative to some neutral reference state), connected by a tunnel junction with capacitance $C_{\rm J}$ and Josephson coupling energy $E_{\rm J}$ to a superconducting electrode. A control gate voltage $V_{\rm g}$ is coupled to the system via a gate capacitor $C_{\rm g}$. Suitable values of the junction capacitance, which can be fabricated routinely by present-day technologies, are in the range of Femtofarad and below, $C_{\rm J} \leq 10^{-15}$ F, while the gate capacitances can be chosen still smaller. The relevant energy scale, the single-electron charging energy $E_{\rm C} \equiv e^2/2(C_{\rm g}+C_{\rm J})$, which depends on the total capacitance of the island, is then in the range of Kelvin [2] or above, $E_{\rm C} \geq 1$ K. The Josephson coupling energy $E_{\rm J}$ is proportional to the critical current of the Josephson junction (see e.g. Tinkham 1996). Typical values considered here are in the range of 100 mK.

We choose a material such that the superconducting energy gap Δ is the largest energy in the problem, larger even than the single-electron charging energy. In this case quasiparticle tunneling is suppressed at low temperatures, and a situation can be reached where no quasiparticle excitation is found on the island [3]. Under these

[2]Throughout this review we frequently use temperature units for energies.

[3]In the ground state the superconducting state is totally

conditions only Cooper pairs tunnel – coherently – in the superconducting junction, and the system is described by the Hamiltonian:

$$\mathcal{H} = 4E_{\rm C}(n - n_{\rm g})^2 - E_{\rm J}\cos\Theta \ . \tag{2.1}$$

Here, n is the number operator of (excess) Cooper pair charges on the island, and Θ, the phase of the superconducting order parameter of the island, is its quantum mechanically conjugate, $n = -i\hbar\,\partial/\partial(\hbar\Theta)$. The dimensionless gate charge, $n_{\rm g} \equiv C_{\rm g}V_{\rm g}/2e$, accounts for the effect of the gate voltage and acts as a control parameter. Here we consider systems where the charging energy is much larger than the Josephson coupling energy, $E_{\rm C} \gg E_{\rm J}$. In this regime a convenient basis is formed by the charge states, parameterized by the number of Cooper pairs n on the island. In this basis the Hamiltonian (2.1) reads

$$\mathcal{H} = \sum_n \Big\{ 4E_{\rm C}(n-n_{\rm g})^2|n\rangle\langle n| \\ -\frac{1}{2}E_{\rm J}\Big(\,|n\rangle\,\langle n+1| + |n+1\rangle\,\langle n|\,\Big)\Big\} \ . \tag{2.2}$$

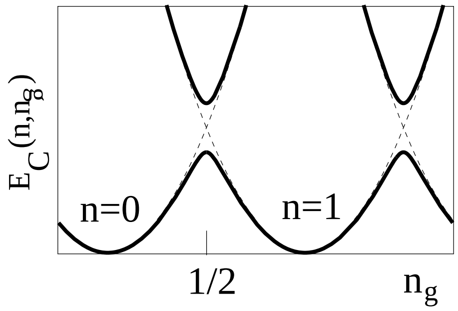

FIG. 2. The charging energy of the superconducting electron box is shown as a function of the gate charge $n_{\rm g}$ for different numbers of extra Cooper pairs n on the island (dashed parabolas). Near degeneracy points the weaker Josephson coupling mixes the charge states and modifies the energy of the eigenstates (solid lines). In the vicinity of these points the system effectively reduces to a two-state quantum system.

For most values of $n_{\rm g}$ the energy levels are dominated by the charging part of the Hamiltonian. However, when $n_{\rm g}$ is approximately half-integer and the charging energies of two adjacent states are close to each other (e.g., at $V_{\rm g} = V_{\rm deg} \equiv e/C_{\rm g}$), the Josephson tunneling mixes them strongly (see Fig. 2). We concentrate on such a voltage range near a degeneracy point where only two charge states, say $n = 0$ and $n = 1$, play a role, while all other charge states, having a much higher energy, can be ignored. In this case the superconducting charge box (2.1) reduces to a two-state quantum system (qubit) with Hamiltonian which can be written in spin-$\frac{1}{2}$ notation as

$$\mathcal{H}_{\rm ctrl} = -\frac{1}{2}B_z\hat{\sigma}_z - \frac{1}{2}B_x\hat{\sigma}_x \ . \tag{2.3}$$

The charge states $n = 0$ and $n = 1$ correspond to the spin basis states $|\!\uparrow\rangle \equiv \binom{1}{0}$ and $|\!\downarrow\rangle \equiv \binom{0}{1}$, respectively. The charging energy splitting, which is controlled by the gate voltage, corresponds in spin notation to the z-component of the magnetic field

$$B_z \equiv \delta E_{\rm ch} \equiv 4E_{\rm C}(1 - 2n_{\rm g}) \ , \tag{2.4}$$

while the Josephson energy provides the x-component of the effective magnetic field

$$B_x \equiv E_{\rm J} \ . \tag{2.5}$$

For later convenience we rewrite the Hamiltonian as

$$\mathcal{H}_{\rm ctrl} = -\frac{1}{2}\Delta E(\eta)\,(\cos\eta\ \sigma_z + \sin\eta\ \sigma_x) \ \ , \tag{2.6}$$

where the mixing angle $\eta \equiv \tan^{-1}(B_x/B_z)$ determines the direction of the effective magnetic field in the x-z-plane, and the energy splitting between the eigenstates is $\Delta E(\eta) = \sqrt{B_x^2 + B_z^2} = E_{\rm J}/\sin\eta$. At the degeneracy point, $\eta = \pi/2$, it reduces to $E_{\rm J}$. The eigenstates are denoted in the following as $|0\rangle$ and $|1\rangle$. They depend on the gate charge $n_{\rm g}$ as

$$|0\rangle \ = \ \ \ \cos\frac{\eta}{2}\,|\!\uparrow\rangle + \sin\frac{\eta}{2}\,|\!\downarrow\rangle \\ |1\rangle = -\sin\frac{\eta}{2}\,|\!\uparrow\rangle + \cos\frac{\eta}{2}\,|\!\downarrow\rangle \ . \tag{2.7}$$

We can further express the Hamiltonian in the basis of eigenstates. To avoid confusion we introduce a second set of Pauli matrices, $\boldsymbol{\rho}$, which operate in the basis $|0\rangle$ and $|1\rangle$, while reserving the operators $\boldsymbol{\sigma}$ for the basis of charge states $|\!\uparrow\rangle$ and $|\!\downarrow\rangle$. By definition the Hamiltonian then becomes

$$H = -\frac{1}{2}\Delta E(\eta)\rho_z \ . \tag{2.8}$$

The Hamiltonian (2.3) is similar to the ideal single-qubit model (A1) presented in Appendix A. Ideally the bias energy (effective magnetic field in z-direction) and the tunneling amplitude (field in x-direction) are controllable. However, at this stage we can control – by the

---

paired, which requires an even number of electrons on the island. A state with an odd number of electrons necessarily costs an extra quasi-particle energy Δ and is exponentially suppressed at low T. This 'parity effect' has been established in experiments below a crossover temperature $T^* \approx \Delta/(k_{\rm B}\ln N_{\rm eff})$, where $N_{\rm eff}$ is the number of electrons in the system near the Fermi energy (Tuominen et al. 1992, Lafarge et al. 1993, Schön & Zaikin 1994, Tinkham 1996). For a small island, T^* is typically one order of magnitude lower than the superconducting transition temperature.

gate voltage – only the bias energy, while the tunneling amplitude has a constant value set by the Josephson energy. Nevertheless, by switching the gate voltage we can perform the required one-bit operations (Shnirman et al. 1997). If, for example, one chooses the idle state far to the left from the degeneracy point, the eigenstates $|0\rangle$ and $|1\rangle$ are close to $|\uparrow\rangle$ and $|\downarrow\rangle$, respectively. Then, switching the system suddenly to the degeneracy point for a time Δt and back produces a rotation in spin space,

$$U_{1-\mathrm{bit}}(\alpha) = \exp\left(i\frac{\alpha}{2}\sigma_x\right) = \begin{pmatrix} \cos\frac{\alpha}{2} & i\sin\frac{\alpha}{2} \\ i\sin\frac{\alpha}{2} & \cos\frac{\alpha}{2} \end{pmatrix}, \quad (2.9)$$

where $\alpha = E_\mathrm{J}\Delta t/\hbar$. Depending on the value of Δt, a spin flip can be produced, or, starting from $|0\rangle$, a superposition of states with any chosen weights can be reached. (This is exactly the operation performed in the experiments of Nakamura et al. (1999); see Subsection II.D). Similarly, a phase shift between the two logical states can be achieved by changing the gate voltage n_g for some time by a small amount, which modifies the energy difference between the ground and excited states.

Several remarks are in order:

(1) Unitary rotations by B_x and B_z are sufficient for all manipulations of a single qubit. By using a sequence of no more than three such elementary rotations we can achieve any unitary transformation of a qubit's state.

(2) The example presented above, with control of B_z only, provides an *approximate* spin flip for the situation where the idle point is far from degeneracy and $E_\mathrm{C} \gg E_\mathrm{J}$. But a spin flip in the logical basis can also be performed *exactly*. It requires that we switch from the idle point η_idle to the point where the effective magnetic field is orthogonal to the idle one, $\eta = \eta_\mathrm{idle} + \pi/2$. This changes the Hamiltonian from $H = -\frac{1}{2}\Delta E(\eta_\mathrm{idle})\rho_z$ to $H = -\frac{1}{2}\Delta E(\eta_\mathrm{idle} + \pi/2)\rho_x$. To achieve this, the dimensionless gate charge n_g should be increased by $E_\mathrm{J}/(4E_\mathrm{C}\sin 2\eta_\mathrm{idle})$. For the limit discussed above, $\eta_\mathrm{idle} \ll 1$, this operating point is close to the degeneracy point, $\eta = \pi/2$.

(3) An alternative way to manipulate the qubit is to use resonant pulses, i.e., ac-pulses with frequency close to the qubit's level-spacing. We do not describe this technique here as it is well known from NMR methods.

(4) So far we were concerned with the time dependence during elementary rotations. However, frequently the quantum state should be kept unchanged for some time, for instance, while other qubits are manipulated. Even in the idle state, $\eta = \eta_\mathrm{idle}$, because the energies of the two eigenstates differ, their phases evolve relative to each other. This leads to the 'coherent oscillations', typical for a quantum system in a superposition of eigenstates. We have to keep track of this time dependence with high precision and, hence, of the time t_0 from the very beginning of the manipulations. The time-dependent phase factors can be removed from the eigenstates if all the calculations are performed in the interaction representation, with zero-order Hamiltonian being the one at the idle point. However, the price for this simplification is an additional time dependence in the Hamiltonian during operations, introduced by the transformation to the interaction representation. This point has been discussed in more detail by Makhlin et al. (2000*b*).

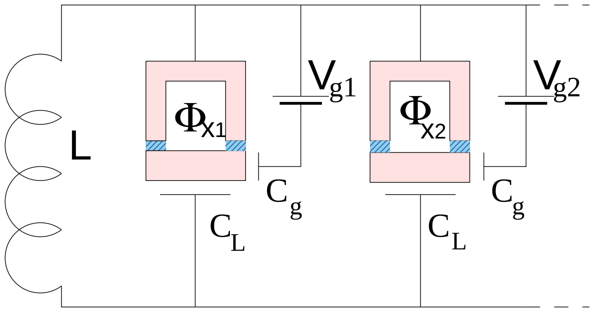

FIG. 3. A register of charge qubits coupled to an inductor via separate capacitors $C_L \sim C_\mathrm{J}$, independent from the gate capacitors C_g.

(5) The choice of the logical basis of the qubit is by no means unique. As follows from the preceding discussion, we can perform x- and z-rotations in the charge basis, $|\uparrow\rangle$, $|\downarrow\rangle$, which provides sufficient tools for any unitary operation. On the other hand, since we can perform *any* unitary transformation, we can choose any other basis as logical basis as well. The Hamiltonian at the idle point is diagonal in the eigenbasis (2.7), while the controllable part of the Hamiltonian, the charging energy, favors the charge basis. The preparation procedure (thermal relaxation at the idle point) is easier described in the eigenbasis, while coupling to the meter (see Section V) is diagonal in the charge basis. So, the choice of the logical states remains a matter of convention.

(6) A final comment concerns normal-metal single-electron systems. While they may serve as classical bits and logic devices, they are ruled out as potential quantum logic devices. The reason is that due to the large number of electron states involved, their phase coherence is destroyed in the typical sequential tunneling processes.

B. Charge qubit with tunable coupling

A further step towards the ideal model (A1), where the tunneling amplitude (x-component of the field) is controlled as well, is the ability to tune the Josephson coupling. This is achieved by the design shown in Fig. 4, where the single Josephson junction is replaced by two junctions in a loop configuration (Makhlin et al. 1999). This dc-SQUID is biased by an external flux Φ_x, which is coupled into the system through an inductor loop.

If the self-inductance of the SQUID loop is low (Tinkham 1996), the SQUID-controlled qubit is described by a Hamiltonian of the form (2.1) with modified potential energy:

$$-E_{\mathrm{J}}^{0}\cos\left(\Theta+\pi\frac{\Phi_{\mathrm{x}}}{\Phi_{0}}\right)-E_{\mathrm{J}}^{0}\cos\left(\Theta-\pi\frac{\Phi_{\mathrm{x}}}{\Phi_{0}}\right)= -2E_{\mathrm{J}}^{0}\cos\left(\pi\frac{\Phi_{\mathrm{x}}}{\Phi_{0}}\right)\cos\Theta\,. \quad (2.10)$$

Here $\Phi_0 = hc/2e$ denotes the flux quantum. We assumed that the two junctions are identical [4] with the same E_{J}^0. The effective junction capacitance is the sum of individual capacitances of two junctions, in symmetric cases $C_{\mathrm{J}} = 2C_{\mathrm{J}}^0$.

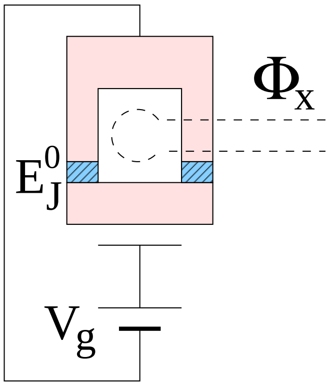

FIG. 4. A charge qubit with tunable effective Josephson coupling. The single Josephson junction is replaced by a flux-threaded SQUID. The flux in turn can be controlled by a current carrying loop placed on top of the structure.

When parameters are chosen such that only two charge states play a role, we arrive again at the Hamiltonian (2.3), but the effective Josephson coupling,

$$B_x = E_{\mathrm{J}}(\Phi_{\mathrm{x}}) = 2E_{\mathrm{J}}^{0}\cos\left(\pi\frac{\Phi_{\mathrm{x}}}{\Phi_{0}}\right)\,, \quad (2.11)$$

is tunable. Varying the external flux Φ_{x} by amounts of order Φ_0 changes the coupling between $2E_{\mathrm{J}}^0$ and zero [5].

The SQUID-controlled qubit is, thus, described by the ideal single-bit Hamiltonian (A1), with field components $B_z(t) = \delta E_{\mathrm{ch}}(V_{\mathrm{g}}(t))$ and $B_x(t) = E_{\mathrm{J}}(\Phi_{\mathrm{x}}(t))$ controlled independently by the gate voltage and the flux. If we fix in the idle state $V_{\mathrm{g}} = V_{\mathrm{deg}}$ and $\Phi_{\mathrm{x}} = \Phi_0/2$, the Hamiltonian is zero, $\mathcal{H}_{\mathrm{qb}}^0 = 0$, and the state does not evolve in time. Hence, there is no need to control the total time from the beginning of the manipulations, t_0. If we change the voltage or the current, the modified Hamiltonian generates rotations around the z- or x-axis, which are elementary one-bit operations. Typical time spans of single-qubit logic gates are determined by the corresponding energy scales and are of order $\hbar/E_{\mathrm{J}}$, $\hbar/\delta E_{\mathrm{ch}}$ for x- and z-rotations, respectively. If at all times at most one of the fields, $B_z(t)$ or $B_x(t)$, are turned on, only the time integrals of their profiles determine the results of the individual operations. Hence these profiles can be chosen freely to optimize speed and simplicity of the manipulations.

The introduction of the SQUID permits not only simpler and more accurate single-bit manipulations, but it also allows us to control the two-bit couplings, as we will discuss next. Furthermore, it simplifies the measurement procedure, which is more accurate at $E_{\mathrm{J}} = 0$ (see Section V).

C. Controlled inter-qubit coupling

In order to perform two-qubit logic gates we need to couple pairs of qubits together and to control the interactions between them. One possibility is to connect the superconducting boxes (i and j) directly, e.g., via a capacitor. The resulting charge-charge interaction is described by a Hamiltonian of the form (A2) with an Ising-type coupling term $\propto \sigma_z^i\sigma_z^j$. Such a coupling allows an easy realization of a controlled-NOT operation. On the other hand, it has severe drawbacks. In order to control the two-bit interaction, while preserving the single-bit properties discussed above, one needs a switch to turn the two-bit interaction on and off. Any externally operated switch, however, connects the system to the dissipative external circuit, thus introducing dephasing effects (see Section IV). They are particularly strong if the switch is attached directly and unscreened to the qubit, which would be required to control the direct capacitive interaction. Therefore alternatives were explored where the control fields are coupled only weakly to the qubits. A solution (Makhlin et al. 1999) is shown in Fig. 5. All N qubits are connected in parallel to a common LC-oscillator mode which provides the necessary two-bit interactions. It turns out that the possibility to control the Josephson couplings by an applied flux, simultaneously allows us to switch the two-bit interaction for each pair of qubits. This brings us close to the ideal model (A2) with a coupling term $\propto \sigma_y^i\sigma_y^j$.

---

[4] While this cannot be guaranteed with high precision in an experiment, we note that the effective Josephson coupling can be tuned to zero exactly by a design with three junctions.

[5] If the SQUID inductance is not small, the fluctuations of the flux within the SQUID renormalize the energy (2.10). But still, by symmetry arguments, at $\Phi_{\mathrm{x}} = \Phi_0/2$ the effective Josephson coupling vanishes.

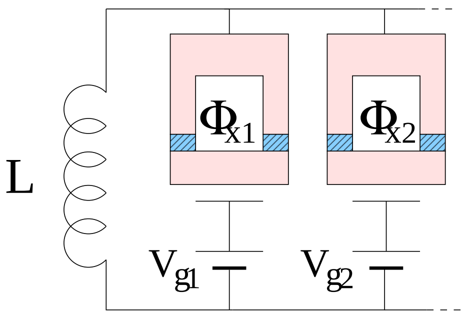

FIG. 5. A register of many charge qubits coupled by the oscillator modes in the LC-circuit formed by the inductor and the qubit capacitors.

In order to demonstrate the mentioned properties of the coupling we consider the Hamiltonian of the chain (register of qubits) shown in Fig. 5. It is

$$\mathcal{H} = \sum_{i=1}^{N} \left\{ \frac{(2en_i - C_g V_{gi})^2}{2(C_J + C_g)} - E_J(\Phi_{xi}) \cos\Theta_i \right\} + \frac{1}{2NC_{qb}} \left(q - \frac{C_{qb}}{C_J} \sum_i 2en_i \right)^2 + \frac{\Phi^2}{2L} \ . \qquad (2.12)$$

Here q denotes the total charge accumulated on the gate capacitors of the array of qubits. Its conjugate variable is the phase drop ϕ across the inductor, related to the flux by $\phi/2\pi = \Phi/\Phi_0$. Furthermore,

$$C_{qb} = \frac{C_J C_g}{C_J + C_g} \qquad (2.13)$$

is the capacitance of the qubit in the external circuit.

Depending on the relations among the parameters the Hamiltonian (2.12) can be reduced. We first consider the situation where the frequency of the (q, Φ) oscillator, $\omega_{LC}^{(N)} = 1/\sqrt{NC_{qb}L}$, is higher than typical frequencies of the qubit's dynamics:

$$\hbar\omega_{LC}^{(N)} \gg E_J, \delta E_{ch} \ . \qquad (2.14)$$

In this case the oscillator modes are not excited, but still their virtual excitation produces an effective coupling between the qubits. To demonstrate this we eliminate the variables q and Φ and derive an effective description in terms of the qubits' variables only. As a first step we perform a canonical transformation, $\tilde{q} = q - (C_{qb}/C_J) \sum 2en_i$ and $\tilde{\Theta}_i = \Theta_i + 2\pi(C_{qb}/C_J)\,(\Phi/\Phi_0)$, while Φ and n_i are unchanged. This step leads to the new Hamiltonian (we omit the tildes):

$$\mathcal{H} = \frac{q^2}{2NC_{qb}} + \frac{\Phi^2}{2L} + \sum_i \left\{ \frac{(2en_i - C_g V_{gi})^2}{2(C_J + C_g)} - E_J(\Phi_{xi}) \cos\left(\Theta_i - \frac{2\pi}{\Phi_0} \frac{C_{qb}}{C_J} \Phi \right) \right\} \ . \qquad (2.15)$$

We assume that the fluctuations of Φ are weak

$$\frac{C_{qb}}{C_J} \sqrt{\langle\Phi^2\rangle} \ll \Phi_0 \ , \qquad (2.16)$$

since, otherwise, the Josephson tunneling terms in the Hamiltonian (2.15) are washed out (Shnirman et al. 1997). Assuming (2.16) to be satisfied, we expand the Josephson terms in Eq. (2.15) up to linear terms in Φ. Then we can trace over the variables q and Φ. As a result we obtain an effective Hamiltonian, consisting of a sum of N one-bit Hamiltonians (2.1) and the coupling terms

$$\mathcal{H}_{coup} = -\frac{2\pi^2 L}{\Phi_0^2} \left(\frac{C_{qb}}{C_J} \right)^2 \left[\sum_i E_J(\Phi_{xi}) \sin\Theta_i \right]^2 \ . \qquad (2.17)$$

In spin-$\frac{1}{2}$ notation this becomes [6]

$$\mathcal{H}_{coup} = -\sum_{i<j} \frac{E_J(\Phi_{xi}) E_J(\Phi_{xj})}{E_L} \hat{\sigma}_y^i \hat{\sigma}_y^j \ + \ \text{const} \ , \qquad (2.18)$$

where we introduced the scale

$$E_L = \left(\frac{C_J}{C_{qb}} \right)^2 \frac{\Phi_0^2}{\pi^2 L} \ . \qquad (2.19)$$

The coupling Hamiltonian (2.18) can be understood as the magnetic free energy of the current-biased inductor $-LI^2/2$. This current is the sum of the contributions from the qubits with non-zero Josephson coupling, $I \propto \sum_i E_J^i(\Phi_{xi}) \sin\Theta_i \propto \sum_i E_J^i(\Phi_{xi}) \hat{\sigma}_y^i$.

Note that the strength of the interaction does not depend directly on the number of qubits N in the system. However, the frequency of the (q, Φ)-oscillator $\omega_{LC}^{(N)}$ scales as $1/\sqrt{N}$. The requirement that this frequency should not drop below typical eigenenergies of the qubit, ultimately, limits the number of qubits which can be coupled by a single inductor.

The system with flux-controlled Josephson couplings $E_J(\Phi_{xi})$ and the interaction of the form (2.18) allows us to perform all necessary gate operations in a straightforward way. In the idle state all Josephson couplings are turned off and the interaction (2.18) is zero. Depending on the choice of the idle state we may also tune the qubits by their gate voltages to the degeneracy points, which makes the Hamiltonian vanish, $\mathcal{H} = 0$. The interaction Hamiltonian remains zero during one-bit operations, as long as we perform one such operation at a time, i.e., only for one qubit we have $E_J^i = E_J(\Phi_{xi}) \neq 0$. To perform a

[6] While the expression (2.18) is valid only in leading order in an expansion in $E_J^i/\hbar\omega_{LC}^N$, higher terms also vanish when the Josephson couplings are put to zero. Hence, the decoupling in the idle periods persists.

two-bit operation for any pair of qubits, say, i and j, $E_{\rm J}^i$ and $E_{\rm J}^j$ are switched on simultaneously, yielding the Hamiltonian

$$\mathcal{H} = -\frac{E_{\rm J}^i}{2}\hat{\sigma}_x^i - \frac{E_{\rm J}^j}{2}\hat{\sigma}_x^j - \frac{E_{\rm J}^i E_{\rm J}^j}{E_L}\hat{\sigma}_y^i\hat{\sigma}_y^j\,. \qquad (2.20)$$

While (2.20) is not identical to the form (A2) it equally well allows the relevant non-trivial two-bit operations, which, combined with the one-bit operations discussed above, provide a universal set of gates.

A few comments should be added:
(1) We note that typical time spans of two-bit operations are of the order $\hbar E_L/E_{\rm J}^2$. It follows from the conditions (2.14) and (2.16) that the interaction energy is never much larger than $E_{\rm J}$. Hence, at best the two-bit gate can be as fast as a single-bit operation.
(2) It may be difficult to fabricate a nano-meter-scale inductor with the required inductance L, in particular, since it is not supposed to introduce stray capacitances. However, it is possible to realize such an element by a Josephson junction in the classical regime (with negligible charging energy) or an array of junctions.
(3) The design presented above does not permit performing singe- or two-bit operations simultaneously on different qubits. However, this becomes possible in more complicated designs where parts of the many-qubit register are separated, e.g., by switchable SQUIDs.
(4) In the derivation of the qubit interaction presented here we assumed a dissipation-less high-frequency oscillator mode. To minimize dissipation effects, the circuit, including the inductor, should be made of superconducting material. Still at finite frequencies some dissipation will arise. To estimate its influence, the effect of an Ohmic resistance R in the circuit has been analyzed by Shnirman et al. (1997), with the result that the inter-qubit coupling persists if the oscillator is underdamped, $R \ll \sqrt{L/NC_{\rm qb}}$. In addition the dissipation causes dephasing. An estimate of the resulting dephasing time can be obtained along the lines of the discussion in Section IV. For a reasonably low-loss circuit the dephasing due to the coupling circuit is weaker than the influence of the external control circuit.
(5) The interaction energy (2.18) involves via E_L the ratio of $C_{\rm J}$ and $C_{\rm qb}$. The latter effectively screens the qubit from electromagnetic fluctuations in the voltage source's circuit, and hence should be taken as low as possible (see Section IV). Consequently, to achieve a reasonably high interaction strength and hence speed of two-bit operations a large inductance is needed. For typical values of $E_{\rm J} \sim 100$ mK and $C_{\rm g}/C_{\rm J} \sim 0.1$ one needs an inductance of $L \geq 1$ μH in order not to have the two-bit operation more than ten times slower than the single-bit operation. However, large values of the inductance are difficult to reach without introducing large stray capacitances. To overcome this problem Makhlin et al. (2000a) suggested to use separate gate capacitors to couple the qubits to the inductor, as shown in Fig. 3. As long as the superconducting circuit of the inductor is at most weakly dissipative, there is no need to screen the qubit from the electromagnetic fluctuations in this circuit, and one can choose C_L as large as $C_{\rm J}$ (still larger C_L would decrease the charging energy E_C of the superconducting box), which makes the relevant capacitance ratio in Eq. (2.17) of order one. Hence, a fairly low inductance induces an interaction of sufficient strength. For instance, for the circuit parameters mentioned above, $L \sim 10$ nH would suffice. At the same time, potentially dephasing voltage fluctuations are screened by $C_{\rm g} \ll C_{\rm J}$.
(6) So far we discussed manipulations on time scales much slower than the eigenfrequency of the LC-circuit, which leave the LC-oscillator permanently in the ground state. Another possibility is to use the oscillator as a bus mode, similar to the techniques used for ion traps. In this case an ac-voltage with properly chosen frequency is applied to a qubit to entangle its quantum state with that of the LC-circuit (for instance, by exciting the oscillator conditionally on the qubit's state). Then by addressing another qubit one can absorb the oscillator quantum, simultaneously exciting the second qubit. As a result, a two-qubit unitary operation is performed. This coupling via real excitations is a first-order process, as opposed to the second-order interaction (2.18). Hence, this method allows for faster two-qubit operations. Apart from this technical advantage, the creation of entanglement between a qubit and an oscillator would by itself be a very interesting experimental achievement (Buisson & Hekking 2000).

D. Experiments with Josephson charge qubits

Several of the concepts and properties described above have been verified in experiments. This includes the demonstration of superpositions of charge states, the spectroscopic verification of the spectrum, and even the demonstration of coherent oscillations.

In a superconducting charge box the coherent tunneling of Cooper pairs produces eigenstates which are gate-voltage dependent superpositions of charge states. This property has been first observed, in a somewhat indirect way, in the dissipative current through superconducting single-electron transistors. In this system single-electron tunneling processes (typically treated in perturbation theory) lead to transitions between the eigenstates. Since the eigenstates are not pure charge states, the Cooper-pair charge may also change in a transition. In the resulting combination of coherent Cooper-pair tunneling and stochastic single-electron tunneling the charge transferred is not simply e and the work done by the voltage source not simply eV. (In an expansion in the

Josephson coupling to n-th order the charge $(2n+1)e$ is transferred.) As a result a dissipative current can be transferred at subgap voltages. The theoretical analysis predicted a richly structured I-V characteristic at subgap voltages (Averin & Aleshkin 1989, Maassen van den Brink et al. 1991, Siewert & Schön 1996), which has been qualitatively confirmed by experiments (Maassen van den Brink et al. 1991, Tuominen et al. 1992, Hadley et al. 1998).

A more direct demonstration of eigenstates which arise as superpositions of charge states was found in the Saclay experiments (Bouchiat 1997, Bouchiat et al. 1998). In their setup (see Fig. 6) a single-electron transistor is coupled to a superconducting charge box (in the same way as the measurement setup to be discussed in Section V) and the expectation value of the charge of the box was measured. When the gate voltage is increased adiabatically this expectation value increases in a series of rounded steps near half-integer values of n_{g}. At low temperatures the width of this transition agrees quantitatively with the predicted ground state properties of Eqs. (2.3,2.7). At higher temperatures, the excited state contributes, again as expected from theory.

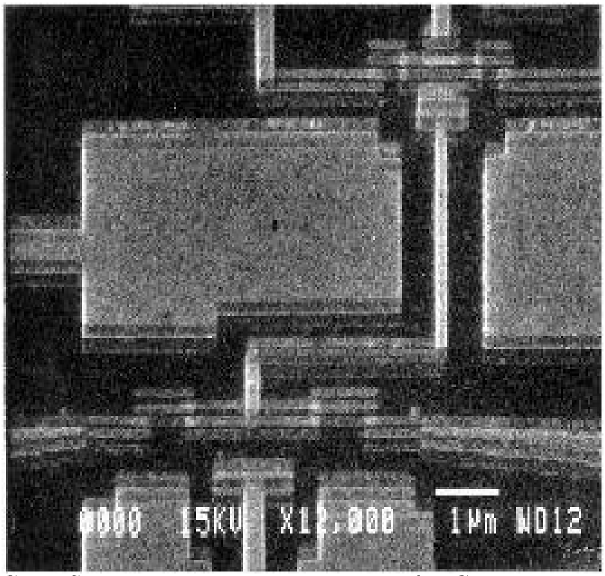

FIG. 6. Scanning electron micrograph of a Cooper-pair box coupled to a single-electron transistor used in the experiments of the Saclay group (Bouchiat 1997, Bouchiat et al. 1998).

Next we mention the experiments of Nakamura et al. (1997) who studied the superconducting charge box by spectroscopic means. When exposing the system to radiation they found resonances (in the tunneling current in a suitable setup) at frequencies corresponding to the difference in the energy between excited and ground state, again in quantitative agreement with the predictions of Eq. (2.3).

The most spectacular demonstration so far of the concepts of Josephson qubits has been provided by Nakamura et al. (1999). Their setup is shown in Fig. 7. In the experiments the Josephson charge qubit is prepared far from the degeneracy point for sufficiently long time to relax to the ground state. In this regime the ground state is close to a charge state, say, $|\uparrow\rangle$. Then the gate voltage is suddenly switched to a different value. Let us, first, discuss the case where it is switched precisely to the degeneracy point. Then the initial state, a pure charge state, is an equal-amplitude superposition of the ground state $|0\rangle$ and the excited state $|1\rangle$. These two eigenstates have different energies, hence in time they acquire different phase factors:

$$|\psi(t)\rangle = \mathrm{e}^{-iE_0\,t/\hbar}\,|0\rangle + \mathrm{e}^{-iE_1\,t/\hbar}\,|1\rangle \ . \tag{2.21}$$

After a delay time Δt the gate voltage is switched back to the original gate voltage. Depending on the delay, the system then ends up either in the ground state $|\uparrow\rangle$ [for $(E_1-E_0)\Delta t/h = 2\nu\pi$ with ν integer], in the excited state $|\downarrow\rangle$ [for $(E_1-E_0)\Delta t/h = (2\nu+1)\pi$], or in general in a Δt-dependent superposition. The probability that, as a result of this manipulation, the qubit is in the excited state is measured by monitoring the current through a probe junction. In the experiments this current was averaged over many repeated cycles, involving relaxation and switching processes, and the oscillatory dependence on Δt described above has been observed.

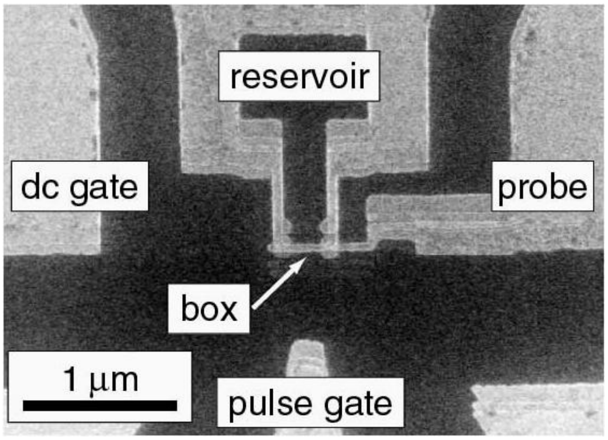

FIG. 7. Micrograph of a Cooper-pair box with flux-controlled Josephson junction and a probe junction (Nakamura et al. 1999).

In fact even more details of the theory have been quantitatively confirmed. For instance one expects and finds an oscillatory behavior also when the gate voltage is switched to a point different from the degeneracy point, with the frequency of oscillations being a function of this gate voltage. Secondly, the frequency of the coherent oscillations depends on the Josephson coupling energy. The latter can be varied, since the Josephson coupling is controlled by a flux-threaded SQUID (see Fig. 4). Also this aspect has been verified quantitatively.

The coherent oscillations with a period of roughly 100 psec could be observed in the experiments of Nakamura et al. (1999) for at least 2 nsec [7]. This puts a lower limit on the phase coherence time τ_ϕ and, in fact, represents its first direct measurement in the time domain. Estimates show that a major contribution to the dephasing is due to the measurement process by the probe junction itself. In the experiments so far the detector was permanently coupled to the qubit and observed it continuously. Still, information about the quantum dynamics could be obtained since the coupling strength was optimized: it was weak enough not to destroy the quantum time evolution too fast and strong enough to produce a sufficient signal. A detector which does not induce dephasing during manipulations should significantly improve the operation of the device. In Section V we suggest to use a single-electron transistor, which performs a quantum measurement only when switched to a dissipative state.

So far only experiments with single qubits have been demonstrated. Obviously the next step is to couple two qubits and to create and detect entangled states. Experiments in this direction have not been successful yet, partially because of difficulties as, for instance, dephasing due to fluctuating background charges. However, the experience with experiments with single qubits demonstrates that extensions to coupled qubits should be possible as well.

E. Adiabatic charge manipulations

Another qubit design, based on charge degrees of freedom in Josephson junction systems was proposed by Averin (1998). It also allows controlling the two-bit coupling at the price of representing each qubit by a chain of Josephson coupled islands. The basic setup is shown in Fig. 8. Each superconducting island (with index i) is biased via its own gate capacitor by a gate voltage V_i. The control of these voltages allows moving the charges along the chain similar to the adiabatic pumping of charges in junction arrays (see e.g. Pekola et al. 1999). The capacitances of the Josephson junctions as well as the gate capacitances are small enough so that the typical charging energy prevails over the Josephson coupling. In this regime the appropriate basis is that of charge states $|n_1, n_2, \ldots\rangle$, where n_i is the number of extra Cooper pairs on island i. There exist gate voltage configurations such that the two charge states with the lowest energy are almost degenerate, while all other charge states have much higher energy. For instance, if all voltages are equal except for the voltages V_m and V_l at two sites, m and l, one can achieve the situation where the states $|0,0,0,\ldots\rangle$ and $|0,\ldots,-1_m,0,\ldots,1_l,\ldots\rangle$ are degenerate. The subspace of these two charge states is used as the logical Hilbert space of the qubit. They are coupled via the Josephson tunneling across the $|m-l|-1$ intermediate junctions.

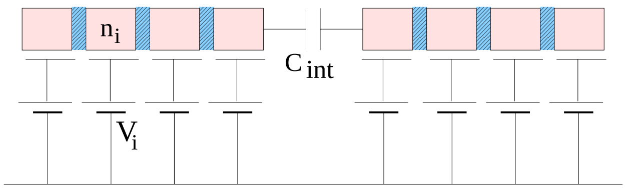

FIG. 8. Two coupled qubits as proposed by Averin (1998).

The parameters of the qubit's Hamiltonian can be tuned via the bias voltages. Obviously, the bias energy $B_z(V_1, V_2, ...)$ between these two states can be changed via the local voltages, V_l and V_m. Furthermore, the effective tunneling amplitude $B_x(V_1, V_2, ...)$ can be tuned by adiabatic pumping of charges along the chain, changing their distance $|m-l|$ and, hence, the effective Josephson coupling, which depends exponentially on this distance. (The Cooper pair must tunnel via $|m-l|-1$ virtual charge states with much higher energy.)

An inter-qubit interaction can be produced by placing a capacitor between the edges (outer islands) of two qubits. If at least one of the charges in each qubit is shifted close towards this capacitor, the Coulomb interaction leads to an interaction of the type $J_{zz}\sigma_z^1\sigma_z^2$. The resulting two-bit Hamiltonian is of the form

$$\mathcal{H} = -\frac{1}{2}\sum_{j=1,2}\left[B_z^j(t)\sigma_z^j + B_x^j(t)\sigma_x^j\right] + J_{zz}(t)\sigma_z^1\sigma_z^2 \ . \tag{2.22}$$

For controlled manipulations of the qubit the coefficients of the Hamiltonian are modified by adiabatic motion of the charges along the junction array. The adiabaticity is required to suppress transitions between different eigenstates of the qubit system. While conceptually satisfying, this proposal appears difficult to implement: It requires many gate voltages for each qubit. Due to the complexity a high accuracy of the operations is required. Its larger size as compared to simpler designs makes the system more vulnerable to dephasing effects, e.g., due to fluctuations of the offset charges.

Adiabatic manipulations of the Josephson charge qubit can lead to Berry phases. Falci et al. (2000) suggested that a Berry phase can accumulate during suitable manipulations of a flux controlled charge qubit with an asymmetric dc-SQUID, and that it can be detected in an experiment similar to that of Nakamura et al. (1999).

[7] In later experiments the same group reported phase coherence times as long as 5 nsec (Nakamura et al. 2000).

If the bare Josephson couplings of the SQUID loop are $E_{\rm J}^1$ and $E_{\rm J}^2$ the effective Josephson energy is given by (cf. Eq.(2.10))

$$-E_{\rm J}^1 \cos\left(\Theta + \pi\frac{\Phi_{\rm x}}{\Phi_0}\right) - E_{\rm J}^2 \cos\left(\Theta - \pi\frac{\Phi_{\rm x}}{\Phi_0}\right) \ . \qquad (2.23)$$

Hence, the corresponding Hamiltonian of the qubit has all three components of the effective magnetic field: $B_x = (E_{\rm J}^1 + E_{\rm J}^2)\cos(\pi\Phi_{\rm x}/\Phi_0)$ and $B_y = (E_{\rm J}^2 - E_{\rm J}^1)\sin(\pi\Phi_{\rm x}/\Phi_0)$, while B_z is given by Eq.(2.4). With three non-zero field components, adiabatic changes of the control parameters $V_{\rm g}$ and $\Phi_{\rm x}$ may result in $\boldsymbol{B}$ enclosing a non-zero solid angle. This results in a Berry phase shift, $\gamma_{\rm B}$, between the ground and excited states. In general, a dynamic phase $\int \Delta E(t)dt$ is also accumulated in the process. To single out the Berry phase, Falci et al. (2000) suggested to encircle the loop in parameter space back and forth, with a NOT operation performed in between. The latter exchanges the ground and excited state, and, as a result, the dynamic phases accumulated during both paths cancel. At the same time the Berry phases add up to $2\gamma_{\rm B}$. This phase shift can be measured by a procedure similar to that used by Nakamura et al. (1999): the system is prepared in a charge state away from degeneracy, abruptly switched to the degeneracy point where adiabatic manipulations and the NOT gate are performed, and then switched back. Finally, the average charge is measured. The probability to find the qubit in the excited charge state, $\sin^2 2\gamma_{\rm B}$, reflects the Berry phase.

The experimental demonstration of topological phases in Josephson junction devices would constitute a new class of "macroscopic" quantum effects in these systems. They can be performed with a single Josephson qubit in a design as used by Nakamura et al. (1999) and thus appear feasible in the near future.

III. QUBITS BASED ON THE FLUX DEGREE OF FREEDOM

In the previous Section we described the quantum dynamics of low capacitance Josephson devices where the charging energy dominates over the Josephson energy, $E_{\rm C} \gg E_{\rm J}$, and the relevant quantum degree of freedom is the charge on superconducting islands. We will now review the quantum properties of superconducting devices in the opposite regime, $E_{\rm J} \gg E_{\rm C}$, where the flux is the appropriate quantum degree of freedom. These systems were proposed by Caldeira & Leggett (1983) in the mid 80s as test objects to study various quantum mechanical effects. This includes the 'macroscopic quantum tunneling' of the phase (or flux) as well as resonance tunneling. Both had been observed in several experiments (Voss & Webb 1981, Martinis et al. 1987, Clarke et al. 1988, Rouse et al. 1995). Another important quantum effect has been reported recently: The groups in Stony Brook (Friedman et al. 2000) and in Delft (van der Wal et al. 2000) demonstrated in experiments the avoided level crossing due to coherent tunneling of the flux in a double well potential. In principle, all other manipulations discussed in the previous section should be possible with Josephson flux devices as well. They have the added advantage not to be sensitive to fluctuations in the background charges. However, attempts to observe 'macroscopic quantum coherent oscillations' in Josephson flux devices have not been successful yet (Leggett 1987, Tesche 1990).

A. Josephson flux (persistent current) qubits

We consider superconducting ring geometries interrupted by one or several Josephson junctions. In these systems persistent currents flow and magnetic fluxes are enclosed. The simplest design of these devices is an rf-SQUID, which is formed by a loop with one junction, as shown in Fig. 9 a. The phase difference across the junction is related to the flux Φ in the loop (in units of the flux quantum $\Phi_0 = h/2e$) by $\varphi/2\pi = \Phi/\Phi_0 +$integer. An externally applied flux $\Phi_{\rm x}$ biases the system. Its Hamiltonian, with Josephson coupling, charging energy, and magnetic contributions taken into account, thus reads

$$\mathcal{H} = -E_{\rm J}\cos\left(2\pi\frac{\Phi}{\Phi_0}\right) + \frac{(\Phi-\Phi_{\rm x})^2}{2L} + \frac{Q^2}{2C_{\rm J}} \ . \qquad (3.1)$$

Here L is the self-inductance of the loop and $C_{\rm J}$ the capacitance of the junction. The charge $Q = -i\hbar\partial/\partial\Phi$ on the leads is canonically conjugate to the flux Φ.

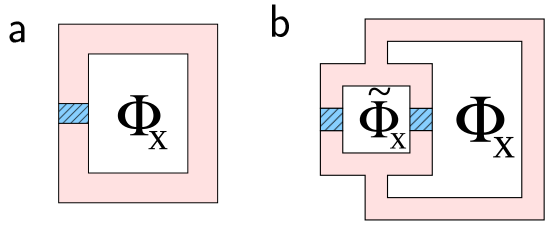

FIG. 9. a) The rf-SQUID, a simple loop with a Josephson junction, forms the simplest Josephson flux qubit. b) An improved design of a flux qubit. The flux $\tilde{\Phi}_{\rm x}$ in the smaller loop controls the effective Josephson coupling of the rf-SQUID.

If the self-inductance is large, such that $\beta_L \equiv E_{\rm J}/(\Phi_0^2/4\pi^2 L)$ is larger than 1 and the externally applied flux $\Phi_{\rm x}$ is close to $\Phi_0/2$, the first two terms in the Hamiltonian form a double-well potential near $\Phi = \Phi_0/2$. At low temperatures only the lowest states in the two wells contribute. Hence the reduced Hamiltonian of this effective two-state system again has the form (2.3), $\mathcal{H}_{\rm ctrl} = -\frac{1}{2}B_z\hat{\sigma}_z - \frac{1}{2}B_x\hat{\sigma}_x$. The diagonal term B_z is the bias, i.e., the asymmetry of the double well potential, given for $\beta_L - 1 \ll 1$ by

$$B_z(\Phi_x) = 4\pi\sqrt{6(\beta_L - 1)}\, E_J\ (\Phi_x/\Phi_0 - 1/2)\ . \tag{3.2}$$

It can be tuned by the applied flux Φ_x. The off-diagonal term B_x describes the tunneling amplitude between the wells. It depends on the height of the barrier and thus on E_J. This Josephson energy, in turn, can be controlled if the junction is replaced by a dc-SQUID, as shown in Fig. 9 b, introducing the flux $\tilde{\Phi}_x$ as another control variable [8]. With these two external control parameters the elementary single-bit operations, i.e., z- and x-rotations can be performed, equivalent to the manipulations described for charge qubits in the previous section. Also for flux qubits we can either perform the operations by sudden switching of the external fluxes Φ_x and $\tilde{\Phi}_x$ for a finite time, or we can use ac-fields and resonant pulses. To enable coherent manipulations the parameter β_L should be chosen larger than unity (so that two wells with well-defined levels appear) but not much larger, since the resulting large separation of the wells would suppress the tunneling.

The rf-SQUID described above had been discussed in the mid 80s as a realization of a 2-state quantum system. Some features of macroscopic quantum behavior were demonstrated such as 'macroscopic quantum tunneling' (MQT) of the flux, resonant tunneling and level quantization (Voss & Webb 1981, Martinis et al. 1987, Clarke et al. 1988, Rouse et al. 1995, Silvestrini et al. 1997). However, only very recently the level repulsion near a degeneracy point has been demonstrated (Friedman et al. 2000, van der Wal et al. 2000).

The group in Stony Brook (Friedman et al. 2000) probed spectroscopically the superposition of *excited* states in different wells. The rf-SQUID used had self-inductance $L = 240$ pH and $\beta_L = 2.33$. A substantial separation of the minima of the double-well potential (of order Φ_0) and a high inter-well barrier made the tunnel coupling between the lowest states in the wells negligible. However, both wells contain a set of higher localized levels – under suitable conditions one state in each well – with relative energies also controlled by Φ_x and $\tilde{\Phi}_x$. Being closer to the top of the barrier these states mix more strongly and form eigenstates, which are superpositions of localized flux states from different wells. External microwave radiation was used to pump the system from a well-localized lowest state in one well to one of these eigenstates. The energy spectrum of these levels was studied for different biases Φ_x, $\tilde{\Phi}_x$, and the properties of the model (3.1) were confirmed. In particular, the level splitting at the degeneracy point indicates a superposition of distinct quantum states. They differ in a macroscopic way: the authors estimated that two superimposed flux states differ in flux by $\Phi_0/4$, in current by 2–3 μA, and in magnetic moment by 10^{10} μ_B.

The Delft group (van der Wal et al. 2000) performed microwave spectroscopy experiments on a similar but much smaller three-junction system, to be described in more detail below. In their system the superpositions of the *lowest* states in two wells of the Josephson potential landscape were probed. In the spectrum they observed a level repulsion at the degeneracy point, confirming the predictions of the two-state model Hamiltonian (2.3) with the parameters B_x, B_z calculated from the potential (3.3).

In spite of this progress, attempts to observe 'macroscopic quantum coherence', i.e., the coherent oscillations of a quantum system prepared in a superposition of eigenstates have not been successful so far (Leggett 1987, Tesche 1990). A possible reason for this failure has been suggested recently by Mooij et al. (1999). They argue that for the designs considered so far the existence of the double-well potential requires that $\beta_L > 1$ which translates into a sufficiently high product of the critical current of the junction and its self-inductance. In practice, only a narrow range of circuit parameters is useful, since high critical currents require a relatively large junction area resulting in a high capacitance which suppresses tunneling. A high self-inductance of the rf-SQUID can be achieved only in large loops. This makes the system very susceptible to external noise.

To overcome this difficulty Mooij et al. (1999) and Feigelman et al. (2000) proposed to use a smaller superconducting loop with three or four junctions, respectively. Here we discuss the 3-junction circuit shown in Fig. 10 a,c. In this low-inductance circuit the flux through the loop remains close to the externally applied value, $\Phi = \Phi_x$. Hence the phase differences across the junctions are constrained by $\varphi_1 + \varphi_2 + \varphi_3 = 2\pi\Phi_x/\Phi_0$, leaving φ_1 and φ_2 as independent dynamical variables. In the plane spanned by these two variables the Josephson couplings produce a potential landscape given by

$$\begin{aligned} U(\varphi_1, \varphi_2) = &-E_J \cos\varphi_1 - E_J \cos\varphi_2 \\ &-\tilde{E}_J \cos(2\pi\Phi_x/\Phi_0 - \varphi_1 - \varphi_2)\,. \end{aligned} \tag{3.3}$$

If $\tilde{E}_J/E_J > 0.5$, a double-well potential is formed within each $2\pi \times 2\pi$ cell in the phase plane. For an optimal value of $\tilde{E}_J/E_J \approx 0.7$–$0.8$ the cells are separated by high barriers, while tunneling between two minima within one cell is still possible. The lowest states in the wells form a two-state quantum system, with two different current configurations. Mooij et al. (1999) and Orlando et al. (1999) discuss junctions with $E_J \sim 2$ K and $E_J/E_C \sim 80$ and loops of micrometer size with very small self-inductance $L \sim 5$ pH (which can be neglected when calculating the

[8] See (Mooij et al. 1999) for suggestions how to control $\tilde{\Phi}_x$ independent of Φ_x.

energy levels). Typical qubit operation parameters are the level splitting $B_z \sim 0.5$ K and the tunneling amplitude $B_x \sim 50$ mK. For the optimal choice of $\tilde{E}_\mathrm{J}/E_\mathrm{J}$ the two minima differ in phases by an amount of order $\pi/2$. Due to the very low inductance and the relatively low critical current $I_\mathrm{c} \sim 200$ nA this translates into a flux difference of $\delta\Phi \sim LI_\mathrm{c} \sim 10^{-3}\Phi_0$. While this corresponds to a still 'macroscopic' magnetic moment of 10^4 to 10^5 μ_B, the two basis states are similar enough to make the coupling to external fluctuating fields and hence the dephasing effects weak (for a further discussion, see Section IV). In this respect the new design is qualitatively superior to the simple rf-SQUID.

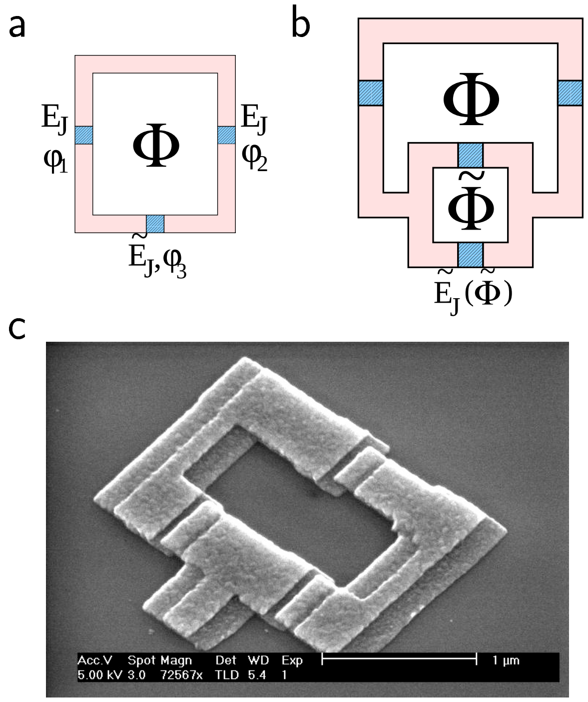

FIG. 10. a) and c) A 3-junction loop as a flux qubit (Mooij et al. 1999). The reduced size and lower inductance of this system as compared to earlier designs (e.g., Fig. 9 a) reduce the coupling to the external world and hence dephasing effects. b) Multi-junction flux qubit with a controlled Josephson coupling (Mooij et al. 1999). Control over two magnetic fluxes, Φ and $\tilde{\Phi}$, allows one to perform all single-qubit logic operations.

In order to obtain more direct evidence for superpositions of localized flux states the Delft group (van der Wal et al. 2000) measured the average flux of the qubit as a function of the external bias B_z. This experiment is similar to that of Bouchiat et al. (1997, 1998) for the single-Cooper-pair box, which was discussed in Section II.D. As the bias is swept across the degeneracy point, one expects the average flux to change from the value in one well to that in the other well. At high temperatures the step is rounded with width set by temperature. As k_BT is lowered below the tunnel splitting B_x this width should saturate at the value of B_x. However, experimentally it saturated much earlier than expected from the spectroscopically measured tunnel splitting. This discrepancy indicates an enhanced population of the excited state which can be caused by noise, either from external sources or due to the dc-SQUID detector.

B. Coupling of flux qubits

In order to couple different flux qubits one can use a direct inductive coupling (Mooij et al. 1999, Orlando et al. 1999) as shown by the dashed line in Fig. 11. A mutual inductance between the qubits can be established in different ways. The dashed loop shown in the figure couples the currents and fluxes in the lower parts of the qubits. Since fluxes through these loops control the barrier heights of the double-well potentials, this gives rise to the interaction term $\propto \hat{\sigma}_x^1\hat{\sigma}_x^2$. Placing the loop differently produces in addition contributions to the interaction Hamiltonian of the form $\hat{\sigma}_z^1\hat{\sigma}_z^2$. The typical interaction energy is of order MI_c^2 where M is the mutual inductance and $I_\mathrm{c} = (2\pi/\Phi_0)E_\mathrm{J}$ is the critical current in the junctions. For their design, Mooij et al. (1999) estimate the typical interaction energy to be of order $0.01E_\mathrm{J} \sim 50$ mK in frequency units, i.e., of the order of single-qubit energies. For a typical rf-SQUID (Friedman et al. 2000) this coupling can be even stronger than the tunneling rate between the flux states of the SQUID.

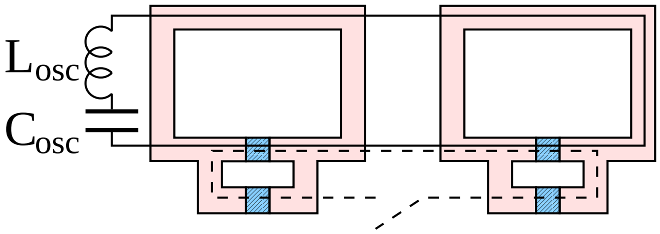

FIG. 11. Flux qubits coupled in two ways. The dashed line induces a direct inductive coupling. Alternatively, an inter-qubit coupling is provided by the LC-circuit indicated by a solid line.

In the simplest form this interaction is always turned on. To turn it off completely, one needs a switch which has to be controlled by high-frequency pulses. The related coupling to the external circuit leads to decoherence (see the discussion at the end of this Section). An alternative is to keep the interaction turned on constantly and use ac driving pulses to induce coherent transitions between the levels of the two-qubit system (cf. Shnirman et al. 1997, Mooij et al. 1999). A disadvantage of this approach is that permanent couplings result in an unwanted accumulation of relative phases between the 2-

qubit states even in the idle periods. Keeping track of these phases, or their suppression by repeated refocusing pulses (see Section IV), require a high precision and complicate the operation.

A controllable inter-qubit coupling without additional switches is achieved in the design shown by the solid line in Fig. 11 (Makhlin et al. 2000*c*). The coupling is mediated by an LC-circuit, with self-inductance $L_{\rm osc}$ and capacitance $C_{\rm osc}$, which is coupled inductively to each qubit. Similar to the design of the charge qubit register in Section II.C, the coupling depends on parameters of of individual qubits and can be controlled in this way. The effective coupling can be found again by integrating out the fast oscillations in the LC-circuit. It can be understood in a simple way by noting that in the limit $C_{\rm osc} \to 0$ the qubits establish a voltage drop across the inductor, $V = \sum_i M\dot{\Phi}_i/L$, and the Hamiltonian for the oscillator mode is $\mathcal{H}_{\rm osc} = \Phi^2/2L_{\rm osc} + Q^2/2C_{\rm osc} - VQ$, with the charge Q being conjugate to the flux Φ through the LC-circuit. Here Φ_i is the flux in the loop of qubit i, L is the self-inductance of the loop and M is its mutual inductance with the LC-circuit. Continuing as described in Section II.C we obtain the inter-qubit interaction term $-C_{\rm osc}V^2/2$. In the limit of weak coupling to the LC-circuit, we have $\dot{\Phi}_i = \frac{i}{\hbar}[\mathcal{H}_i, \Phi_i] = \delta\Phi_i B_x^i \hat{\sigma}_y^i/\hbar$, where $\delta\Phi_i$ is the separation between two minima of the potential and B_x^i is the tunneling amplitude. Hence, the interaction is given by

$$\mathcal{H}_{\rm int} = -\pi^2 \left(\frac{M}{L}\right)^2 \sum_{i<j} \frac{\delta\Phi_i \delta\Phi_j}{\Phi_0^2} \frac{B_x^i B_x^j}{e^2/C_{\rm osc}}\, \hat{\sigma}_y^i \hat{\sigma}_y^j \,. \qquad (3.4)$$

To turn off the interaction one should suppress the tunneling amplitudes B_x^i. This can be done with exponential precision by increasing the height of the potential barrier via $\tilde{\Phi}_x$. Note, that in this case also unwanted fluctuations of B_x^i and resulting dephasing effects are exponentially suppressed. All needed single and two-qubit manipulations can be performed by turning on the fields B_x^i and B_z^i, in complete analogy to what we discussed in Section II.C. We also encounter the equivalent drawbacks: the design shown in Fig. 11 does not allow simultaneous manipulations on different qubit pairs, and the conditions of high oscillator frequencies and weak renormalization of qubit parameters by the coupling, similar to Eqs.(2.14), (2.16), limit the two-qubit coupling energy. The optimization of this coupling requires $\sqrt{L_{\rm osc}/C_{\rm osc}} \approx R_{\rm K}(\delta\Phi/\Phi_0)^2(M/L)^2$ and ω_{LC} not far above the qubit frequencies. For rf-SQUIDs (Friedman et al. 2000) the resulting coupling can reach the same order as the single-bit terms. On the other hand, for the design of Mooij et al. (1999), where two basis phase states differ only slightly in their magnetic properties, the coupling term is much weaker than the single-bit energies.

C. "Quiet" superconducting phase qubits

The circuits considered so far in this Section are vulnerable to external noise. First, they need for their operation an external bias in the vicinity of $\Phi_0/2$, which should be kept stable for the time of manipulations. In addition, the two basis flux states of the qubit have different current configurations, which may lead to magnetic interactions with the environment and possible crosstalk between qubits. To a large extent the latter effect is suppressed already in the design of Mooij et al. (1999). To further reduce these problems several designs of so-called "quiet" qubits have been suggested (Ioffe et al. 1999, Blatter et al. 1999, Zagoskin 1999, Blais & Zagoskin 2000). They are based on intrinsically doubly degenerate systems, e.g., Josephson junctions with d-wave leads and energy-phase relation (e.g., $\cos 2\phi$) with two minima, or the use of π-junctions which removes the need for a constant magnetic bias near $\Phi_0/2$. As a result the relevant two states differ only in their distribution of *internal* currents in the Josephson junctions while *external* loops carry no current. As a result the coupling of the qubit to the electromagnetic environment is substantially reduced and coherence is preserved longer.

The mentioned designs are similar and we discuss them in parallel. Ioffe et al. (1999) suggested to use an SD tunnel junction with the s-wave lead matched to the (110) boundary of the d-wave superconductor. In this geometry the first harmonic, $\propto \cos\varphi$, in the Josephson coupling vanishes due to symmetry reasons, and one obtains a bistable system with the potential energy $E_{\rm J}\cos 2\varphi$ and minima at $\pm\varphi_0$ with $\varphi_0 = \pi/2$. (A similar current-phase relation was observed recently by Il'ichev et al. (1998) in a DD junction with a mismatch angle of 45°.) Zagoskin (1999) proposed to use DND, or D–grain-boundary–D Josephson junctions formed by two d-wave superconductors with different spatial orientation of the order parameter, connected by a normal metal. The energy-phase relation for such junctions also has two degenerate minima, at the phase differences $\pm\varphi_0$. The separation $2\varphi_0$ of these minima, and hence the tunneling amplitude, are controlled by the mismatch angle of the d-wave leads.

In a later development a 'macroscopic analogue' of d-wave qubits was discussed (Blatter et al. 1999). Instead of an SD-junction, it is based on a five-junction loop, shown in Fig. 12, which contains one strong π-junction and four ordinary junctions. The presence of the π-junction is equivalent to magnetically biasing the loop with a half superconducting flux quantum. Four other junctions, frustrated by the π-phase shift, have two lowest-energy states with the phase difference of $\pm\pi/2$ between the external legs in the figure. In this respect the 5-junction loop is similar to the SD-junction discussed above and can be called a $\pi/2$-junction.

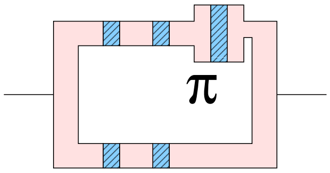

FIG. 12. A five-junction loop, a basic bistable element of "quiet" superconducting qubits (Blatter et al. 1999), is made of four ordinary junctions and one stronger π-junction. In two stable configurations the phase difference across this element is $\pm\pi/2$.

In all these designs the bistability is a consequence of the time-reversal symmetry (which changes the signs of all the phases) of the Hamiltonian. Thus the degeneracy persists also in systems containing different Josephson junctions, although the phase differences in the two lowest-energy states and their separation can change. If charging effects with $E_{\rm C} \ll E_{\rm J}$ are taken included, one arrives at a double-well system with tunneling between the wells. Such a qubit can be operated by connecting or disconnecting it from external elements, as described below.

The first issue to be addressed is the question how to store the qubit's state, i.e., how to freeze the evolution. This can be achieved by connecting the qubit in parallel to a large capacitor (Ioffe et al. 1999). This makes the phase degree of freedom very massive, thus suppressing the tunneling and restoring the needed degeneracy. In order to perform a $\hat{\sigma}_x$-rotation the inter-well tunneling is turned on by disconnecting the capacitor. This means a switch is needed in the circuit.

The $\hat{\sigma}_z$-rotation or phase shift can be accomplished by lifting the degeneracy between the wells. This can be done by connecting another, much stronger $\pi/2$-junction (DS-junction or 5-junction loop) and a weak ordinary, s-wave junction (with Josephson energy $\propto \cos\varphi$) in series to the qubit, to form a closed loop. This again requires a switch. The auxiliary $\pi/2$-junction shifts the phase differences of the potential minima of the qubit to 0 and π. Hence the s-junction is in the ground state or frustrated depending on the qubit's phase drop. The corresponding energy difference produces the needed phase shift between two qubit's states.

To perform two-qubit manipulations and control the entanglement Ioffe et al. (1999) proposed to form a loop, connecting in series two qubits and one s-junction with weak Josephson coupling $E_{\rm J}^s \ll E_{\rm J}$. The phase state of each qubit is characterized by the phase difference of $\pm\varphi_0$, i.e., the total phase drop on the qubits is equal to $\pm 2\varphi_0$ or 0 depending on whether the qubits are in the same state or in a different ones. When the connection between the qubits and the s-junction is turned on, this phase drops across the s-junction, and its energy differs by $E_{\rm J}^s(1-\cos 2\varphi_0)$ for the states $|00\rangle$, $|11\rangle$ as compared to the states $|01\rangle$, $|10\rangle$. The net effect is an Ising-type interaction between the pair of qubits, which allows performing unitary two-qubit transformations.

Another way of operation was discussed by Blais & Zagoskin (2000). They suggested to use a magnetic force microscope tip for single-bit manipulations (local magnetic field lifts the degeneracy of two phase states) and for the read-out of the phase state. The tip should be moved towards or away from the qubit during manipulations. The short time scales of qubit operation make this proposal difficult to realize.

Even in "quiet" designs, in both SD and DD systems, there are microscopic persistent currents flowing inside the junctions which differ for the two logical states (Blatter et al. 1999, Zagoskin 1999). These weak currents still couple to the outside world and to other qubits, thus spoiling the ideal behavior. Furthermore, all the designs mentioned require externally operated switches to connect and disconnect qubits. We discuss the associated problems in the following subsection.

To summarize, the "quiet" designs require rather complicated manipulations as well as circuits with many junctions, including π-junctions or d-wave junctions, which are difficult to fabricate in a controlled and reliable way. In addition, many constraints imposed on the circuit parameters (in particular, on the hierarchy of Josephson couplings) appear difficult to satisfy. In our opinion the "quiet" phase qubit designs belong to a higher complexity class than the previously discussed charge and flux qubits, and their experimental realization may remain a challenge for some time.

D. Switches

Switches may be used in variety of contexts in quantum nano-circuits. They are needed, e.g., for a direct capacitive coupling between charge qubits or magnetic coupling of flux qubits. They are also a major tool for controlling the dynamics of "quiet" qubits. Ideal switches should decouple qubits from the environment and at the same time let through control signals. They should operate on the very fast time scale of the qubit dynamics and have a high "switching ratio", that is the ratio of the interaction with the switch in the on- or off-state. Such switches are hard to realize. In this subsection we compare the characteristics of several Josephson-junction-based switches and the associated problems.

Possible switches are dc-SQUIDs as well as SSETs (single-Cooper-pair transistors) in a mode where they act as Josephson junctions with an externally controlled coupling. Then the switching ratio is the ratio of the minimal and maximal values of the coupling. In a dc-SQUID with Josephson energies of its junctions equal to $E_{\rm J}^1$ and $E_{\rm J}^2$, this ratio is $(E_{\rm J}^1 - E_{\rm J}^2)/(E_{\rm J}^1 + E_{\rm J}^2)$. It reached a value below 1% in the experiment of Rouse et al. (1995). However, fast switching of the bias flux may be difficult to perform. In a SSET the effective coupling is controlled by a gate voltage, which can be switched fast. However, the switching ratio of order $E_{\rm J}/E_{\rm C}$ ($E_{\rm J}$ and $E_{\rm C}$ are characteristics of the SSET) is hardly below several percent. These non-idealities lead to unwanted interactions when the switch is supposed to be disconnected.

Since a dc-SQUID requires an external bias to be operated as a switch, Blatter et al. (1999) suggested a similar construction with the bias provided by $\pi/2$-junctions instead of an external magnetic field. Namely, one can insert two $\pi/2$-junctions into one arm of the SQUID-loop. Depending on whether the phase drops across these junctions are equal or opposite, they simulate an external bias of a half flux quantum or no bias. Accordingly, the Josephson couplings of two s-junctions in the SQUID add up or cancel each other. The switching is realized via a voltage pulse which drives one $\pi/2$-junction between $+\pi/2$- and $-\pi/2$-states. Blatter et al. (1999) also suggest to use an array of n such switches, reducing the overall Josephson coupling in the off-state by a factor $[(E_{\rm J}^1 - E_{\rm J}^2)/E_{\rm C}]^n$. Unfortunately, in the on-state the overall coupling through the array is also reduced with growing n, although this reduction may be weaker than in the off-state, i.e., the switching ratio increases with n. Still the quality of the switch in the on-state is reduced. Moreover, to operate the switch one would need to send simultaneously voltage pulses to n intermediate elements which complicates the operation. Note that this design is reminiscent of the qubit design proposed by Averin (1998) which is presented in Subsection II.E. However, while Blatter et al. (1999) suggest to control the coupling, $\propto (E_{\rm J}/E_{\rm C})^n$, by controlling $E_{\rm J}$, Averin proposes to change the distance n of the tunneling process.

While switches of the type as described above may be useful in first experiments with simple quantum nanocircuits, further work is needed before they can be used in more advanced designs which require high precision of manipulations and phase coherence for a long time.

IV. ENVIRONMENT AND DISSIPATION

A. Identifying the problem

For an ideal quantum system the time evolution is described by deterministic, reversible unitary operations. The concepts of quantum state engineering and computation heavily rely on this quantum coherence, with many potential applications requiring a large number of coherent manipulations of a large number of qubits. On the other hand, for any real physical quantum system the time evolution may be disturbed in various ways, and the number of coherent manipulations is limited. Possible sources of errors are inaccuracies in the preparation of the initial state, inaccuracies in the manipulations (logic gates), uncontrolled couplings between qubits, undesired excitations out of the two-state Hilbert space (Fazio et al. 1999), and – unavoidable in devices which are to be controlled externally – interactions with the environment. Due to the coupling to the environment the quantum state of the qubits gets entangled with the environmental degrees of freedom. As a consequence the phase coherence is destroyed after a time scale called the dephasing time. In this Section we will describe the influence of the environment on the qubit. We determine how the dephasing time depends on system parameters and how it can be optimized.

Some of the errors can be corrected by 'software' tools. One known from NMR and, in particular, NMR-based quantum logic operations (see e.g. Chang 1998) are the *refocusing* techniques. They serve to suppress the effects of undesired terms in the Hamiltonian, e.g., deviations of the single-bit field terms from their nominal values or uncontrolled interactions like stray direct capacitive couplings of charge qubits or inductive couplings of flux qubits. As an example we consider the error due to a single-bit term $\delta B_x \sigma_x$, which after some time has produced an unwanted rotation by α. Refocusing is based on the fact that a π-pulse about the z-axis reverses the influence of this term, i.e., $U_z(\pi)U_x(\alpha)U_z(\pi) = U_x(-\alpha)$. Hence, fast repeated inversions of the bias $B_z(t)$ (with $|B_z| \gg \delta B_x$) eliminate the effects associated with δB_x. The technique can also be applied to enhance the precision of non-ideal control switches: one first turns off the coupling term to a low value and then further suppresses it by refocusing. The examples demonstrate that refocusing requires very fast repeated switchings with a period much shorter than the elementary operation time. This may make it hard to implement.

It was therefore a major breakthrough when the concepts of quantum error-correction were discovered (see e.g. Steane 1998, Preskill 1998). When applied they should make it possible, even in the presence of dephasing processes – provided that the dephasing time is not too short – to perform coherent sequences of quantum manipulations of arbitrary length. The price to be paid is an increase in system size (by roughly an order of magnitude), and a large number of steps are needed for error correction before another computational step can be performed (increasing the number of steps by roughly 3 orders of magnitude). This imposes constraints on the dephasing time. The detailed analysis shows that error correction can be successful if the dephasing time is of the order of 10^4 times longer than the time needed for an elementary logic gate.

In the Josephson junction systems, discussed here, the environment is usually composed of resistive elements in the circuits needed for the manipulations and the measurements. They produce voltage and current noise. In many cases such fluctuations are Gaussian distributed with a Johnson-Nyquist power spectrum, coupling linearly to the quantum system of interest. They can thus be described by a harmonic oscillator bath with suitable frequency spectrum and coupling strength (Leggett et al. 1987, Weiss 1999). For charge qubits, for instance, fluctuations in the gate voltage circuit, coupling to σ_z, as well as the fluctuations in the current, which control the Josephson energy and couple to σ_x, can be described in this way (Shnirman et al. 1997). In this section we will first describe these noise sources and the dephasing introduced in this way. We later comment on other noise sources such as telegraph noise, typically with a $1/f$ power spectrum due to switching two-level systems (e.g., 'background charge' fluctuations), or the shot noise resulting from the tunneling in a single-electron transistor coupled to a qubit for the purpose of a measurement.

Depending on the relation between typical frequencies of the coherent (Hamiltonian) dynamics and the dephasing rates we distinguish two regimes. In the first, "Hamiltonian-dominated" regime, where the controlled part of the qubit Hamiltonian $\mathcal{H}_{\rm ctrl} = -(1/2)\boldsymbol{B}\boldsymbol{\sigma}$, governing the deterministic time evolution and logic gates, is large, it is convenient to describe the dynamics in the eigenbasis of $\mathcal{H}_{\rm ctrl}$. The coupling to the environment is weak, hence the environment-induced transitions are slow. One can then distinguish two stages: a) *dephasing* processes, in which the relative phase between the eigenstates becomes random; b) *energy relaxation* processes, in which the occupation probabilities of the eigenstates change.

In the other, "environment-dominated" regime $\mathcal{H}_{\rm ctrl}$ is too weak to support its eigenstates as the preferred basis. The qubit's dynamics in this situation is governed by dissipative terms and depends on details of the structure of the coupling to the environment. In general the evolution is complicated, and the distinction between relaxation and dephasing may be impossible.

Both regimes may be encountered during manipulations. Obviously, the Hamiltonian should dominate when a coherent manipulation is performed. On the other hand, if in the idle state the Hamiltonian vanishes (a very useful property as outlined in Section II.A, II.B), the environment-dominated regime is realized. One has to ensure that the phase coherence rate in this regime is still low enough.

B. Spin-boson model

Before we proceed discussing specific physical systems, we recall what is known about the spin-boson model, which has been studied extensively (see reviews by Leggett et al. 1987, Weiss 1999). It models the environment as an oscillator bath coupled to one component of the spin. The Hamiltonian reads

$$\mathcal{H} = \mathcal{H}_{\rm ctrl} + \sigma_z \sum_a \lambda_a x_a + \mathcal{H}_{\rm B} \ , \tag{4.1}$$

where

$$\mathcal{H}_{\rm ctrl} = -\frac{1}{2} B_z \, \sigma_z - \frac{1}{2} B_x \, \sigma_x \tag{4.2}$$

$$= -\frac{\Delta E}{2} (\cos\eta \, \sigma_z + \sin\eta \, \sigma_x) \tag{4.3}$$

is the controlled part of the Hamiltonian (cf. Eqs. 2.3 and 2.6), while

$$\mathcal{H}_{\rm B} = \sum_a \left(\frac{p_a^2}{2m_a} + \frac{m_a \omega_a^2 x_a^2}{2} \right) \tag{4.4}$$

is the Hamiltonian of the bath. The bath operator $X = \sum_a \lambda_a x_a$ couples to σ_z. In thermal equilibrium one finds for the Fourier transform of the symmetrized correlation function of this operator

$$\langle X_\omega^2 \rangle \equiv \frac{1}{2} \langle \{X(t), X(t')\} \rangle_\omega = \hbar J(\omega) \coth \frac{\omega}{2k_{\rm B}T} \ , \tag{4.5}$$

where the bath spectral density is defined by

$$J(\omega) \equiv \frac{\pi}{2} \sum_a \frac{\lambda_a^2}{m_a \omega_a} \delta(\omega - \omega_a) \, . \tag{4.6}$$

This spectral density has typically a power-law behavior at low frequencies (Leggett et al. 1987). Of particular interest is Ohmic dissipation, corresponding to a spectrum

$$J(\omega) = \frac{\pi}{2} \, \alpha \hbar \omega \ , \tag{4.7}$$

which is linear at low frequencies up to some high-frequency cutoff ω_c. The dimensionless parameter α reflects the strength of dissipation. Here we concentrate on weak damping, $\alpha \ll 1$, since only this regime is relevant for quantum state engineering. But still the Hamiltonian-dominated and the environment-dominated regimes are both possible depending on the ratio between the energy scale $\Delta E = \sqrt{B_z^2 + B_x^2}$, characterizing the coherent evolution, and the dephasing rate (to be determined below).

The Hamiltonian-dominated regime is realized when $\Delta E \gg \alpha k_{\rm B} T$. In this regime it is natural to describe the evolution of the system in the eigenbasis (2.7) which diagonalize $\mathcal{H}_{\rm ctrl}$:

$$\mathcal{H} = -\frac{1}{2} \Delta E \rho_z + (\sin\eta \, \rho_x + \cos\eta \, \rho_z) \, X + \mathcal{H}_{\rm B} \ . \tag{4.8}$$

Two different time scales characterize the evolution (Weiss & Wollensak 1989, Görlich et al. 1989, Weiss 1999). On a first, dephasing time scale τ_φ the off-diagonal (in the preferred eigenbasis) elements of the qubit's reduced density matrix decay to zero. They are represented by the expectation values of the operators

$\rho_\pm \equiv (1/2)(\rho_x \pm i\rho_y)$. Dephasing leads to the following time-dependence (at long times):

$$\langle\rho_\pm(t)\rangle = \langle\rho_\pm(0)\rangle\, e^{\mp i\Delta E t}\, e^{-t/\tau_\varphi}\ . \tag{4.9}$$

On the second, relaxation time scale $\tau_{\rm relax}$ the diagonal entries tend to their thermal equilibrium values:

$$\langle\rho_z(t)\rangle = \rho_z(\infty) + [\rho_z(0) - \rho_z(\infty)]\, e^{-t/\tau_{\rm relax}}\ , \tag{4.10}$$

where $\rho_z(\infty) = \tanh(\Delta E/2k_{\rm B}T)$.

The dephasing and relaxation times were originally evaluated for the spin boson model in a path integral technique (Leggett et al. 1987, Weiss 1999). The rates are [9]

$$\tau_{\rm relax}^{-1} = \pi\alpha\ \sin^2\eta\, \frac{\Delta E}{\hbar} \coth\frac{\Delta E}{2k_{\rm B}T}\ , \tag{4.11}$$

$$\tau_\varphi^{-1} = \frac{1}{2}\,\tau_{\rm relax}^{-1} + \pi\alpha\ \cos^2\eta\, \frac{2k_{\rm B}T}{\hbar}\ . \tag{4.12}$$

In some cases these results can be derived in a simple way, which we present here to illustrate the origin of different terms. As is apparent from the Hamiltonian (4.8) the problem can be mapped on the dynamics of a spin-1/2 particle in the external magnetic field ΔE pointing in z-direction and a fluctuating field in the x-z-plane. The x-component of this fluctuating field, with magnitude proportional to $\sin\eta$, induces transitions between the eigenstates (2.7) of the unperturbed system. Applying the Golden Rule for this term one obtains readily the relaxation rate (4.11).

The longitudinal component of the fluctuating field, proportional to $\cos\eta$ does not induce relaxation processes. It does, however, contribute to dephasing since it leads to random fluctuations of the eigenenergies and, thus, to a random relative phase between the two eigenstates. As an example we analyze its effect on the dephasing rate in an exactly solvable limit.

The unitary operator

$$U \equiv \exp\left(-i\sigma_z\frac{\Phi}{2}\right) \quad \text{with} \quad \Phi \equiv \sum_a \frac{2\lambda_a p_a}{\hbar m_a\omega_a^2} \tag{4.13}$$

transforms the Hamiltonian (4.1–4.4) to a rotating spin-frame (Leggett et al. 1987):

$$\tilde{\mathcal{H}} = U\mathcal{H}U^{-1} = -(1/2)\Delta E\cos\eta\,\sigma_z \\ -(1/2)\Delta E\sin\eta\left(\sigma_+ e^{-i\Phi} + \text{h.c.}\right) + \mathcal{H}_{\rm B}\ . \tag{4.14}$$

[9] Note that in the literature usually the evolution of $\langle\sigma_z(t)\rangle$ has been studied. To establish the connection to the results (4.11,4.12) one has to substitute Eqs. (4.9,4.10) into the identity $\sigma_z = \cos\eta\ \rho_z + \sin\eta\ \rho_x$ Furthermore, we neglect renormalization effects, since they are weak for $\alpha \ll 1$.

Here we recognize that in the limit $\eta = 0$ the spin and the bath are decoupled, which allows an exact treatment. The trivial time evolution in this frame, $\sigma_\pm(t) = \exp(\mp i\Delta E t)\sigma_\pm(0)$, translates in the laboratory frame to

$$\sigma_\pm(t) = e^{\mp i\Phi(t)} e^{\pm i\Phi(0)} e^{\mp i\Delta E t}\sigma_\pm(0)\ . \tag{4.15}$$

To average over the bath we need the correlator

$$P(t) \equiv \langle e^{i\Phi(t)}\, e^{-i\Phi(0)}\rangle = \langle e^{-i\Phi(t)}\, e^{i\Phi(0)}\rangle \tag{4.16}$$

which was studied extensively by many authors (Leggett et al. 1987, Panyukov & Zaikin 1988, Odintsov 1988, Nazarov 1989, Devoret et al. 1990). It can be expressed as $P(t) = \exp[K(t)]$, where

$$K(t) = \frac{4}{\pi\hbar}\int_0^\infty d\omega\, \frac{J(\omega)}{\omega^2} \\ \times\left[\coth\left(\frac{\hbar\omega}{2k_BT}\right)(\cos\omega t - 1) - i\sin\omega t\right]\ . \tag{4.17}$$

For the Ohmic bath (4.7) for $t > \hbar/2k_{\rm B}T$ one has ${\rm Re}K(t) \approx -(2k_{\rm B}T/\hbar)\,\pi\,\alpha\,t$. Thus we reproduce Eq. (4.9) with τ_φ given by (4.12) in the limit $\eta = 0$. While it is not so simple to derive the general result for arbitrary η, it is clear from Eqs. (4.11) and (4.12) that the effects of the perpendicular ($\propto \sin\eta$) and longitudinal ($\propto\cos\eta$) terms in (4.8) add up independently.

In the environment-dominated regime, $\Delta E \ll \alpha k_{\rm B}T$, the qubit's Hamiltonian is too weak to fix the basis, while the coupling to the bath becomes the dominant part of the total Hamiltonian. Therefore one should discuss the problem in the eigenbasis of the observable σ_z to which the bath is coupled. The spin can tunnel incoherently between the two eigenstates of σ_z. To find the tunneling rate one can again use the canonical transformation (4.13) leading to the Hamiltonian (4.14). In the Golden Rule approximation one obtains (Leggett et al. 1987) the following relaxation rate (for $\Delta E \ll \alpha k_{\rm B}T$):

$$\tau_{\rm relax}^{-1} = \frac{2\pi}{\hbar}\frac{\Delta E^2\sin^2\eta}{4}\left[\tilde{P}(\Delta E\cos\eta) + \tilde{P}(-\Delta E\cos\eta)\right] \\ \approx \frac{\Delta E^2\sin^2\eta}{2\pi\hbar\alpha k_{\rm B}T}\ , \tag{4.18}$$

where $\tilde{P}(..)$ is the Fourier transform of $P(t)$. To find the dephasing rate we use again Eq. (4.15) and obtain

$$\tau_\varphi^{-1} \approx 2\pi\alpha k_{\rm B}T/\hbar\ . \tag{4.19}$$

In this regime the dephasing is much faster than the relaxation. Moreover, we observe that $\tau_{\rm relax}^{-1} \propto (\alpha k_{\rm B}T)^{-1}$ while $\tau_\varphi^{-1} \propto \alpha k_{\rm B}T$. This implies that the faster is the dephasing, the slower is the relaxation. Such a behavior is an indication of the Zeno (watchdog) effect (Harris & Stodolsky 1982): the environment frequently "observes" the state of the spin, thus preventing it from tunneling.

C. Several fluctuating fields and many qubits

Next we consider the general case of a qubit coupled to several fluctuation sources (baths) via different spin components and below we discuss a many-qubit system. It is described by the following generalization of the spin-boson model:

$$\mathcal{H} = \mathcal{H}_{\rm ctrl} + \sum_i \boldsymbol{\sigma}\boldsymbol{n}_i \left(\sum_a \lambda_a^i x_a^i \right) + \sum_i \mathcal{H}_{\rm B}^i \ , \qquad (4.20)$$

where the index i labels the different (Ohmic) baths and the unit vectors $\boldsymbol{n}_i$ determine the spin components to which the baths are coupled. The Hamiltonian-dominated regime is realized when $\Delta E \gg \sum_i \alpha_i k_{\rm B}T$, where α_i correspond to the bath i. In this case one should divide the fluctuations of all baths into transverse and longitudinal ones, as in Eq. (4.8), with each bath being characterized by the angle η_i between $\boldsymbol{n}_i$ and the field direction ($\cos\eta_i = \boldsymbol{B}\boldsymbol{n}_i/|\boldsymbol{B}|$). The transverse fluctuations will add up to the relaxation rate as

$$\tau_{\rm relax}^{-1} = \sum_i \pi\alpha_i \ \sin^2\eta_i \ \frac{\Delta E}{\hbar} \coth\frac{\Delta E}{2k_{\rm B}T} \ , \qquad (4.21)$$

while the longitudinal fluctuations lead to the dephasing rate

$$\tau_\varphi^{-1} = \frac{1}{2}\ \tau_{\rm relax}^{-1} + \sum_i \pi\alpha_i \ \cos^2\eta_i \ \frac{2k_{\rm B}T}{\hbar} \ . \qquad (4.22)$$

In the simplest environment-dominated situation one of the baths ($i = i_0$) is much stronger than all others, $\alpha_{i_0} \gg \sum_{i\neq i_0} \alpha_i$, and satisfies $\alpha_{i_0} k_{\rm B}T \gg \Delta E$. Then, the dephasing is described in the eigenbasis of $\boldsymbol{\sigma}\boldsymbol{n}_{i_0}$ corresponding to this bath. The rate is

$$\tau_\varphi^{-1} \approx 2\pi\alpha_{i_0} k_{\rm B}T/\hbar \ . \qquad (4.23)$$

The relaxation rate in this basis may be estimated using the Golden Rule:

$$\tau_{\rm relax}^{-1} \approx \frac{\Delta E^2 \sin^2\eta_{i_0}}{2\pi\hbar\alpha_{i_0}\ k_{\rm B}T} + \sum_{i\neq i_0} 2\pi\alpha_i \sin^2\chi_i \ \frac{k_{\rm B}T}{\hbar} \ , \qquad (4.24)$$

where $\cos\chi_i = (\boldsymbol{n}_i\boldsymbol{n}_{i_0})$. This rate is smaller than the dephasing rate (4.23). Note that the relaxation rates due to the other than the strongest baths do not show the Zeno effect.

In the most complicated case of the environment-dominated regime with several baths coupled to different spin components and characterized by constants α_i of the same order it is difficult to make quantitative predictions. However, we expect that the time scale for a quantum state destruction (either dephasing or relaxation) will be longer than $(\sum_i 2\pi\alpha_i k_{\rm B}T/\hbar)^{-1}$.

So far we were concerned with dissipative effects in a single qubit. However, any but the simplest applications of quantum state engineering make use of many coupled qubits and entangled states, i.e., states whose properties can not be reduced to the single-bit ones. Therefore the question arises how dissipation affects multi-qubit systems and entangled states.

As a first step we analyze the effect of dissipation on an N-qubit system during an idle period when the single-bit terms and two-bit interactions are switched off, $\mathcal{H}_{\rm ctrl} = 0$. We assume that each qubit is coupled to an independent oscillator bath, with no correlations between the baths, and we choose a basis where this coupling is diagonal, i.e., the bath is coupled to the σ_z-component. In this case the time evolution operator, governing the density matrix, $\hat\rho_{\nu_1\ldots\nu_N;\mu_1\ldots\mu_N}(t)$, factorizes. We perform for each qubit i the unitary rotation (4.13) with the result:

$$\rho_{\nu_1\ldots\nu_N;\mu_1\ldots\mu_N}(t) \propto \prod_{i=1}^N \left\langle e^{i\Phi_i(t)(\nu_i-\mu_i)} e^{-i\Phi_i(0)(\nu_i-\mu_i)} \right\rangle . \qquad (4.25)$$

Averaging over the baths yields in the long-time limit the following time dependence of the density matrix:

$$\rho_{\nu_1\ldots\nu_N;\mu_1\ldots\mu_N}(t) \ \propto \prod_{\{i:\nu_i\neq\mu_i\}} \exp\left(-t/\tau_\varphi^i\right) . \qquad (4.26)$$

Here the product is over all qubits i which have off-diagonal entries in the density matrix. This form shows that the dissipation has the strongest effect on those entries of $\hat\rho$ which are off-diagonal with respect to each qubit. For instance, the dephasing rate of $\rho_{0\ldots0;1\ldots1}(t)$ is $1/\tau_\varphi = \sum_i 1/\tau_\varphi^i$. It scales linearly with the number of qubits.

The result (4.26) applies independent of the initial state, i.e., equally for product states or entangled states of the multi-qubit system. However, it is valid only if the controlled parts of the Hamiltonian are switched off. The question how dissipation influences the dynamics of entangled states in general situations, e.g., during logic operations when the many-qubit Hamiltonian is non-zero, remains open. Further work is needed to analyze this interesting and important problem.

D. Dephasing in charge qubits

We now turn to the specific case of a Josephson charge qubit coupled to the environment and determine how the dephasing and relaxation rates depend on system parameters. The system is sensitive to various electro-magnetic fluctuations in the external circuit and the substrate, as well as to background charge fluctuations. We first estimate the effect of fluctuations originating from the circuit of the voltage sources. In Fig. 13 the equivalent circuit of a qubit coupled to an impedance $Z(\omega)$ is shown. The latter has intrinsic voltage fluctuations with Johnson-Nyquist power spectrum. When embedded in the circuit shown in Fig. 13 but with $E_{\rm J} = 0$, the voltage fluctuations between the terminals of $Z(\omega)$ are characterized by the spectrum

$$\langle \delta V \delta V \rangle_\omega = \mathrm{Re}\{Z_{\rm t}(\omega)\}\hbar\omega \coth\left(\frac{\hbar\omega}{2k_{\rm B}T}\right) . \qquad (4.27)$$

Here $Z_{\rm t}(\omega) \equiv \left[i\omega C_{\rm qb} + Z^{-1}(\omega)\right]^{-1}$ is the total impedance between the terminals of $Z(\omega)$ and $C_{\rm qb}$ is the capacitance (2.13) of the qubit in the circuit.

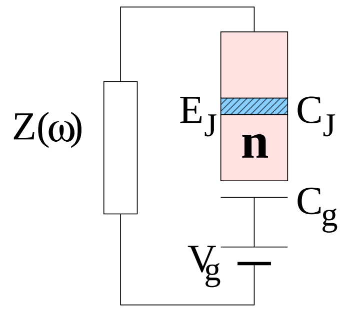

FIG. 13. A qubit in an electro-magnetic environment characterized by the impedance $Z(\omega)$.

Following Caldeira & Leggett (1983) we model the dissipative element $Z(\omega)$ by a bath of harmonic oscillators described by the Hamiltonian $\mathcal{H}_{\rm B}$ as in Eq. (4.4) (Shnirman et al. 1997). The voltage fluctuations between the terminals of $Z(\omega)$ are represented by $\delta V = \sum_\alpha \lambda_\alpha x_\alpha$, while the spectral function (4.6) has to be chosen as $J(\omega) = \omega \mathrm{Re}\{Z_{\rm t}(\omega)\}$ in order to reproduce the fluctuation spectrum (4.27).

To derive the Hamiltonian we introduce an auxiliary variable, the charge q on the gate capacitor, and add a term which couples q to the bath (a natural choice since the current through the impedance is $\dot{q}$). For simplicity of derivation it is convenient also to add a small inductance in series with the impedance Z to provide a 'mass' for the q-mode. Allowing for a time-dependent external voltage $V_{\rm g}(t)$ and integrating out q, we find the Hamiltonian:

$$\mathcal{H} = \frac{[2en - C_{\rm g}V_{\rm g}(t)]^2}{2(C_{\rm J}+C_{\rm g})} - E_{\rm J}\cos\Theta + \sum_a \frac{p_a^2}{2m_a}$$
$$+ \sum_a \frac{m_a\omega_a^2}{2}\left[x_a - \frac{\lambda_a}{m_a\omega_a^2}\left\{2en\frac{C_{\rm qb}}{C_{\rm J}} + C_{\rm qb}V_{\rm g}(t)\right\}\right]^2 . \qquad (4.28)$$

The voltage $V_{\rm g}(t)$ in the last term (coupling to the bath) is relevant only if it depends on time and is usually dropped in the literature. Its role is to provide the RC time delay. This means that when $V_{\rm g}$ is changed the qubit feels the change only after the RC time. In the systems described here this delay is much shorter than the other relevant time scales and, thus, need not to be discussed further.

To be specific we will concentrate in the following on the fluctuations due to an Ohmic resistor $Z(\omega) = R_V$ in the bias voltage circuit. In the two-state approximation, using the relations $n = (1/2)(1+\sigma_z)$ and $\cos\Theta = (1/2)\sigma_x$, we thus arrive at the Hamiltonian of the spin-boson model (4.1) with B_z and B_x given by Eq. (2.4) and (2.5), respectively. The dimensionless parameter $\alpha_z^{\rm ch}$, characterizing the effect of fluctuations coupling to σ_z of the charge qubit, is given by

$$\alpha_z^{\rm ch} = \frac{4R_V}{R_{\rm K}}\left(\frac{C_{\rm qb}}{C_{\rm J}}\right)^2 . \qquad (4.29)$$

The circuit resistance is compared to the quantum resistance $R_{\rm K} = h/e^2 \approx 25.8\ \mathrm{k}\Omega$. Since the parameter $\alpha_z^{\rm ch}$ directly relates the dephasing rate to typical energy scales, its inverse determines the number of coherent single-qubit manipulations which can be performed within the dephasing time. From Eq. (4.29) we see that in order to keep the dissipative effects of external voltage fluctuations weak one has to use a voltage source with low resistance and choose the gate capacitance $C_{\rm g} \approx C_{\rm qb} \ll C_{\rm J}$ as low as possible. The latter screens out the voltage fluctuations, at the expense that one has to apply larger gate voltages for the manipulations. At high frequencies discussed here the typical impedance of the voltage circuit is $R_{\rm V} \approx 50\ \Omega$, and one obtains $\alpha_z^{\rm ch} \approx 10^{-2}(C_{\rm g}/C_{\rm J})^2$. Taking the ratio [10] $C_{\rm g}/C_{\rm J} = 10^{-2}$ one can reach the dissipation as weak as $\alpha_z^{\rm ch} \approx 10^{-6}$, allowing in principle for 10^6 coherent single-bit manipulations.

The fluctuations of the externally controlled flux through the SQUID loop of a charge qubit with tunable Josephson coupling (see Fig. 4) also destroy the phase coherence. As can be seen from Eq. (2.10) these fluctuations couple to $\cos\Theta \propto \sigma_x$. Analogously to the voltage fluctuations considered above, their strength can be expressed by the effective impedance of the current circuit which supplies the flux. For an estimate we take this impedance R_I to be purely real. At typical high frequencies of the qubit's operation it is of order of the vacuum impedance, $R_I \sim 100\ \Omega$. In terms of this resistance the effect of fluctuations in the flux is characterized by the parameter

$$\alpha_x^{\rm ch} = \frac{R_{\rm K}}{4R_I}\left(\frac{M}{\Phi_0}\frac{\partial E_{\rm J}(\Phi_{\rm x})}{\partial \Phi_{\rm x}}\right)^2 , \qquad (4.30)$$

[10] Nakamura et al. (1999) reached an even smaller ratio for the qubit, but the probe circuit introduced a high stray capacitance.

where the flux-controlled Josephson coupling $E_J(\Phi_x)$ is given by Eq.(2.11). The effect is weak for low values of the mutual inductance. For $M \approx 0.01 - 0.1$ nH and $E_J^0 \approx 0.1$ K we obtain $\alpha_x^{\rm ch} \approx 10^{-6} - 10^{-8}$. The dephasing and relaxation times, if only flux fluctuations need to be considered, are thus given by Eqs. (4.11), (4.12), (4.30), but with a substitution $\tan\eta = B_z/B_x$ since the noise terms couple to σ_x. When both the gate voltage and the flux fluctuate a multi-bath situation described by Eq. (4.20) is realized.

For typical parameters, e.g., for those of the experiments of Nakamura et al. (1999), one can estimate the dephasing time associated with the noise in the external circuit to be of the order of 100 ns. These experiments allow a direct probing of the phase coherence. Coherent oscillations have been observed for 5 ns. Hence the theoretical estimate appears to be of the right order [11].

Another important source of decoherence in charge qubits are fluctuations of the background charge. It was found experimentally that they lead to $1/f$ noise at low frequencies. Typically, their contribution to fluctuations of the effective gate voltage, $Q_g = C_g V_g$, is of order $S_Q(\omega) = 10^{-8} e^2/\omega$. These fluctuations limit the time of coherent evolution and can hardly be improved by present-day experimental techniques [12]. Fortunately, for the ideas of quantum state engineering, the configurations of background charges change rarely, on a typical slow relaxation time scale which can reach minutes or even hours. Thus during each cycle of manipulations these charges provide random static gate voltages, which do not destroy, e.g., coherent oscillations. Their effect can be suppressed using refocusing techniques. On the other hand, when averaging over many experimental runs (as done by Nakamura et al. (1999)), then an ensemble-average is formed and the dephasing rate can be extracted.

When the qubit is coupled to a measurement device, which necessarily implies a coupling to a macroscopic variable with dissipative dynamics, the feedback introduces fluctuations and causes dephasing. We will discuss this explicitly in the next section for the case where a Josephson charge qubit is coupled to a dissipative single-electron transistor. We find that the shot noise of the tunneling current in the SET introduces dephasing and relaxation processes.

E. Dephasing in flux qubits

Flux qubits have the advantage that they are practically insensitive to the background charge fluctuations and are advertised for this reason (Mooij et al. 1999). Still their phase coherence can be destroyed by a number of effects as well. Some sources of dissipation for flux qubits have been discussed by Tian et al. (2000) and estimates have been provided for the parameters of the circuits of Mooij et al. (1999) and Orlando et al. (1999). This includes the effect of background charge fluctuations ($\tau_\varphi \approx 0.1$ s) as well as quasiparticle tunneling in the superconductor with a non-vanishing subgap conductance ($\tau_\varphi \approx 1$ ms). The effect of nuclear spins in the substrate producing fluctuating magnetic fields is similar to the effect of background charges on charge qubits. While the static random magnetic field may induce substantial changes of the qubit frequencies of order $\delta\Omega_{\rm nucl} \approx 30$ MHz (which can be suppressed, in principle, by using refocusing pulses), they cause no dephasing for the qubits until a typical nuclear spin relaxation time T_1, which can reach minutes. Other sources of dephasing studied by Tian et al. (2000) include the electro-magnetic radiation ($\tau_\varphi \approx 10^3$ s), much weaker than in typical rf-SQUID designs, and unwanted dipole-dipole magnetic couplings between qubits, which for the inter-qubit distance of 10 μm produces substantial effects after a relatively short time $\tau \approx 0.2$ ms. Variations of the design were suggested to reduce the latter effect.

An important source of dissipation of flux qubits are the fluctuations in the external circuit which supplies fluxes through the loops. They can be analyzed along the same lines as presented above. Since they couple to σ_z, the relevant parameter is $\alpha_z^{\rm fl}$. It is fixed by the impedance Z_I of the current source in the input loop providing the flux bias, and the mutual inductance of the input and the qubit's loop, M:

$$\alpha_z^{\rm fl} = \frac{a}{4} R_K \, {\rm Re}\, Z_I^{-1} \left(\frac{4\pi^2 E_J M}{\Phi_0^2} \right)^2 . \tag{4.31}$$

The numerical prefactor in Eq. (4.31) is $a = 6(\beta_L - 1)/\pi^2$ for the rf-SQUID and $a = b^2\sqrt{4b^2 - 1}/\pi^2$ for the design of Mooij et al. (1999) with $b \equiv \tilde{E}_J/E_J$ being the ratio of critical currents for the junctions in the loop (see Section III.A). The dephasing is slow for small loops and

[11] In the experiments of Nakamura et al. (1999) actually much of the dephasing can be attributed to the measurement device, a dissipative tunnel junction which was coupled permanently to the qubit. Its tunneling resistance was optimized to be large enough not to destroy the qubits quantum coherence completely, but low enough to allow for a measurable current. Single-electron tunneling processes, occurring on a time scale of the order of 10 ns, destroy the state of the qubit (escape out of the two-state Hilbert space) thus putting an upper limit on the time when coherent time evolution can be observed. For a more detailed discussion of the experiment and the measurement process we refer to the article by Choi et al. (2000).

[12] See, however, recent work of Krupenin et al. (2000) where the $1/f$-noise was suppressed by fabricating a metallic island on top of an electrode instead of placing it on the substrate.

junctions with low critical currents. Indeed, the argument in the bracket in (4.31) can be represented as the product of the 'screening ratio' M/L and the quantity $\beta_L = 4\pi^2 L E_{\rm J}/\Phi_0^2$. While the latter should be larger than one for the rf-SQUID, it can be much smaller for the design of Mooij et al. (1999), resulting in a slower dephasing.

The impedance $Z_I(\omega)$ and the bath spectrum $J(\omega) = \hbar\omega\,\mathrm{Re}\,Z_I^{-1}(\omega)$ are frequency-dependent. They can lead to resonances, e.g., if the current source is attached to the qubit via low-loss lines. Care has to be taken in experiments to avoid these resonances. In addition, the dephasing and relaxation times have to be estimated for this situation. The analysis of the Hamiltonian (4.8) with general bath spectrum shows that they can be defined as the times when the quantities $\cos^2\eta\,\langle(\int_0^t X(\tau)d\tau)^2\rangle$ and $\sin^2\eta\,\langle|\int_0^t X(\tau)e^{\pm i\Delta E\tau}d\tau|^2\rangle$ reach values of order one, respectively. The first quantity can be expressed as $t\int d\omega\langle X_\omega^2\rangle\tilde\delta(\omega)$ involving the function $\tilde\delta(\omega) \equiv 2\sin^2(\omega t/2)/(\pi t\omega^2)$ which is peaked at $\omega = 0$ and has the width t^{-1}. Recalling that $\langle X_\omega^2\rangle$ is related to the bath spectrum (4.5), one finds that only the low-frequency part of the impedance $Z_I(\omega)$, with $\omega < \tau_\varphi^{-1}$, determines the dephasing rate. On the other hand, the relaxation rate depends on the values of $Z_I(\omega)$ at frequencies in the vicinity of $\omega = \Delta E/\hbar$ in a range of width $\tau_{\rm relax}^{-1}$.

The choice of a high dc resistance of the remote current source strongly suppresses the fluctuations at low frequencies. Using Eqs. (4.31, 4.12) we can estimate the dephasing rate for the parameters of Mooij et al. (1999). Assuming $Z_I(\omega\approx 0) \sim 1\ \mathrm{M}\Omega$ and $M \approx L$ we find $\alpha_z^{\rm fl} \sim 10^{-9}$, which implies a negligible dephasing. At higher frequencies of order ΔE, even if resonances are suppressed, $Z_I(\omega\approx\Delta E)$ is of order 100 Ω, leading to $\alpha_z^{\rm fl} \sim 10^{-5}$. This determines the relaxation rate via Eq. (4.11). For Mooij et al.'s (1999) parameters we estimate a relaxation time of $\sim 5\ \mu$s at the degeneracy point.

The effect of fluctuations of the σ_x-term in the Hamiltonian (in the flux circuit of the dc-SQUID-loop which controls the Josephson coupling) can be described in a similar way (Makhlin et al. 1999). The effect of these fluctuations is relatively weak for the operation regimes discussed by Mooij et al. (1999).

While a further analysis of the dephasing effects in flux qubits may be needed, the above-mentioned estimates of τ_φ suggest that the observation of coherent flux oscillations is feasible in the near future. However, an open problem remains the fact that the *observation* requires an efficient quantum detector, e.g., a quantum magnetometer. We discuss this issue in the next section.

V. THE QUANTUM MEASUREMENT PROCESS

A. General concept of quantum measurements

Quantum state engineering requires controlled quantum manipulations but also quantum measurement processes. They are needed, e.g., at the end of a computation to read out the final results, or even in the course of the computation for the purpose of error correction. The problem of quantum measurement has always attracted considerable attention, and it still stirs controversy. In most of the literature on quantum information theory the measurement process is expressed simply as a "wave function collapse", i.e., as a non-unitary projection, which reduces the quantum state of a qubit to one of the possible eigenstates of the observed quantity with state-dependent probabilities.

On the other hand, in reality any measurement is performed by a device which itself is a physical system, suitably coupled to the measured quantum system and with a macroscopic read-out variable. This is accounted for in the approaches described below, which are based on the concepts of the dissipative quantum mechanics (Leggett et al. 1987, Weiss 1999, Zurek 1991). The qubit and the measuring device are described as coupled quantum systems. Initially there exist no correlations between the qubit and the meter but, due to the coupling, such correlations (entanglement) emerge in time. This is precisely the concept of measurement of von Neumann (1955). Furthermore, the meter is actually a dissipative system, coupled to the environment. The dissipation eventually reduces the entanglement between the qubit and the meter to classical correlations between them. This is exactly what is needed for the measurement.

Several groups have studied problems related to quantum measurement processes in mesoscopic systems. Aleiner et al. (1997), Levinson (1997), and Gurvitz (1997) investigated the effect of a dissipative conductor, whose conductance depends on the state of quantum system, onto this system itself. Such a configuration is realized in recent experiment (Buks et al. 1998, Sprinzak et al. 1999), where a quantum dot is embedded in one of the paths of a 'which path' interferometer. The flow of a dissipative current through a nearby quantum point contact, with conductance which depends on the charge on the dot, amounts to a 'measurement' of the path chosen by the electrons in the interferometer. And indeed the flow of a current through the point contact leads to an observable reduction of the flux-dependence of the current through the interferometer. On the other hand, no real measurement was performed. The experiments merely demonstrated that the amount of dephasing can be controlled by a dissipative current through the QPC, but they did not provide information about the path chosen by each individual electron.

In what follows we will discuss systems in which one is not only able to study the dephasing but also, e.g., by measuring a dissipative current, to extract information about the quantum state of the qubit. As an explicit example we investigate a single-electron transistor (SET) in the sequential tunneling regime coupled capacitively to a charge qubit (Shnirman & Schön 1998, Schoelkopf et al. 1998). Our purpose is not philosophical but rather practical. We do not search for an ideal measurement device, instead we describe the properties of a realistic system, known to work in the classical regime, and investigate whether it can serve as quantum measurement device. At the same time we keep in mind that we should come as close as possible to the projective measurement picture assumed in quantum algorithms. With the same goal, namely, to establish their potential use as quantum detectors, various other mesoscopic devices have been studied recently. These include a quantum point contact (QPC) coupled to a quantum dot (Gurvitz 1997, Korotkov 1999), a single-electron transistor in the co-tunneling regime (Averin 2000*a*, Maassen van den Brink 2000), or a superconducting SET (SSET) (Averin 2000*b*, Cottet et al. 2000). For a flux qubit a dc-SQUID, or suitable modifications of it, can serve as a quantum detector.

Technically the measurement process is described by the time evolution of the reduced density matrix of the coupled system of qubit and meter. To analyze it we first derive a Bloch-master equation for the time-evolution of the system of a Josephson charge qubit and a dissipative single-electron transistor (SET) coupled to it. This derivation demonstrates how the unitary time evolution of system plus detector can lead to a quantum measurement. It also allows us to follow the dynamics of the system and detector and to analyze the mutual influence of their variables. During the measurement the qubit looses its phase coherence on a short dephasing time scale τ_φ [13]. This means that the off-diagonal elements of the qubit's density matrix (in a preferred basis, which depends on relative strengths of the coupling constants) vanish, while the diagonal ones still remain unchanged. At the same time the information about the initial state of the qubit is transferred to the macroscopic state of the detector (the current in the SET). Under suitable conditions, after another time scale $\tau_{\rm meas}$, this information can be read out. Finally, on a longer, mixing (or relaxation) time scale $\tau_{\rm mix}$ the detector acts back onto the qubit and destroys the information about the initial state. The diagonal entries of the density matrix tend to their stationary values. (These are either determined by the detector or they are thermally distributed, depending on the relative strength of the measurement device and residual interactions with the bath.) One has to chose parameters such that this back-action does not change the occupation probabilities of the qubit's state before the information is actually read out, $\tau_{\rm mix} \gg \tau_{\rm meas} \geq \tau_\varphi$.

The different times scales characterizing the measurement process by a SET, show up also in equilibrium properties, e.g., in the noise spectrum of the fluctuations in the SET. This can be extracted from the time evolution of the coupled density matrix as well.

Ideally, the meter is coupled to the qubit only during the measurement. In practice, however, this option is hard to realize for mesoscopic devices. Rather the meter and the qubit are coupled permanently but the former is kept in a non-dissipative state. To perform a measurement, the meter is switched to the dissipative regime which, as we mentioned above, is an important requirement for the effective quantum measurement. For instance, in a SET, due to the Coulomb blockade phenomena, no dissipative currents are flowing in the meter as long as the transport voltage is switched off. Applying a voltage bias above the Coulomb threshold induces a dissipative current through the SET, which leads to dephasing and, at the same time, provides the macroscopic read-out variable.

Various ways of operation can be used, depending on details of a particular setting. For instance, one can switch the meter abruptly into the dissipative regime and monitor the response of dissipative currents to the qubit. Another possibility is to change the bias gradually until the system switches into the dissipative regime. The value of the bias at which the switching occurs provides information about the qubit's state. Conceptually, these techniques are similar. For definiteness, below we discuss the former operation strategy.

B. Single-electron transistor as a quantum electrometer

Since the relevant quantum degree of freedom of a Josephson charge qubit is the charge of its island, the natural choice of measurement device is a single-electron transistor (SET). This system is shown in Fig. 14. The left hand part is the qubit, with state characterized by the number of extra Cooper pairs n on the island, and controlled by its gate voltage $V_{\rm g}^{\rm qb}$. The right hand part shows a normal island between two normal leads, which form the SET. Its charging state is characterized by the number of extra single-electron charges N on the middle island. It is controlled by gate and transport voltages, $V_{\rm g}^{\rm SET}$ and $V_{\rm tr}$, and further, due to the capacitive coupling to the qubit, by the state of the latter. A similar setup has been studied in the experiments of Bouchiat

[13] In this section τ_φ denotes the dephasing time during a measurement. It is usually much shorter than the dephasing time during the controlled manipulations discussed in the previous sections. from the context it should be clear which situation we refer to.

(1997) and Bouchiat et al. (1998), where it was used to demonstrate that the ground state of a single Cooper pair box is a coherent superposition of different charge states.

During the quantum manipulations of the qubit the transport voltage $V_{\rm tr}$ across the SET transistor is kept zero and the gate voltage of the SET, $V_{\rm g}^{\rm SET}$, is chosen to tune the island away from degeneracy points. Therefore at low temperatures Coulomb blockade effects suppress exponentially a dissipative current flow in the system, and the transistor merely modifies the capacitances of the system [14]. To perform a measurement one tunes the SET by $V_{\rm g}^{\rm SET}$ to the vicinity of its degeneracy point and applies a small transport voltage $V_{\rm tr}$. The resulting normal current through the transistor depends on the charge configuration of the qubit, since different charge states induce different voltages on the island of the SET. While these properties are well established as operation principle of a SET as electro-meter in the classical limit, it remains to be demonstrated that they also allow resolving different quantum states of the qubit. For this purpose we have to discuss various noise factors, including the shot noise associated with the tunneling current and the measurement induced transitions between the states of the qubit. They can be accounted for by analyzing the time evolution of the density matrix of the combined system.

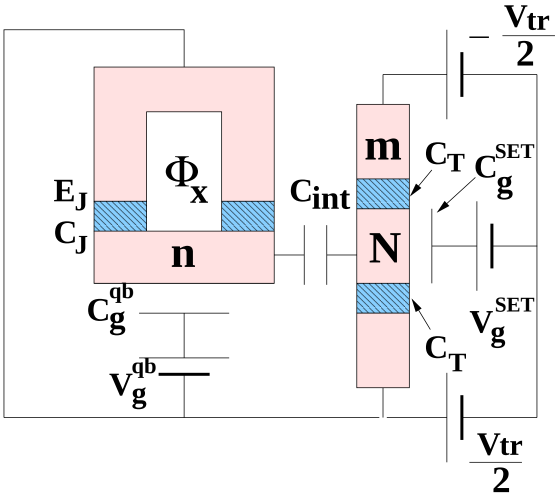

FIG. 14. The circuit consisting of a qubit plus a single-electron transistor used as a measuring device.

The Hamiltonian of the combined system consists of the parts describing the qubit, the SET and the interaction between them:

$$\mathcal{H} = \mathcal{H}_{\rm ctrl} + \mathcal{H}_{\rm SET} + \mathcal{H}_{\rm int} \ . \tag{5.1}$$

[14] More precisely, the leading contribution are co-tunneling processes, which are weak in high-resistance junctions.

Except for a redefinition and renormalization of parameters, the qubit's part is identical to that of the bare qubit (2.3),

$$\mathcal{H}_{\rm ctrl} = -\frac{1}{2} B_z \hat{\sigma}_z - \frac{1}{2} B_x \hat{\sigma}_x \ ,$$

with $B_z = 4E_{\rm C,qb}(1-2n_{\rm g,qb})$ and $B_x = E_{\rm J}(\Phi_x)$. For a detailed derivation and precise definition of the parameters see Appendix C. Here it is sufficient to know that the qubit's Hamiltonian can be controlled by gate voltages and the flux through the SQUID. After diagonalization of (2.8), $\mathcal{H}_{\rm ctrl} = -(1/2)\Delta E(\eta)\, \rho_z$, the characteristic energy scale of the qubit, $\Delta E(\eta) = \sqrt{B_z^2 + B_x^2}$, becomes apparent.

The Hamiltonian of the SET reads

$$\begin{aligned}\mathcal{H}_{\rm SET} &= E_{\rm C,SET}(N - N_{\rm g,SET})^2 \\ &\quad + \mathcal{H}_{\rm L} + \mathcal{H}_{\rm R} + \mathcal{H}_{\rm I} + \mathcal{H}_{\rm T} \ ,\end{aligned} \tag{5.2}$$

where the transistor's charging energy is given by (C2) and the gate charge $N_{\rm g,SET} \equiv -eV_N/2E_{\rm C,SET}$, defined in Eq. (C4), can be controlled by $V_{\rm g}^{\rm SET}$. The three terms $\mathcal{H}_{\rm L}$, $\mathcal{H}_{\rm R}$, and $\mathcal{H}_{\rm I}$ describe microscopic degrees of freedom of noninteracting electrons in the two leads and the middle island of the SET transistor:

$$\mathcal{H}_r = \sum_{k\sigma} \epsilon^r_{k\sigma} c^{r\dagger}_{k\sigma} c^r_{k\sigma} \quad (r = \mathrm{L,R,I}) \ . \tag{5.3}$$

The index $r = \mathrm{L,R,I}$ labels the electrodes "left", "right" (viewed from a suitable angle) and island, σ labels transverse channels including the spin, while k refers to the wave vector within one channel. Note that similar terms should have been written for the electrode and island of the qubit; however, for this superconducting non-dissipative element the microscopic degrees of freedom can be integrated out (Ambegaokar et al. 1982, Schön & Zaikin 1990), resulting in the "macroscopic" quantum description presented in Sections II and III. In this limit the tunneling terms reduce to the Josephson coupling $\mathcal{H}_{\rm J} = -E_{\rm J}\cos\Theta$, expressed in a collective variable describing the coherent transfer of Cooper pairs, $e^{i\Theta}|n\rangle = |n+1\rangle$.

The normal-electron tunneling in the SET transistor is described by the standard tunneling Hamiltonian, which couples the microscopic degrees of freedom:

$$\begin{aligned}\mathcal{H}_{\rm T} = & \sum_{kk'\sigma} T^L_{kk'\sigma} c^{\rm L\dagger}_{k\sigma} c^{\rm I}_{k'\sigma} e^{-i\phi} \\ & + \sum_{k'k''\sigma} T^R_{k'k''\sigma} c^{\rm R\dagger}_{k''\sigma} c^{\rm I}_{k'\sigma} e^{-i\phi} e^{i\psi} + \text{h.c.} \ .\end{aligned} \tag{5.4}$$

To make the charge transfer explicit, (5.4) displays two "macroscopic" operators, $e^{\pm i\phi}$ and $e^{\pm i\psi}$. The first one describes changes of the charge on the transistor island due to the tunneling: $e^{i\phi}|N\rangle = |N+1\rangle$. If the total number of electrons on the island is large it may be treated as an independent degree of freedom. We further include the operator $e^{\pm i\psi}$, which acts on m, the number of electrons which have tunneled through the SET transistor, $e^{i\psi}|m\rangle = |m+1\rangle$. Since the chemical potential of the right lead is controlled, m does not appear in any charging part of the Hamiltonian. However, we have to keep track of it, since it is the measured quantity, related to the current through the SET transistor.

Finally, $\mathcal{H}_{\rm int} = E_{\rm int} N(2n-1)$ describes the capacitive interaction between the charge on the qubit's island and the SET island. In detail it originates from the mixed term in Eq. (C1), where $E_{\rm int}$ is given by Eq. (C2). In the 2-state approximation for the qubits, $n = (1+\sigma_z)/2$, we obtain

$$\mathcal{H}_{\rm int} = N\delta\mathcal{H}_{\rm int} \equiv N E_{\rm int}\, \sigma_z \ . \tag{5.5}$$

The operator $\delta\mathcal{H}_{\rm int}$, introduced here for later convenience, is the part of the interaction Hamiltonian which acts in the qubit's Hilbert space.

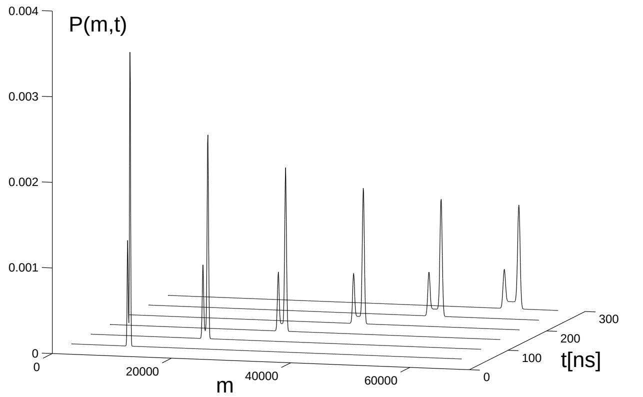

FIG. 15. $P(m,t)$, the probability that m electrons have tunneled during time t (measured in nanoseconds). The initial amplitudes of the qubit's states are $|a|^2 = 0.25$, $|b|^2 = 0.75$. $E_{\rm J} = 0.1$ K, the remaining parameters are given later in the text.

C. Density matrix and description of measurement

The total system composed of qubit and SET is described by a total density matrix $\hat{\varrho}(t)$. We can reduce it, by tracing out the microscopic electron states of the left and right leads and of the island, to

$$\hat{\rho}(t) = {\rm Tr}_{\rm L,R,I}\{\hat{\varrho}(t)\} \, . \tag{5.6}$$

This reduced density matrix $\hat{\rho}(i,i';N,N';m,m')$ is still a matrix in the indices i, which label the quantum states of the qubit $|0\rangle$ or $|1\rangle$, in N, and in m. In the following we will assume that initially, as a result of previous quantum manipulations, the qubit is prepared in some quantum state and it is disentangled from the SET, i.e., the initial density matrix of the whole system may be written as a product $\hat{\rho}_0 = \hat{\rho}_0^{\rm qb} \otimes \hat{\rho}_0^{\rm SET}$. At time $t=0$ we switch on a transport voltage of the SET and follow the resulting time evolution of the density matrix of the whole system. For specific questions we may further reduce the total density matrix in two ways, either one providing complementary information about the measurement process.

The first, common procedure (Gurvitz 1997) is to trace over N and m. This yields a reduced density matrix of the qubit $\hat{\rho}_{ij} \equiv \sum_{N,m} \hat{\rho}(i,j;N,N;m,m)$. At $t=0$ one has $\hat{\rho}_{ij} = (\hat{\rho}_0^{\rm qb})_{ij}$. Depending on the relation among the energy scales and coupling strengths (see Section IV) a preferred basis may exist in which the dynamics of the diagonal and the off-diagonal elements of $\hat{\rho}_{ij}$ decouple. We study how fast the off-diagonal elements (in that special basis) vanish after the SET is switched to the dissipative state, i.e., we determine the rate of dephasing induced by the SET. And we determine how fast the diagonal elements change their values. This process we call 'mixing'.

The rates of 'dephasing' and 'mixing' refer to the quantum properties of the measured system in the presence of the measurement device. These quantities have also been analyzed in Refs. (Levinson 1997, Aleiner et al. 1997, Gurvitz 1997, Buks et al. 1998). They do not tell us, however, anything about the quantity measured in an experiment, namely, the current flowing through the SET. Therefore the second way to reduce the density matrix is important as well. By tracing the density matrix over the qubit's variables and the state N of the island,

$$P(m,t) \equiv \sum_{i,N} \hat{\rho}(i,i;N,N;m,m)(t) \, , \tag{5.7}$$

we obtain the probability distribution for the experimentally accessible number of electrons m which have tunneled through the SET during time t. Its detailed analysis will be presented below. In order to provide a feeling we first present and describe some representative results: At $t=0$ no electrons have tunneled, so $P(m,0) = \delta_{m,0}$. Then, as illustrated in Fig. 15, the peak of the distribution moves to nonzero values of m and, simultaneously, widens due to shot noise. If the two states of the preferred basis correspond to different tunneling currents, and hence different m-shifts, and if the mixing in this basis is sufficiently slow, then after some time the peak splits into two with weights corresponding to the initial values of the diagonal elements of $\hat{\rho}_0^{\rm qb}$ in the preferred basis (we will denote these values $|a|^2$ and $|b|^2 = 1 - |a|^2$). Provided that after sufficient separation of the two peaks their weights are still close to the original values, a good quantum measurement can be performed by measuring m. After a longer time, due to transitions between the states of the preferred basis (mixing) the two peaks transform into a broad plateau. Therefore there is an optimum time for the measurement, such that, on one hand, the two peaks are separate and, on the other hand, the mixing has not yet influenced the process.

Having introduced the relevant time scales, we can mention that the which-path interferometry (Buks et al. 1998) can be thought of as a very short measurement process. Each particular electron – the observed quantum system – spends only a short time within the dot. This time of interaction with the meter may be shorter than the dephasing time. Therefore the coupling leads only to a slight suppression of the interference pattern.

D. Master equation

The time evolution of the density matrix leads to Bloch-type master equations with coherent terms. Examples of this type have recently been analyzed in various contexts (Nazarov 1993, Schoeller & Schön 1994, Stoof & Nazarov 1996, Gurvitz & Prager 1996, Gurvitz 1997). Schoeller & Schön (1994) developed a diagrammatic technique which provides a formally exact master equation for a SET as an expansion in the tunneling term $\mathcal{H}_{\rm T}$, while all other terms, including the charging energy, constitute the zeroth order Hamiltonian $\mathcal{H}_0$. The time evolution of the reduced density matrix, $\hat\rho(t) = \hat\rho(0)\Pi(0,t)$ is expressed by a propagator $\Pi(t',t)$, which is expanded and displayed diagrammatically and finally summed in a way reminiscent of a Dyson equation. Examples are shown in Fig. 16 and Appendix D. In contrast to equilibrium many-body expansions, since the time dependence of the density matrix is described by a forward and a backward time-evolution operator, there are two propagators, which are represented by two horizontal lines (Keldysh contour). The two bare lines describe the coherent time evolution of the system. They are coupled due to the tunneling in the SET. The sum of all distinct transitions defines a 'self-energy' diagram Σ. Below we will present the rules for calculating Σ and present a suitable approximate form. The Dyson equation is equivalent to a Bloch-master equation for the density matrix, which reads

$$\frac{d\hat\rho(t)}{dt} - \frac{i}{\hbar}[\hat\rho(t), \mathcal{H}_0] = \int_0^t dt' \hat\rho(t')\Sigma(t-t') \ . \qquad (5.8)$$

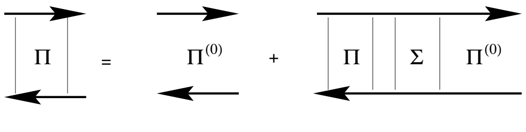

FIG. 16. The Dyson-type equation governing the time evolution of the density matrix. It is equivalent to the generalized master equation (5.8). The 'self-energy' diagrams Σ describe the transitions due to tunneling in the SET transistor.

In principle, the density matrix $\hat\rho(i,i';N,N';m,m') \equiv \hat\rho^{i',N',m'}_{i,\,N,\,m}$ is a matrix in all three indices i, N, and m, and the (generalized) transition rates due to single-electron tunneling processes (in general of arbitrary order), $\Sigma^{i',N',m'\to\bar i',\bar N',\bar m'}_{i\ ,N\ ,m\ \to\,\bar i,\,\bar N,\,\bar m}(t-t')$, connect these diagonal and off-diagonal states. But a closed set of equations for the time evolution of the system can be derived (Schoeller & Schön 1994) which involves only the elements of $\hat\rho$ diagonal in N. The same is true for the matrix structure in m. I.e., we need to consider only the following elements of the density matrix $\hat\rho^{ij}_N(m) \equiv \hat\rho^{i,N,m}_{j,N,m}$. Accordingly, of all the transition rates we need to calculate only the corresponding matrix elements $\Sigma^{i',N',m'\to i,N,m}_{j',N',m'\to j,N,m}(\Delta t)$.

If the temperature is low and the applied transport voltage not too high, the leading tunneling processes in the SET are sequential transitions between two adjacent charge states, say, $N=0$ and $N=1$. We concentrate here on this case (to avoid confusion with the states of the qubit we continue using the notation N and $N+1$). The transition rates can be calculated diagrammatically in the framework of the real-time Keldysh contour technique. The derivation is presented in Appendix D. A simplification arises, since the coherent part of the time evolution of the density matrix, which evolves on the time scale set by the qubits energies, is slow compared to the 'tunneling time', given by the inverse of the energy transfer in the tunneling process (see arguments in square brackets in Eqs. 5.11, 5.12 below). As a result the self-energy effectively reduces to a delta-function, $\Sigma(\Delta t) \propto \delta(\Delta t)$, and the Bloch-master equation (5.8) reduces to a *Markovian* dynamics.

The resulting master equation is translationally invariant in m-space. Hence a Fourier transformation is appropriate, $\hat\rho^{ij}_N(k) \equiv \sum_m e^{-ikm}\hat\rho^{ij}_N(m)$. As a result Eq. (D8) factorizes in k-space and we get a finite rank (8×8) system of equations for each value of k. This system may be presented in a compact form if we combine the eight components of the density matrix into a pair $(\hat\rho_N, \hat\rho_{N+1})$ of the 2×2-matrices $\hat\rho^{ij}_N(k)$, corresponding to N and $N+1$:

$$\hbar\frac{d}{dt}\begin{pmatrix} \hat\rho_N \\ \hat\rho_{N+1}\end{pmatrix} + \begin{pmatrix} i[\mathcal{H}_{\rm ctrl}, \hat\rho_N] \\ i[\mathcal{H}_{\rm ctrl} + \delta\mathcal{H}_{\rm int}, \hat\rho_{N+1}]\end{pmatrix} = \begin{pmatrix} -\check\Gamma_{\rm L} & e^{-ik}\check\Gamma_{\rm R} \\ \check\Gamma_{\rm L} & -\check\Gamma_{\rm R}\end{pmatrix}\begin{pmatrix} \hat\rho_N \\ \hat\rho_{N+1}\end{pmatrix} \ . \qquad (5.9)$$

The operator $\delta\mathcal{H}_{\rm int} \equiv E_{\rm int}\sigma_z = E^{\parallel}_{\rm int}\rho_z + E^{\perp}_{\rm int}\rho_x$ was introduced in Eq. (5.5). The tunneling rates in the left and right junctions are represented by operators $\check\Gamma_{\rm L}$ and $\check\Gamma_{\rm R}$, acting on the qubit's density matrix:

$$\begin{aligned} \check\Gamma_{\rm L}\hat\rho_N &\equiv \Gamma_{\rm L}\hat\rho_N + \pi\alpha_{\rm L}\,[\delta\mathcal{H}_{\rm int}, \hat\rho_N]_+ \ , \\ \check\Gamma_{\rm R}\hat\rho_{N+1} &\equiv \Gamma_{\rm R}\hat\rho_{N+1} - \pi\alpha_{\rm R}\,[\delta\mathcal{H}_{\rm int}, \hat\rho_{N+1}]_+ \ . \end{aligned} \qquad (5.10)$$

Here $\alpha_{\rm L/R} \equiv R_{\rm K}/(4\pi^2 R^{\rm T}_{\rm L/R})$ is the tunneling conductance of the left/right junction, measured in units of the resistance quantum $R_K = h/e^2$. The tunneling rates in the junctions are determined by the potentials $\mu_{L/R}$ of the leads and the induced charge $N_{g,SET}$ on the SET's island:

$$\Gamma_L = 2\pi\alpha_L[\mu_L - (1 - 2N_{g,SET})E_{C,SET}] \tag{5.11}$$

$$\Gamma_R = 2\pi\alpha_R[(1 - 2N_{g,SET})E_{C,SET} - \mu_R] \tag{5.12}$$

$$\Gamma \equiv \Gamma_L\Gamma_R/(\Gamma_L + \Gamma_R) \, . \tag{5.13}$$

They combine into the parameter Γ which gives the conductance of the SET in the classical (e.g., high voltage) regime. As a result of the last terms in the Eqs. (5.10) the effective rates and thus the current in the SET are sensitive to the state of the qubit, which makes the measurement possible.

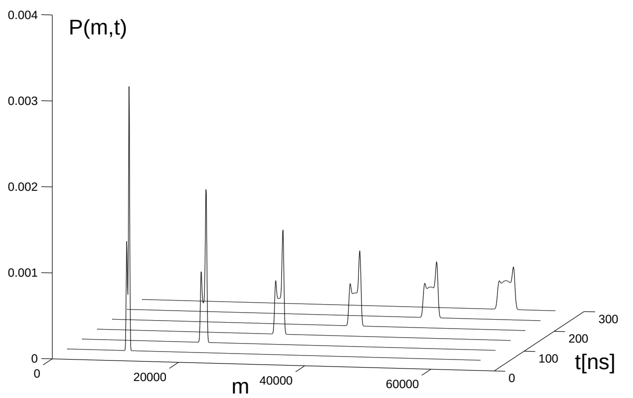

FIG. 17. $P(m,t)$, the probability that m electrons have tunneled during time t. The parameters are the same as in Fig. 15 except that $E_J = 0.25$ K.

To provide a feeling for the types of solutions we present here numerical solutions of Eq. (5.9) for the following system parameters: $B_z = 2$ K, $E_{int} = 0.25$ K, $\alpha_L = \alpha_R = 0.03$, $\Gamma_L = 1.8$ K, and $\Gamma_R = 7.8$ K. We plot the results for $E_J = 0.1$ K (Fig. 15) and for $E_J = 0.25$ K (Fig. 17). We see that for the smaller value of E_J (the eigenbasis of $\mathcal{H}_{ctrl}$ is closer to the charge basis) the probability distribution $P(m,t)$ develops a two-peak structure. The weights of the peaks are equal to the initial values of the diagonal elements of the qubit's density matrix. For the larger value of E_J the two-peak structure can also be seen but the valley between the peaks is filled. This indicates that the mixing transitions take place on the same time scale as that of peak separation, and no good measurement can be performed. In Fig. 18 the probability distribution $P(m,t)$ is plotted for longer times. (In order to cover many decades of the time it is necessary to rescale the m axis as well.) The parameters are the same as in Fig. 15 ($E_J = 0.1$ K). The figure displays clearly the measurement stage and the third stage on the mixing time scale. The valley between the two peaks fills up and a single, broad (note the rescaled m axis) peak develops.

As one can see from (5.9) the Hamiltonian of the qubit switches between $\mathcal{H}_{ctrl}$ and $\mathcal{H}_{ctrl} + \delta\mathcal{H}_{int}$ after each tunneling event in the SET. This leads, in general, to a complicated dynamics. Above we showed representative numerical results. Next we will analyze Eq. (5.9) perturbatively which provides insight into the physics of the measurement process.

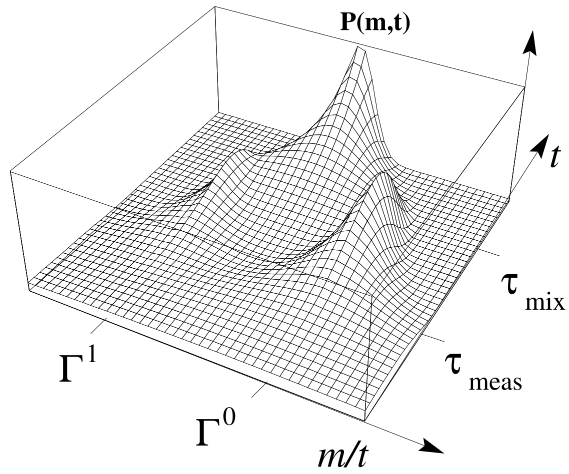

FIG. 18. $P(m,t)$ obtained in the two-mode approximation (5.33), plotted versus t (on a logarithmic scale) and m/t. The initial probabilities of the qubit's states are $|a|^2 = 0.75$, $|b|^2 = 0.25$.

In general, the two Hamiltonians $\mathcal{H}_{ctrl}$ and $\mathcal{H}_{ctrl}+\delta\mathcal{H}_{int}$ are not close and their respective eigenbases may be quite different. In this situation a better choice for the qubit's Hamiltonian would be the "average" Hamiltonian

$$\mathcal{H}_{av} \equiv \mathcal{H}_{ctrl} + \langle N\rangle\delta\mathcal{H}_{int} \ , \tag{5.14}$$

where $\langle N\rangle \equiv \Gamma_L/(\Gamma_L + \Gamma_R)$ is the steady state average of N. (The left-right asymmetry follows from the specific choice of the sequential tunneling regime: $N = 0 \to N = 1$ in the *left* junction and $N = 1 \to N = 0$ in the *right* junction.) Relevant energy scales are, then, the level splitting of the "average" Hamiltonian,

$$\mathcal{H}_{av} = -\frac{1}{2}\Delta E_{av}\rho_z \ , \tag{5.15}$$

the capacitive coupling energy E_{int}, and the bare tunneling rates $\Gamma_{L/R}$. For definiteness we consider the case

$$E_{int} \ll \Gamma_L + \Gamma_R \ . \tag{5.16}$$

I.e., we exclude the regimes of too strong coupling or too weak tunneling in the SET, which could be treated similarly to what is presented below. The main simplification of the regime (5.16) is that the spectrum of fluctuations of the electron number N on the SET island is white in a wide enough range of frequencies, characterized by the zero frequency noise power $S_N(\omega\to 0)\equiv 2\langle\delta N^2_{\omega\to 0}\rangle$. When the SET is detached from the qubit and switched to the dissipative regime, this spectrum is given by $S_N(\omega\to 0)=4\Gamma/(\Gamma_{\rm L}+\Gamma_{\rm R})^2$. The related back-action noise randomizes the relative phase between the charge states of the qubit. In the absence of other sources for dynamics the rate of this process is

$$\tau_{\varphi 0}^{-1}=E_{\rm int}^2 S_N(\omega\to 0)=\frac{4E_{\rm int}^2\Gamma}{(\Gamma_{\rm L}+\Gamma_{\rm R})^2}\ . \qquad (5.17)$$

It is an important scale for the distinction between different sub-regimes of (5.16), which will be described in the following.

E. Hamiltonian-dominated regime

Let us first consider the case where the qubit's "average" Hamiltonian dominates over the dephasing due to the back-action of the SET, $\Delta E_{\rm av}\gg\tau_{\varphi 0}^{-1}$. Then, a perturbative analysis in the eigenbasis of $\mathcal{H}_{\rm av}$ is appropriate, where the operator $\delta\mathcal{H}_{\rm int}$ can be rewritten as $\delta\mathcal{H}_{\rm int}=E_{\rm int}^{\|}\rho_z+E_{\rm int}^{\perp}\rho_x$, where $E_{\rm int}^{\|}\equiv E_{\rm int}\cos\eta_{\rm av}$, $E_{\rm int}^{\perp}\equiv E_{\rm int}\sin\eta_{\rm av}$, and $\sin\eta_{\rm av}\equiv E_{\rm J}/\Delta E_{\rm av}$. In the following we treat the off-diagonal part of $\delta\mathcal{H}_{\rm int}$, i.e., $E_{\rm int}^{\perp}\rho_x$, (which leads to mixing, see below) perturbatively. In zeroth order, i.e., for $E_{\rm int}^{\perp}=0$, the time evolution of $(\hat\rho_N^{ij}(k),\hat\rho_{N+1}^{ij}(k))$ with different (i,j) are decoupled from each other. For diagonal elements, $i=j=0$ or 1, we obtain

$$\frac{d}{dt}\begin{pmatrix}\hat\rho_N^{00/11}\\ \hat\rho_{N+1}^{00/11}\end{pmatrix}=\begin{pmatrix}-\Gamma_{\rm L}^{0/1} & e^{-{\rm i}k}\Gamma_{\rm R}^{0/1}\\ \Gamma_{\rm L}^{0/1} & -\Gamma_{\rm R}^{0/1}\end{pmatrix}\begin{pmatrix}\hat\rho_N^{00/11}\\ \hat\rho_{N+1}^{00/11}\end{pmatrix}\ , \qquad (5.18)$$

where $\Gamma_L^{0/1}=\Gamma_L\pm 2\pi\alpha_L E_{\rm int}^{\|}$ and $\Gamma_R^{0/1}=\Gamma_R\mp 2\pi\alpha_R E_{\rm int}^{\|}$. We obtain four eigenmodes ($\propto e^{\lambda t}$), two for each element (00 or 11). Most interesting are small values $k\ll 1$. In this case, two modes with eigenvalue $\lambda_-^{ii}(k)\approx -{\rm i}\Gamma^i k-\frac{1}{2}f^i\Gamma^i k^2$ and eigenvectors $V_-^{ii}(k)$ given by $\hat\rho_N^{ii}(k)/\hat\rho_{N+1}^{ii}(k)\approx\Gamma_{\rm R}^i/\Gamma_{\rm L}^i$, describe waves in m-space propagating with group velocity

$$\Gamma^i\equiv\frac{\Gamma_{\rm L}^i\Gamma_{\rm R}^i}{\Gamma_{\rm L}^i+\Gamma_{\rm R}^i}\ . \qquad (5.19)$$

The wave-packets widen with time as $\sqrt{2f^i\Gamma^i t}$ due to shot-noise effects. The so called Fano factors,

$$f^i\equiv({\Gamma_{\rm L}^i}^2+{\Gamma_{\rm R}^i}^2)/(\Gamma_{\rm L}^i+\Gamma_{\rm R}^i)^2\,, \qquad (5.20)$$

determine the suppression of the shot noise in the sequential tunneling regime. The second pair of eigenmodes decay fast, $\lambda_+^{ii}(k)\approx -(\Gamma_{\rm L}^i+\Gamma_{\rm R}^i)$. For their eigenvectors we obtain $\hat\rho_N^{ii}(k)/\hat\rho_{N+1}^{ii}(k)\approx -1$. This fast decay means that after a few tunneling events, on the time scale $(\Gamma_{\rm L}^i+\Gamma_{\rm R}^i)^{-1}$, detailed balance $\hat\rho_N^{ii}(k)/\hat\rho_{N+1}^{ii}(k)\approx\Gamma_{\rm R}^i/\Gamma_{\rm L}^i$ is established. For larger values of k ($k\sim 1$) one can check that both $\hat\rho_N^{ii}(k)$ and $\hat\rho_{N+1}^{ii}(k)$ decay fast.

For the off-diagonal elements we obtain

$$\frac{d}{dt}\begin{pmatrix}\hat\rho_N^{01/10}\\ \hat\rho_{N+1}^{01/10}\end{pmatrix}=\left[\begin{pmatrix}-\Gamma_{\rm L} & e^{-{\rm i}k}\Gamma_{\rm R}\\ \Gamma_{\rm L} & -\Gamma_{\rm R}\end{pmatrix}\pm\begin{pmatrix}i\Delta E_N & 0\\ 0 & i\Delta E_{N+1}\end{pmatrix}\right]\begin{pmatrix}\hat\rho_N^{01/10}\\ \hat\rho_{N+1}^{01/10}\end{pmatrix}\ , \qquad (5.21)$$

where $\Delta E_N=\Delta E_{\rm av}+2\langle N\rangle E_{\rm int}^{\|}$, and $\Delta E_{N+1}=\Delta E_{\rm av}-2(1-\langle N\rangle)E_{\rm int}^{\|}$. Again, there are two pairs of eigenmodes with eigenvalues such that $\lambda_\pm^{10}(k)=[\lambda_\pm^{01}(-k)]^*$. One pair of eigenmodes with ${\rm Re}\lambda_+^{01/10}(k\ll 1)\approx -(\Gamma_{\rm L}+\Gamma_{\rm R})$ decay fast. For the second pair $\lambda_-^{10/01}(k\ll 1)\approx\pm i\Delta E_{\rm av}-\tau_\varphi^{-1}$ where

$$\tau_\varphi^{-1}\approx\frac{4\Gamma {E_{\rm int}^{\|}}^2}{(\Gamma_{\rm L}+\Gamma_{\rm R})^2}={E_{\rm int}^{\|}}^2 S_N(\omega\to 0)=\tau_{\varphi 0}^{-1}\cos^2\eta_{\rm av}\ . \qquad (5.22)$$

Thus after detailed balance is established, the λ_-^{10} and λ_-^{01} modes describe coherent oscillations of the off-diagonal matrix elements with frequency of order $\Delta E_{\rm av}$ and decay rate τ_φ^{-1}. For larger values of k the decay times are of the same order or shorter than those for $k\approx 0$.

The fast decaying diagonal modes $\lambda_+^{00/11}$ do not contribute to $P(m,t)$, since for these modes $\hat\rho_N^{ii}(k)+\hat\rho_{N+1}^{ii}(k)\approx 0$. Thus there are only two modes contributing, with eigenvalues $\lambda_-^{00}(k)$ and $\lambda_-^{11}(k)$. Starting from the initial occupation probabilities $|a|^2$ and $|b|^2$ we obtain

$$P(k,t)\approx |a|^2 e^{\lambda_-^{00}(k)\,t}+|b|^2 e^{\lambda_-^{11}(k)\,t}\ , \qquad (5.23)$$

where $P(m,t)\equiv\int dk/(2\pi)\,P(k,t)\,e^{{\rm i}km}$. This form describes the evolution of the distribution $P(m,t)$ from the initial $\delta(m)$ at $t=0$ into two peaks. The peaks shift to positive m-values linear in t with velocities Γ^0 and Γ^1, and they grow in widths as $\sqrt{2f^i\Gamma^i t}$. This time dependence implies that only after a certain time, which we denote as "measurement time" $\tau_{\rm meas}$, the two peaks emerge from the broadened distribution. The associated rate is

$$\tau_{\rm meas}^{-1}=\left(\frac{\Gamma^0-\Gamma^1}{\sqrt{2f^0\Gamma^0}+\sqrt{2f^1\Gamma^1}}\right)^2\ . \qquad (5.24)$$

In the linear response regime, when Γ^0 and Γ^1 are close, we obtain

$$\tau_{\rm meas}^{-1}=\frac{(\Delta I)^2}{4S_I}\ , \qquad (5.25)$$

where S_I is the zero frequency power of the shot noise in the SET and $\Delta I = e(\Gamma^0 - \Gamma^1)$. The weights of the peaks are given by the initial weights of the eigenstates of $\mathcal{H}_{\rm av}$, $|a|^2$ and $|b|^2$. Measuring the charge m thus constitutes a perfect quantum measurement (Shnirman & Schön 1998).

Next we analyze the effect of the perturbation $E_{\rm int}^{\perp}\rho_z$ in the master equation (5.9). It appears in both the coherent (LHS) and incoherent (RHS) parts of Eq. (5.9) and leads to the mixing. As usual the perturbation has the strongest effect when it lifts a (near) degeneracy, since in this case the eigenvectors within the degenerate subspace may change substantially. Therefore we first treat the two near degenerate modes, i.e., we restrict ourselves to the two-dimensional subspace spanned by $V_-^{00}(k=0)$ and $V_-^{11}(k=0)$, and check how the degeneracy between these two modes is lifted in second order of perturbative expansion. To account for this we approximate the diagonal part of the density matrix as

$$\hat{\rho}_{\rm diag}(k,t) \approx A^0(k,t)V_-^{00}(k=0) + A^1(k,t)V_-^{11}(k=0) \ , \tag{5.26}$$

(the LHS should be understood as an eight-column vector consisting of all matrix elements of $\hat{\rho}_{\rm diag}$) for which we obtain an effective (reduced) master equation:

$$\frac{d}{dt}\begin{pmatrix} A^0(k) \\ A^1(k) \end{pmatrix} = M_{\rm red}\begin{pmatrix} A^0(k) \\ A^1(k) \end{pmatrix} \ , \tag{5.27}$$

where

$$M_{\rm red} = \begin{pmatrix} \lambda_-^{00}(k) & 0 \\ 0 & \lambda_-^{11}(k) \end{pmatrix} + \frac{1}{2\tau_{\rm mix}}\begin{pmatrix} -1 & 1 \\ 1 & -1 \end{pmatrix} . \tag{5.28}$$

The second term in (5.28) results from the perturbative expansion and, indeed, lifts the degeneracy between the two modes. The mixing rate is obtained in second order perturbation expansion as

$$\tau_{\rm mix}^{-1} = \frac{4\Gamma {E_{\rm int}^{\perp}}^2}{\Delta E_{\rm av}^2 + (\Gamma_{\rm R}+\Gamma_{\rm L})^2} = {E_{\rm int}^{\perp}}^2 S_N\left(\omega = \frac{\Delta E_{\rm av}}{\hbar}\right) . \tag{5.29}$$

In the approximation (5.26) we have $A^i(k,t) = \sum_N \hat{\rho}_N^{ii}(k)$. At $t=0$ these are occupation probabilities of the eigenstates of $\mathcal{H}_{\rm av}$, $A^0(k,t=0) = |a|^2$, $A^1(k,t=0) = |b|^2$, for all k. It is straightforward to diagonalize Eq. (5.28) to find the eigenvalues. While the sum of the occupation probabilities is conserved, $A^0(k=0,t) + A^1(k=0,t) = 1$, the difference decays, $A^0(k=0,t) - A^1(k=0,t) \propto \exp(-t/\tau_{\rm mix})$. Thus both occupations tend to $1/2$ in the long-time limit. This implies that the evolution of $P(m,t)$ is given by Eq. (5.23) only for times $t \ll \tau_{\rm mix}$, and in order to perform a measurement one must have $\tau_{\rm mix} \gg \tau_{\rm meas}$. As $\tau_{\rm meas}^{-1} \propto {E_{\rm int}^{\parallel}}^2 \propto \cos^2\eta_{\rm av}$ and $\tau_{\rm mix}^{-1} \propto {E_{\rm int}^{\perp}}^2 \propto \sin^2\eta_{\rm av}$, a good measurement may always be achieved by choosing $\tan^2\eta_{\rm av}$ small enough.

Another effect of the mixing perturbation is that the dephasing rate, i.e., the rate of vanishing of the off-diagonal elements of the density matrix is changed as

$$\tau_\varphi^{-1} = \tau_{\varphi 0}^{-1}\cos^2\eta_{\rm av} + 1/2\tau_{\rm mix} \ . \tag{5.30}$$

This is analogous to the relation between the dephasing (4.12) and relaxation (4.11) rates in the spin-boson model. It reflects the fact that the relaxation of the diagonal elements of the density matrix leads also to additional suppression of the off-diagonal ones. Thus even when $\eta_{\rm av} = \pi/2$, the off-diagonal elements vanish with the rate $1/2\tau_{\rm mix}$.

The long-time behavior of the qubit and detector, excluding the period of the initial dephasing, is dominated by the two slowly decaying modes. In this regime we obtain from Eqs. (5.27,5.28) the reduced time evolution operator

$$U_{\rm red}(k,t) \equiv \exp[M_{\rm red}(k)\,t] \ . \tag{5.31}$$

Its Fourier transform $U_{\rm red}(m,t)$ yields the expression for the distribution

$$P(m,t) = (1,\,1)\cdot U_{\rm red}(m,t)\cdot\begin{pmatrix} |a|^2 \\ |b|^2 \end{pmatrix} . \tag{5.32}$$

This Fourier transform can be performed analytically (Makhlin et al. 2000*d*), and we arrive at

$$P(m,t) = \sum_{m'=-\infty}^{\infty} \tilde{P}(m-m',t)\,\frac{e^{-m'^2/2f\bar{\Gamma}t}}{\sqrt{2\pi f\bar{\Gamma}t}} \ , \tag{5.33}$$

where

$$\tilde{P}(m,t) = P_{\rm pl}\left(2\frac{m-\bar{\Gamma}t}{\delta\Gamma\,t}\,,\ \frac{t}{2\tau_{\rm mix}}\right) + e^{-t/2\tau_{\rm mix}}\left[|a|^2\delta\left(m-\Gamma^0 t\right) + |b|^2\delta\left(m-\Gamma^1 t\right)\right] \tag{5.34}$$

and

$$\Gamma^{0/1} \equiv \bar{\Gamma} \pm \delta\Gamma/2 \ . \tag{5.35}$$

We observe that the solution is constructed from two delta-peaks, smeared by the convolution with the shot-noise Gaussian, and a plateau between them, which for $|x|<1$ is given by

$$P_{\rm pl}(x,\tau) = e^{-\tau}\frac{1}{2\,\delta\Gamma\,\tau_{\rm mix}}\left\{I_0\left(\tau\sqrt{1-x^2}\right) + \left[1 + x(|a|^2-|b|^2)\right] I_1\left(\tau\sqrt{1-x^2}\right)/\sqrt{1-x^2}\right\} , \tag{5.36}$$

while $P_{\rm pl} = 0$ for $|x| > 1$. Here I_0, I_1 are the modified Bessel functions. We work in the limit of weak qubit-detector coupling, where the Fano factors (5.20) are close, and we denote them simply by f. For short times, $t \ll \tau_{\rm mix}$, the peaks dominate, while the plateau is low. At longer times the initial peaks disappear while the plateau is transformed into a single central peak (see Fig. 18).

We complement the results for the charge distribution function $P(m,t)$ by a derivation of the distribution function for the values of the current. The measured quantity is actually the current averaged over a certain time interval Δt, i.e., $I_{\Delta t} \equiv [m(t+\Delta t) - m(t)]/\Delta t \equiv \Delta m/\Delta t$. Accordingly the quantity of interest $P(I_{\Delta t}, t)$ can be expressed by the joint probability that m electrons have tunneled at time t and $m + \Delta m$ electrons at a later time $t + \Delta t$:

$$P(I_{\Delta t}, t) = \sum_m P(m, t; m+\Delta m, t+\Delta t) = \sum_m {\rm Tr}' \left[U(\Delta m, \Delta t)\, U(m,t) \hat\rho_0\right] . \qquad (5.37)$$

Here we made use of the Markovian approximation (see Section V.D). The trace is taken over all degrees of freedom except m, and also $\hat\rho_0$ refers to their initial state. In the two-mode approximation (5.27,5.28), sufficient at long times, we replace U again by $U_{\rm red}$ and obtain

$$P(I_{\Delta t}, t) = (1\ 1) \cdot U_{\rm red}(\Delta m, \Delta t) \cdot \cdot \left\{ \frac{1}{2} \begin{pmatrix} 1 \\ 1 \end{pmatrix} + \frac{|a|^2 - |b|^2}{2} e^{-t/\tau_{\rm mix}} \begin{pmatrix} 1 \\ -1 \end{pmatrix} \right\} \qquad (5.38)$$

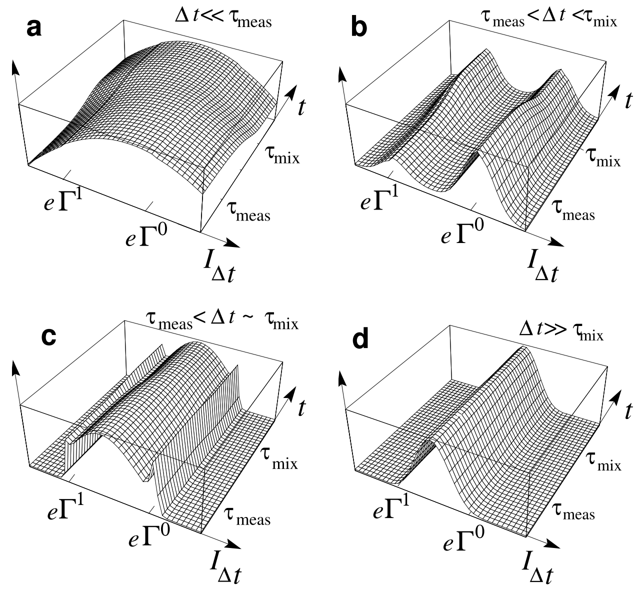

FIG. 19. Probability distribution $P(I_{\Delta t}, t)$ of the current averaged over various time intervals Δt. The time axis is plotted on a logarithmic scale.

The behavior of $P(I_{\Delta t}, t)$ is displayed in Fig. 19 for various values of Δt: (a) If the current is averaged over very short intervals, $\Delta t \ll \tau_{\rm meas}$ [Fig. 19 (a)], the detector does not have enough time to extract the signal from the shot-noise governed background. (b) An effective quantum measurement is achieved if $\tau_{\rm meas} < \Delta t < \tau_{\rm mix}$. In this case the qubit-sensitive signal can be seen on top of the shot noise. Hence, as seen in Fig. 19 (b), the measured value of $I_{\Delta t}$ is either close to $e\Gamma^0$ or to $e\Gamma^1$ (5.19). The corresponding probabilities (the weights of the two peaks) are initially $|a|^2$ and $|b|^2$. They change at longer times, $t > \tau_{\rm mix}$, to a 1/2-1/2-distribution due to the mixing. A typical current pattern is a telegraph signal jumping between $e\Gamma^0$ and $e\Gamma^1$ on a time scale $\tau_{\rm mix}$. (c,d) If the current is averaged over longer times $\Delta t \geq \tau_{\rm mix}$, the meter-induced mixing erases the information about the qubit's state. Several telegraph jumps can occur on this time scale, and for $\Delta t \gg \tau_{\rm mix}$ one measures only the time-averaged current between $e\Gamma^0$ and $e\Gamma^1$, completely insensitive to the initial values. This is shown in Fig. 19 (d), while Fig. 19 (c) displays the crossover between (b) and (d).

Notice, that since $P(I_{\Delta t}, t\!=\!0) = P(m\!=\!I\Delta t, t\!=\!\Delta t)$, the zero-time limits of the surfaces in Figs. 19 (a)–(d) are given by the charge distribution function plotted in Fig. 18.

We point out that in the Hamiltonian dominated regime the current in the SET is sensitive to the occupation probabilities of the *eigenstates* of $\mathcal{H}_{\rm av}$, rather than those in the basis of charge states. This may appear surprising, since the SET couples to the charge operator of the qubit. More precisely, the current is only sensitive to the *expectation value* of the charge in each eigenstate. As a consequence, at the degeneracy point $\eta_{\rm av} = \pi/2$, where the two eigenstates have the same average charge, both eigenstates lead to the same current in the SET and no measurement is possible. The measurement is effective only when charges in the eigenstates differ, $\tan\eta_{\rm av} \ll 1$.

F. Detector-dominated regime

When the back-action dephasing dominates over the average Hamiltonian, $\tau_{\varphi 0}^{-1} \gg \Delta E_{\rm av}$, a perturbative analysis in the charge basis is appropriate. In this basis the perturbation is the Josephson term of the qubit's Hamiltonian $\mathcal{H}_{\rm ctrl}$, i.e., $-(1/2)B_x\sigma_x$. Starting from the zeroth order, $B_x = E_{\rm J} = 0$, we obtain equations similar to Eqs. (5.18, 5.21) with the replacements $\Delta E_{\rm av} \to B_{z,{\rm av}}$ and $E_{\rm int}^{\parallel} \to E_{\rm int}$, where $B_{z,{\rm av}} \equiv B_z - 2\langle N\rangle E_{\rm int}$ is the charging energy of the "average" Hamiltonian. The analysis of the diagonal and the off-diagonal modes is performed similarly. We get for the dephasing rate $\tau_\varphi^{-1} = \tau_{\varphi 0}^{-1}$. For the measurement time we reproduce Eq. (5.24). The dynamics of the two long-living diagonal modes can again be reduced to Eqs. (5.23), (5.26), (5.27) and (5.28) with

$$\tau_{\rm mix}^{-1} \approx E_{\rm J}^2 \tau_{\varphi 0} \ . \tag{5.39}$$

This result is standard for the Zeno regime, i.e., the regime when coherent oscillations are overdamped by dephasing (cf. Eq. 4.18).

The condition for the Zeno regime given above requires a rather strong dephasing, such that $\tau_{\varphi 0}^{-1}$ exceeds both components of the qubit's Hamiltonian (2.3), $\tau_{\varphi 0}^{-1} \gg E_{\rm J}, B_{z,\rm av}$. The second part of this condition can be satisfied by tuning the qubit close to the degeneracy point. In contrast, in the Hamiltonian-dominated regime it is desirable for a good measurement to switch the qubit away from the degeneracy point.

The long-time behavior of the charge and current distributions, $P(m,t)$ and $P(I_{\Delta t},t)$, is again given by Eqs. (5.33, 5.38) but with proper redefinitions of Γ^0, Γ^1, $\tau_{\rm mix}^{-1}$ etc. which now refer to the detector-dominated regime. In particular, the measurement provides information about the initial occupations of the qubit charge states rather than the eigenstates.

To summarize we present the main results for the two regimes in Table I.

TABLE I. Summary of the main results for the Hamiltonian-dominated and detector-dominated regimes.

regime	Hamiltonian dominated (coherent)	fluctuation dominated (Zeno)
leading term	$\mathcal{H}_{\rm av}$	$\delta N(t)\delta\mathcal{H}_{\rm int}$
largest energy	$\Delta E_{\rm av} \gg \tau_{\varphi 0}^{-1}$	$\tau_{\varphi 0}^{-1} \gg \Delta E_{\rm av}$
preferred basis	eigenbasis	charge basis
perturbation	$E_{\rm int} \sin\eta_{\rm av}\, \rho_x$	$E_{\rm J}\, \sigma_x$
τ_φ^{-1}	$\tau_{\varphi 0}^{-1} \cos^2\eta_{\rm av} + \frac{1}{2}\tau_{\rm mix}^{-1}$	$\tau_{\varphi 0}^{-1}$
$\tau_{\rm meas}^{-1}$	$\propto E_{\rm int}^2 \cos^2\eta_{\rm av}$	$\propto E_{\rm int}^2$
$\tau_{\rm mix}^{-1}$	$\dfrac{4\Gamma(E_{\rm int}\sin\eta_{\rm av})^2}{(\Gamma_{\rm L}+\Gamma_{\rm R})^2 + \Delta E_{\rm av}^2}$	$E_{\rm J}^2\, \tau_{\varphi 0}$

G. Flux measurements

To measure the quantum state of a flux qubit (for simplicity we consider here a single junction rf-SQUID), one needs a dissipative device sensitive to the magnetic flux. Natural candidates are dc-SQUIDs, i.e., superconducting loops interrupted by two Josephson junctions. Coupling the qubit and the SQUID inductively, as shown in Fig. 20, one transfers part of the qubit's flux into the loop of the SQUID and, thus, makes the SQUID sensitive to the state of the qubit.

SQUIDs have been used as ultra-sensitive magnetometers for many years, and extensive literature covers the physics of the SQUIDs in much detail (see e.g. Tinkham 1996, Likharev 1996). Here we mention only some of the recent activities and ideas which arose in connection with flux qubits. Two main strategies were proposed. The first one is to use underdamped dc-SQUIDs in the hysteretic regime (Mooij et al. 1999). This regime is realized when the SQUID is unshunted or the shunt resistance is large, $R_{\rm s} \gg (E_{\rm J}/E_{\rm C})\, R_{\rm K}$, where $E_{\rm J}$ and $E_{\rm C}$ are the characteristic Josephson and charging energies of the SQUID. The higher the shunt resistance $R_{\rm s}$, the lower is the noise of the SQUID in the superconducting regime (when no measurement is performed). Therefore, in spite of the permanent presence of the SQUID, the coherent dynamics of the qubit suffers only weak dephasing. To read out the state of the qubit, the current in the SQUID is ramped, and the value of current is recorded where the SQUID switches to the dissipative regime. As this switching current depends on the flux through the SQUID, information about the state of the qubit is obtained. Unfortunately, the current switching is a random process, fluctuating even when the external flux in the SQUID is fixed. For currently available system parameters this spread is larger than the difference in switching currents corresponding to the two states of the qubit. Therefore only statistical (weak repeated) measurements are possible in this regime.

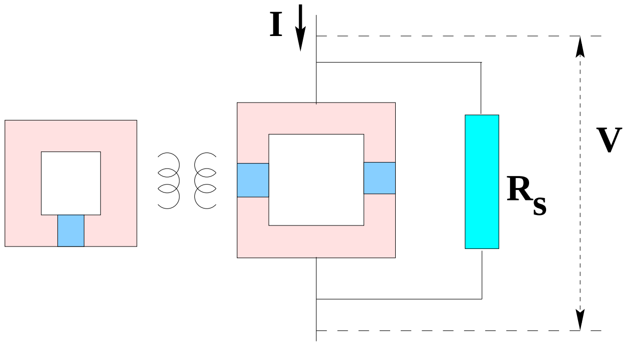

FIG. 20. Measurement setup for a flux qubit. The qubit (the rf-SQUID on the left side) is inductively coupled to the meter (the shunted dc-SQUID on the right side).

The second strategy is to use overdamped SQUIDs, with $R_s < (E_J/E_C)\, R_K$. When the bias current exceeds the critical value, the voltage which develops across the shunt resistor depends on the external flux in the SQUID. Thus by measuring this voltage one learns about the state of the qubit. In this regime the principle of the measurement is identical to the one presented above for the SET. Recently Averin (2000*b*) analyzed continuous (stationary) measurements in this regime and obtained the input and output noise characteristics (cf. Section V.H) which determine the relevant time scales τ_φ, $\tau_{\rm meas}$, $\tau_{\rm mix}$. The main disadvantage of this strategy is that the SQUID induces dephasing during the periods of coherent manipulations when no measurement is performed. The question still remains to be settled whether a reasonable compromise between the underdamped and the overdamped limits can be found.

H. Efficiency of the measuring device

Recently, several devices performing quantum measurements have been analyzed. Apart from SETs in the sequential tunneling regime (Shnirman & Schön 1998, Makhlin et al. 2000*d*, Korotkov 2000*b*, Devoret & Schoelkopf 2000) it includes SETs in the co-tunneling regime (Averin 2000*a*, Maassen van den Brink 2000), superconducting SETs (SSETs) and dc-SQUIDS (Averin 2000*b*), as well as quantum point contacts (QPC) (Korotkov & Averin 2000). All these devices are based on the same basic idea: they are dissipative systems whose response (conductance, resistance) depends on the state of a qubit coupled to them.

The efficiency of a quantum detector has several aspects. From a practical point of view the most important is the ability to perform a strong, single-shot measurement which requires that the mixing is slower than the read-out, $\tau_{\rm mix} \gg \tau_{\rm meas}$. Another desired property is a low back-action noise of the meter in the off-state, which can be characterized by a corresponding dephasing rate.

A further important figure of merit is the ratio of the dephasing and measurement times. Quantum mechanics demands that a quantum measurement should completely dephase a quantum state, i.e. $\tau_\varphi \leq \tau_{\rm meas}$. For the example of a SET coupled to a charge qubit the dephasing time (5.22) is smaller (or even much smaller) than the measurement time (5.24). This means that the information becomes available later than it would be possible in principle. In this sense the efficiency of the SET in the sequential tunneling regime is less then 100% (Shnirman & Schön 1998, Korotkov 1999). The reason for the delay is an entanglement of the qubit with microscopic degrees of freedom in the SET. To illustrate this point consider a situation where the initial state of the system $(a|0\rangle + b|1\rangle)\,|\chi\rangle\,|m=0\rangle$ evolves into $a|0\rangle\,|\chi_0\rangle\,|m_0\rangle + b|1\rangle\,|\chi_1\rangle\,|m_1\rangle$, where $|\chi\rangle$ stands for the quantum state of the uncontrolled environment. One can imagine a situation when $m_0 = m_1$, but $|\chi_0\rangle$ and $|\chi_1\rangle$ are orthogonal. Then the dephasing has occurred but no measurement has been performed. It is interesting to note that the ratio $\tau_\varphi/\tau_{\rm meas}$ grows if the SET is biased in an asymmetric way, creating a strong asymmetry in the tunneling rates, e.g. $\Gamma_{\rm L} \ll \Gamma_{\rm R}$. In other measurement devices the ratio $\tau_\varphi/\tau_{\rm meas}$ may be close to 1. This includes quantum point contacts (Korotkov 1999, Korotkov & Averin 2000) as well as SETs in the co-tunneling regime (Averin 2000*a*, Maassen van den Brink 2000). The common feature of these three examples is that the device consists of one junction or effectively reduces to it. It should be kept in mind, however, that a large ratio of dephasing and measurement times is not the only figure of merit. For instance, in a SET in the co-tunneling regime the current is low and more difficult to detect as compared to a SET in the sequential tunneling regime.

The ratio of dephasing and measurement times $\tau_\varphi/\tau_{\rm meas}$ has been analyzed also in the framework of the theory of linear amplifiers (Averin 2000*b*, Devoret & Schoelkopf 2000). It can be expressed in terms of the noise characteristics of the amplifier which, in turn, determine the sensitivity of the device. In this framework, one considers a detector with the output signal I and input signal ϕ, which is coupled to an observable Q of the detector via a term ϕQ. The input signal causes a variation of the output, which can be characterized by the linear response coefficient $\lambda \equiv d\langle I\rangle/d\phi$. Note that usually one operates in a dissipative, nonequilibrium regime. When used as a quantum detector coupled to a qubit the input variable is $\phi \propto \sigma_z$, and the coupling is $c\sigma_z Q$ (with c being a coupling constant). We first consider a situation where tunneling between the qubit's basis states is suppressed, i.e., $\mathcal{H}_{\rm ctrl} = -B_z\sigma_z/2$. In this case the fluctuations of Q dephase the qubit with rate

$$\tau_\varphi^{-1} = \frac{c^2}{\hbar^2} S_Q \; . \tag{5.40}$$

The symbols S_Q and S_I (introduced below) stand for the noise power of the corresponding observable if the amplifier is decoupled from the qubit: $S_Q = 2\,\langle Q_\omega^2\rangle$ and $S_I = 2\,\langle I_\omega^2\rangle$. A white spectrum is assumed at the relevant frequencies. The two basis states of the qubit produce output signals $I^{0/1} = \bar{I} \pm \Delta I/2$, differing by

$$\Delta I = 2c\lambda \; . \tag{5.41}$$

They can be distinguished after the measurement time

$$\tau_{\rm meas}^{-1} = \frac{(\Delta I)^2}{4S_I} \; . \tag{5.42}$$

Hence, the two times are related by

$$\frac{\tau_{\rm meas}}{\tau_\varphi} = \frac{S_Q S_I}{\hbar^2\lambda^2} = \frac{S_Q S_\phi}{\hbar^2} \ . \tag{5.43}$$

In the last form of Eq. (5.43) $S_\phi \equiv S_I/\lambda^2$ is the output noise in terms of the input, i.e., the noise which should be applied to the input to produce the noise S_I at the output.

If the tunneling is turned on, $\mathcal{H}_{\rm ctrl} = -\frac{1}{2}\Delta E(\cos\eta\,\sigma_x + \sin\eta\,\sigma_z)$, both the measurement rate (5.42) and the rate of pure dephasing (5.40) acquire an additional factor $\cos^2\eta$, while their ratio (5.43) persists. Apart from that, the finite tunneling introduces mixing, with rate

$$\tau_{\rm mix}^{-1} = \frac{c^2}{\hbar^2} S_Q \sin^2\eta \ . \tag{5.44}$$

For the particular case of the SET, which motivates the notations, I is the transport current, $Q = eN$ the charge of its central island, and ϕ the gate potential externally applied to the middle island of the SET (ϕ consists of V_N and a contribution of the qubit, see Eq. C4). The coupling constant is $c = E_{\rm int}/e$ and the linear response is given by $\lambda = \Delta I/(2c) = e^2\delta\Gamma/(2E_{\rm int})$ with $\delta\Gamma$ defined by Eq. (5.35). In this case, Eqs. (5.40, 5.42) are consistent with what has been described before in Eqs. (5.22, 5.25).

The quantity $\sqrt{S_Q S_\phi}$ is proportional to the "noise energy", discussed by Devoret & Schoelkopf (2000), measured in units of the energy quanta at the given frequency. For the noise spectra S_Q and S_ϕ one can obtain an inequality, similar to the Heisenberg uncertainty principle (Braginsky & Khalili 1992): $S_Q S_\phi \geq \hbar^2$. Indeed, by virtue of Eq. (5.43) this relation coincides with the constraint

$$\tau_\varphi \leq \tau_{\rm meas} \ . \tag{5.45}$$

Moreover, one can show (Braginsky & Khalili 1992, Averin 2000*b*) that a stronger inequality holds. Namely, the quantity [15]

$$\epsilon \equiv \frac{1}{2}\left(S_Q S_\phi - {\rm Re}^2 S_{\phi Q}\right)^{1/2} \ , \tag{5.46}$$

is limited by $\epsilon \geq \hbar/2$. Here $S_{\phi Q} \equiv S_{IQ}/\lambda$, where $S_{IQ} \equiv 2\int dt' \langle I(t) Q(t')\rangle$ characterizes cross-correlations between the input and the output. Thus one has

$$\frac{\tau_{\rm meas}}{\tau_\varphi} = \left(\frac{\epsilon}{\hbar/2}\right)^2 + \frac{({\rm Re}\,S_{\phi Q})^2}{\hbar^2} \ . \tag{5.47}$$

The optimization of this ratio requires that the detector reaches the quantum limit of sensitivity, $\epsilon = \hbar/2$, and the cross-correlations vanish, ${\rm Re}\,S_{\phi Q} = 0$. Averin (2000*b*) made the observation that the quantum limit is (nearly) reached in several measurement devices: For a quantum point contact, an overdamped dc-SQUID, a resistively shunted superconducting SET, or a normal SET in the co-tunneling regime (Averin 2000*a*) the following two relations hold under certain conditions:

$$S_I S_Q \approx |S_{IQ}|^2 \tag{5.48}$$

and

$$\lambda \approx {\rm Im}\, S_{IQ} \ . \tag{5.49}$$

They immediately imply that $\epsilon = \hbar/2$. Note, that the relations (5.48,5.49) are requirements for a quantum limited measurement device. They are not valid in general. E.g., the near equality in (5.48) should in general be replaced by the $\geq$ sign. Even for the detectors where they were found they break down (making $\epsilon > \hbar/2$), e.g., at finite temperatures or at bias voltages close to the Coulomb blockade threshold (Averin 2000*a*).

As for Eq. (5.49), by definition the response coefficient is $\lambda = -i\int dt'\theta(t-t')\langle[I(t), Q(t')]\rangle = 2{\rm Im}\int dt'\theta(t-t')\langle I(t)Q(t')\rangle$. Hence, Eq. (5.49) implies a vanishing reciprocal response coefficient $\lambda' = 2{\rm Im}\int dt'\theta(t-t')\langle Q(t)I(t')\rangle$. While in equilibrium Onsager's relations imply $\lambda = -\lambda'$, such an asymmetry can arise in a nonequilibrium stationary state. It is a characteristic feature of linear measuring devices (Braginsky & Khalili 1992).

As for the cross-correlations, ${\rm Re}\,S_{\phi Q}$, they vanish, e.g., in a dc-SQUID with two identical Josephson junctions, a QPC, symmetrically coupled to a quantum dot, or a SSET (Averin 2000*b*).

I. Statistics of the current and the noise spectrum

In previous subsections we have discussed the statistics of the charge m, which passed through the detector, and the corresponding current I after a measurement has been started. In this subsection we complement this discussion by investigating the noise properties of the charge and the current in the stationary regime, i.e., a long time after the qubit-detector coupling was turned on. The noise spectrum reflects the intrinsic properties of the system of qubit and meter and their coupling and depends on the corresponding time scales. We obtain additional evidence for the telegraph behavior of the current.

We study first the charge-charge correlator, which is derived from the joint probability distribution of charges at different times (5.37), and obtain

$$\langle m(t_1)\, m(t_2)\rangle = -{\rm Tr}'\hat\rho_0 \partial_k \left[U(k,\Delta t)\,\partial_k U\left(k, \bar t - \frac{\Delta t}{2}\right)\right]_{k=0} \ , \tag{5.50}$$

[15] This quantity is denoted as "energy sensitivity" by Averin (2000*b*), but Devoret & Schoelkopf (2000) use this term for a different quantity.

where $\Delta t \equiv |t_1 - t_2|$ and $\bar{t} \equiv (t_1+t_2)/2$. We employ again the two-mode approximation and use Eqs. (5.28,5.31) to arrive, after taking time derivatives, at

$$\langle I(t_1)\, I(t_2)\rangle = e^2\bar{\Gamma}^2 + e^2\, f\, \bar{\Gamma}\delta(\Delta t) + e^2\, \frac{\delta\Gamma^2}{4} e^{-\Delta t/\tau_{\rm mix}} + (\ldots)\, e^{-\bar{t}/\tau_{\rm mix}} \; . \tag{5.51}$$

Here $\Gamma^{0/1} \equiv \bar{\Gamma} \pm \delta\Gamma/2$ are the tunneling rates (5.35) for the two qubit states. The Fano factor f is defined after Eq. (5.34). In the stationary limit, $\bar{t} \gg \tau_{\rm mix}$, we thus obtain for the noise spectrum

$$S_I(\omega) = 2e^2 f\bar{\Gamma} + \frac{e^2\delta\Gamma^2\tau_{\rm mix}}{1+\omega^2\tau_{\rm mix}^2} \; . \tag{5.52}$$

The first, ω-independent term corresponds to the shot noise, while the second term originates from the telegraph noise. The ratio of the telegraph and shot noise amplitudes at $\omega = 0$ is

$$\frac{S_{\rm telegraph}}{S_{\rm shot}} = \frac{\delta\Gamma^2\tau_{\rm mix}}{2f\bar{\Gamma}} \approx 4\frac{\tau_{\rm mix}}{\tau_{\rm meas}} \; . \tag{5.53}$$

Note that the telegraph noise becomes noticeable on top of the shot noise in the parameter regime of an effective quantum measurement ($\tau_{\rm mix} \gg \tau_{\rm meas}$).

While the shot-noise contribution reflects intrinsic properties of the detector (SET), the telegraph noise characterizes the qubit. This structure of the noise of the output signal is quite general (Korotkov & Averin 2000, Averin 2000*b*, Korotkov 2000*a*). For the qubit coupled to the meter, the following relation for the noise of the output signal I was derived (using linear response and certain other approximations):

$$S_I(\omega) = S_I^0(\omega) + c^2\lambda^2 S_{\sigma_z}(\omega) \; , \tag{5.54}$$

Here the notations introduced in Section V.H are used, with the only difference that S_I now denotes the noise in the *presence* of the qubit. The first term, S_I^0, in the RHS of Eq. (5.54) represents the noise of the meter decoupled from the qubit ($S_{\rm shot}$ for a SET). The second term arises from the qubit and is governed by the dynamics of the its density matrix. In the preferred basis (cf. Section V.D–V.F) the diagonal elements decay to their stationary values on the mixing time scale, while the off-diagonal elements precess with frequency $\Delta E/\hbar$ and decay within the dephasing time. Depending on the qubit's Hamiltonian, both or one of these processes contribute to the dynamics of $\sigma_z(t)$. Hence, the qubit's contribution, $S_{\sigma_z}(\omega) \equiv 2\int dt \langle\sigma_z(0)\sigma_z(t)\rangle \exp(-i\omega t)$, has a "coherent" peak at the qubit's eigenfrequency, $\Delta E/\hbar$, of width τ_φ^{-1}, and a "telegraph" peak at zero frequency with width $\tau_{\rm mix}^{-1}$.

To derive the noise spectrum of the qubit under the influence of the detector, one can use a Bloch-type master equation for the joint density matrix [e.g., Eq.(5.9) at $k = 0$ for a SET]. Under certain conditions, namely, if the noise spectrum $S_Q(\omega)$ is white in an interval of frequencies at least up to the qubit's level spacing ΔE (in the SET it is white only up to $\Gamma_{\rm R} + \Gamma_{\rm L}$) a simpler set of equations is sufficient (Averin 2000*b*):

$$\begin{aligned} \dot{\rho}_{00} &= B_x \,{\rm Im}\, \rho_{01} \; , \\ \dot{\rho}_{01} &= (iB_z - \tau_{\varphi 0}^{-1})\rho_{01} - \tfrac{i}{2}B_x(\rho_{00} - \rho_{11}) \; . \end{aligned} \tag{5.55}$$

Here ρ_{ij} is the qubit's density matrix in the eigenbasis of σ_z, $\tau_{\varphi 0}^{-1} \equiv c^2 S_Q/\hbar^2$ describes the back-action (5.40), and B_x and B_z form the Hamiltonian of the qubit (2.3). These equations were used, for instance, for the analysis of a quantum point contact coupled to a double quantum dot (Gurvitz 1997, Korotkov & Averin 2000).

At zero bias, $B_z = 0$, one can solve Eq. (5.55) exactly, to obtain (Korotkov & Averin 2000)

$$S_{\sigma_z} = \frac{4B_x^2\tau_{\varphi 0}}{(\omega^2 - B_x^2)^2\tau_{\varphi 0}^2 + \omega^2} \; . \tag{5.56}$$

In the Hamiltonian-dominated limit, $\tau_{\varphi 0}^{-1} \ll B_x$, at this bias point no telegraph peak appears. Still, the qubit contributes to the noise via the last term in Eq. (5.54). This coherent peak at B_x has the height

$$c^2\lambda^2 S_{\sigma_z}^{\rm max} = 4c^2\lambda^2\tau_{\varphi 0} = (\Delta I)^2\tau_{\varphi 0} \; . \tag{5.57}$$

Here ΔI is the difference in the output current (5.41) for the two eigenstates of σ_z (charge states). Recalling that it is related to the measurement rate (5.42) in the detector-dominated regime, one concludes that the signal-to-noise ratio in Eq. (5.54) is limited, by virtue of Eq. (5.45), as

$$\frac{c^2\lambda^2 S_{\sigma_z}^{\rm max}}{S_I^0} = 4\,\frac{\tau_{\varphi 0}}{\tau_{\rm meas}} \le 4 \; . \tag{5.58}$$

Thus, the requirements for the observation of coherent oscillations in the noise spectrum of the measuring device is directly expressed by the ratio of dephasing and measurement time.

In the opposite, detector-dominated regime $B_x \ll \tau_{\varphi 0}^{-1}$, the noise spectrum (5.56) exhibits a telegraph-noise Lorentzian (5.52) at low frequencies, $4\tau_{\rm mix}/(\omega^2\tau_{\rm mix}^2 + 1)$, where $\tau_{\rm mix}^{-1} = B_x^2\tau_{\varphi 0}$.

At a general bias point $B_z \ne 0$ in the Hamiltonian-dominated regime the dynamics of σ_z exhibits features at both frequencies, $\omega = 0$ and $\omega = \Delta E$, and its noise spectrum has two peaks. This was shown numerically by Korotkov & Averin (2000) and it is consistent with the result (5.52). A higher-order analysis of the master equation (5.9), which accounts for the corrections to the oscillating modes (5.21) due to the mixing, allows us to obtain the coherent peak which is, however, suppressed due to the strong dephasing (cf. Eq. 5.58).

J. Conditional master equation

We finally would like to comment on recent studies (Korotkov 1999, Korotkov 2000*a*, Goan et al. 2000) where the so-called selective or conditional approach, popular in quantum optics, was employed. Its purpose is to develop a framework for the analysis of statistical properties of qubit-related quantities *conditioned* on the dynamics of the output signal, $I(t)$, at earlier times. In other words, the goal is to predict the outcome of a measurement of the qubit's state at time t given the results of the current read-out at $t' < t$. A related problem is to produce typical, fluctuating current-time patterns $I(t)$ which one can encounter in a given experiment.

These problems can be addressed using the proper master equation for the coupled system (e.g., Eq. 5.9). Monitoring the current amounts to repeated measurements of the charge m, at sufficiently short time-intervals Δt. Since a closed master equation can be formulated which involves only the m-diagonal entries of the density matrix $\hat\rho(m)$, the effect of a measurement with the result m_0 amounts to choosing the corresponding $\hat\rho(m_0)\delta_{mm_0}$ as the new density matrix (properly rescaled to ensure the normalization). Thus a simulation of the evolution proceeds as follows: From the the master equation with initial matrix $\hat\rho\delta_{m0}$ at $t=0$ one obtains $\rho(\Delta m, \Delta t)$ at the time of the first read-out. Then, to simulate an experiment, one selects a "measured" value of Δm with the corresponding probability $P(\Delta m, \Delta t) = \mathrm{tr}\,\hat\rho(\Delta m, \Delta t)$ (cf. Section V.E) and uses the corresponding density matrix as initial value for the further evolution during the next time interval. Repeating this step many times one produces a typical dependence of $m(t)$ and a density matrix $\hat\rho_{\mathrm{cond}}(t)$ which can be used to study the conditional statistics of further measurements.

This procedure can be simplified if sufficiently frequent read-outs are performed. An expansion in Δt allows one to present the step-by-step evolution of the density matrix $\hat\rho_{\mathrm{cond}}$ as a continuous process (cf. Korotkov 2000*b*):

$$\frac{d}{dt}\hat\rho = -i[\mathcal{H}_{\mathrm{ctrl}}, \hat\rho] - \frac{1}{4}\gamma_\varphi^0[\sigma_z, [\sigma_z, \hat\rho]] + \frac{\Delta I}{2S_I^0}[I(t) - \bar I]\,[\{\sigma_z, \hat\rho\} - 2\,\mathrm{tr}(\sigma_z\hat\rho)\hat\rho] \ , \qquad (5.59)$$

where ΔI is defined in Eq. (5.41). The measured value of the output signal, $I(t) = \Delta m/\Delta t$, as described above, should be chosen randomly with the distribution $P(\Delta m, \Delta t)$. Using the properties of $P(m, \Delta t)$ at short Δt, one can further simplify this procedure and choose $I(t)$ as

$$I(t) = \bar I + \frac{\Delta I}{2}\,\mathrm{tr}(\sigma_z\hat\rho) + \delta I(t) \ , \qquad (5.60)$$

where $\delta I(t)$ is a random quantity with the noise properties identical to those of the current in the detector decoupled from the qubit.

We can mention that, similar to Eq. (5.55), in the derivation of Eq. (5.59) we assumed the back-action noise of the detector to be white. Furthermore, γ_φ^0 is the dephasing rate due to the environment and accounts for non-ideality of the detector (see Section V.H). After averaging over the detector dynamics, $I(t)$, Eq. (5.55) is recovered. Note that $\tau_{\varphi 0}^{-1} > \gamma_\varphi^0$ since the random signal (5.60) produces additional dephasing.

The equations (5.59, 5.60) form a Langevin-type evolution equation which can be used to produce typical outcomes of the measurement and to study statistics of the qubit conditioned on these outcomes.

VI. CONCLUSIONS

Josephson junction systems in a suitable parameter range can be manipulated in a quantum coherent fashion. They are promising physical realizations (the hardware) of future devices to be used for quantum state engineering. We discussed their modes of operation in different designs (in the charge and the flux dominated regimes), the constraints on the parameters, various dephasing effects, and also the physical realization of the quantum mechanical measurement process. We pointed out the advantages of these nano-electronic devices as compared to other physical realizations.

We add a few remarks and comparisons. First, in order to demonstrate that the constraints on the circuit parameters, which were derived in previous sections, can be met by available technologies, we summarize them here and suggest a suitable set.
(i) Necessary conditions for a Josephson charge qubit are: $\Delta > E_{\mathrm{C}} \gg E_{\mathrm{J}}\,,\, k_{\mathrm{B}}T$. The superconducting energy gap Δ has to be chosen large to suppress quasiparticle tunneling. The temperature has to be low to assure the initial thermalization, $k_{\mathrm{B}}T \ll E_{\mathrm{C}}, \hbar\omega_{LC}$, and to reduce dephasing effects. A sufficient choice is $k_{\mathrm{B}}T \sim E_{\mathrm{J}}/2$, since further cooling does not reduce the dephasing (relaxation) rate in a qualitative way. (Of course, it does so far from the degeneracy point, i.e., for $\eta = 0$, or if we switch off the Hamiltonian, $\mathcal{H}_{\mathrm{ctrl}} = 0$. However during manipulations E_{J} is the typical energy difference and sets the time scale for both the manipulation times and the dephasing.)

As an explicit example we suggest the following parameters (the circuit parameters of Nakamura et al. (1999) are in this regime) and estimate the corresponding time scales: We choose junctions with capacitance $C_{\mathrm{J}} = 10^{-15}$ F, corresponding to a charging energy (in temperature units) $E_{\mathrm{C}} \sim 1$ K, and a smaller gate capacitance $C_{\mathrm{g}} = 0.5 \cdot 10^{-17}$ F to reduce the coupling to the environment. Thus at the working temperature of $T = 50$ mK the initial thermalization is assured. The superconducting gap has to be slightly higher, $\Delta > E_{\mathrm{C}}$.

Thus aluminum is a suitable material. We further choose $E_J = 100$ mK, i.e., the time scale of one-qubit operations is $\tau_{\rm op}^{(1)} = \hbar/E_J \sim 10^{-10}$ s.
(ii) A realistic value of the resistor in the gate voltages circuit is $R \sim 50\ \Omega$. Its voltage fluctuations limit the dephasing time (4.12) to values of order $\tau_\varphi \sim 10^{-4}$ s, thus allowing for $\tau_\varphi/\tau_{\rm op}^{(1)} \sim 10^6$ coherent manipulations of a single qubit [16].
(iii) To assure sufficiently fast 2-bit operations we choose for the design of Fig. 3 $L \sim 10$ nH and $C_{\rm L} \approx C_{\rm J}$. Then the 2-bit operations are about 10^2 times slower than the 1-bit operations and, accordingly, their maximum number is reduced.
(iv) The quantum measurement process introduces additional constraints on the parameters, which can be met in realistic devices as demonstrated by the following concise example. The parameters of the qubit are those mentioned before. For the junction and gate capacitances of the normal tunnel junctions of the SET we chose $C_{\rm T} = 1.5\cdot 10^{-17}$ F and $C_{\rm g}^{\rm SET} = 0.5\cdot 10^{-17}$ F, respectively, and for the coupling capacitance between SET and qubit: $C_{\rm int} = 0.5\cdot 10^{-17}$ F. We thus obtain: $E_{\rm C,SET} \approx 25$ K, $E_{\rm C,qb} \approx 1$ K, $E_{\rm int} \approx 0.25$ K (for precise definitions see Appendix C). We further take $n_{\rm g,qb} = 0.25$, $N_{\rm g,SET} = 0.2$ and $\mu_{\rm L} = -\mu_{\rm R} = eV_{\rm tr}/2 = 24$ K and $\alpha_{\rm L} = \alpha_{\rm R} = 0.03$. This gives $B_z \approx 2$ K and $\Gamma_{\rm L} = 1.8$ K and $\Gamma_{\rm R} = 7.8$ K (note that due to the gate voltage the applied transport voltage is split asymmetrically). Thus the measurement time in this regime is $\tau_{\rm meas} \approx 1.5\cdot 10^{-8}$ s. Since for this choice of parameters $\tau_{\varphi 0}^{-1} \approx 4.0\cdot 10^{-3}$ K $\ll B_z \approx \Delta E_{\rm av}$, the "Hamiltonian dominated" regime is realized. Assuming $E_J = 0.1$ K we obtain $\tau_{\rm mix} \approx 0.7\cdot 10^{-6}$ s. Thus $\tau_{\rm mix}/\tau_{\rm meas} \approx 45$ and the separation of peaks should be observable early enough before the mixing dominates. Indeed, the numerical simulation of the system (5.9) for these parameters shows almost ideal separation of peaks (see Fig. 15). On the other hand, for $E_J = 0.25$ K we obtain $\tau_{\rm mix}/\tau_{\rm meas} \approx 7$. This is a marginal situation. The numerical simulation in this case (see Fig. 17) shows that the peaks first start to separate, but, soon, the valley between the peaks fills in due to the mixing transitions.

The requirements on the parameters of a flux qubit circuit can be summarized in a similar way. First, the parameters should be chosen to allow the reduction of the double-well potential to the two ground states forming a two-state quantum system. It is also desirable that these two basis states have macroscopically different flux or phase configurations. The double well is formed by joining either several Josephson junctions (Mooij et al. 1999) or a Josephson junction and an inductive term of similar strength ($E_J \sim \Phi_0^2/4\pi^2 L$) in an rf-SQUID (Friedman et al. 2000)). Since the level spacing within each well is of order $E_0 \sim \sqrt{E_J E_C}$ and the barrier height of order E_J, all these requirements can be satisfied by 'classical' Josephson junctions with $E_J \gg E_C$. Furthermore, the asymmetry of the double well B_z, which is controlled by external fluxes, and the tunnel splitting B_x should be smaller than E_0 in order to suppress leakage to higher states. Finally, the temperature should be low enough to allow the initialization of the qubit's state and to ensure slow dephasing. In summary, the following conditions have to be satisfied: $k_B T \le B_x \ll \sqrt{E_J E_C} \ll E_J$. As pointed out above, it is sufficient to choose $k_B T \sim B_x/2$. These requirements can be satisfied, e.g., by the parameters of the rf-SQUID used by Friedman et al. (2000) ($E_J \approx 70$ K, $E_C \approx 1$ K, $B_x \approx 0.1$ K, and $T \approx 40$ mK) or by similar values discussed by Mooij et al. (1999) ($E_J \sim 10$ K, $E_C \sim 0.1$ K, $B_x \sim 50$ mK, and $T \sim 30$ mK).

At present, the most advanced quantum manipulations of a solid state system, i.e., the coherent oscillations observed by Nakamura et al. (1999), have been demonstrated for a Josephson charge qubit. But flux systems might soon catch up. In the long run, it is not clear whether charge or flux systems will bring faster progress and further reaching demonstrations of complex quantum physics. In fact, a combination of both appears feasible as well. Therefore we compare shortly the properties of the simplest charge and flux qubits.

A very important quantity is the phase coherence time τ_φ, which has to be compared to the typical operation time scale of the qubit's dynamics $\tau_{\rm op}$. While effects of various dissipative mechanisms have been estimated theoretically, further experimental work is needed to understand dephasing in charge and flux qubits. One potentially dangerous source of dephasing, the coupling to the external circuit, can be described by an Ohmic oscillator bath. If this contribution to the dephasing dominates, the above-mentioned ratio of times is determined by the dimensionless parameter $\tau_{\rm op}/\tau_\varphi \sim \alpha$ (see Section IV). For "unscreened" charge qubits it is of order of $\alpha \approx 10^{-2}$, but it can be substantially reduced by the 'screening ratio' of capacitances (see Section IV). Putting in numbers corresponding to those of Nakamura et al.'s (2000) experiment (without probe junctions), we estimate τ_φ to reach several tens of microseconds. Coherent oscillations for about 5 ns have been observed already in this system, in spite of the presence of a non-ideal detector limiting the phase coherent evolution by quasiparticle tunneling

[16] This may be overly optimistic, and indicating that other sources of dephasing need to be considered as well. For instance, at these slow time scales the background charge fluctuations may dominate. We also note that in the experiment of Nakamura et al. (1999) a stray capacitance in the probe circuit, larger than $C_{\rm g}$, renders the dephasing time shorter.

in the probe junction and also providing a strong coupling to the external circuit. The phase coherence time should be compared to the qubit operation time scale of $\tau_{\rm op} \approx 10$ to 100 ps.

For flux qubits considered by Mooij et al. (1999) the current circuit may produce $\alpha \sim 10^{-5}$ and the relaxation times of order 10 μs, while other dephasing mechanisms studied would destroy coherence after times of order of hundreds of microseconds or longer. At the same time, the qubit level spacing sets the fastest operation time to $\tau_{\rm op} \approx 0.1$ to 1 ns.

A major source of errors and dephasing for all charge-degrees of freedom are the fluctuations of the 'offset charges'. They arise due to charge transfers in the substrate, e.g., between impurity sites, and are detrimental for many of the potential applications of single-charge systems. Fortunately, they occur typically on long time scales, and may not take place during a 'computation', i.e., a series of coherent manipulations. Similarly for flux qubits nuclear spins provide random magnetic fields. Also these fields change only on a long spin-relaxation time scale and cause no dephasing in shorter 'computations'.

Another important point is the efficiency of quantum detectors used to read out the charge or flux state. Estimates show that the newly developed rf-SETs (Schoelkopf et al. 1998) should make single-shot charge measurements possible in principle ($\tau_{\rm mix} \gg \tau_{\rm meas}$). On the other hand, the flux read-out with a SQUID is far from this goal and averaging over a large number of measurements is needed (van der Wal et al. 2000).

As for the experimental achievements, in both charge and flux systems the validity of the two-state model has been confirmed spectroscopically (Nakamura et al. 1997, Friedman et al. 2000, van der Wal et al. 2000). The direct observation of superpositions of basis (charge or flux) states (Bouchiat 1997, Bouchiat et al. 1998) and of the coherent oscillations between the basis states (Nakamura et al. 1999) so far was successful only in the charge design.

To conclude, the fabrication and controlled coherent manipulations of Josephson junction qubits are possible using present-day technologies. In these systems fundamental properties of macroscopic quantum-mechanical systems can be explored. First experiments on elementary systems have been performed successfully. More elaborate designs as well as further progress of nanotechnology will provide longer coherence times and allow sequences of coherent manipulations as well as scaling to larger numbers of qubits. The application of Josephson junction systems as elements of a quantum computer, i.e., with a very large number of manipulations and large number of qubits, will remain a challenging issue. On the other hand, many aspects of quantum information processing can initially be tested on simple circuits as proposed here. We also expect further spin-offs, once the techniques of quantum state engineering get further developed.

We have further shown that a dissipative quantum system coupled to a qubit may serve as a quantum measuring device in an accessible range of parameters. Explicitly we studied a single-electron transistor coupled capacitively to a charge qubit. We have described the process of measurement by deriving the time evolution of the reduced density matrix of the coupled system. We found that the dephasing time is shorter than the measurement time, and we have estimated the mixing time, i. e., the time scale on which the transitions induced by the measurement occur. Similar scenarios are discussed for flux qubits measured by a SQUID coupled to it inductively.

ACKNOWLEDGMENTS

We thank T. Beth, C. Bruder, R. Fazio, Z. Hermon, J. König, A. Korotkov, Y. Levinson, J.E. Mooij, Y. Nakamura, H. Schoeller, and F. Wilhelm for stimulating discussions. This work has been supported by the 'Schwerpunktprogramm Quanten-Informationsverarbeitung' and the SFB 195 of the German Science Foundation (DFG).

APPENDIX A: AN IDEAL MODEL

The model Hamiltonian

Quantum state engineering requires coherent manipulations of suitable quantum systems. The needed quantum manipulations can be performed if we have sufficient control over the fields and interaction terms in the Hamiltonian. As an introduction and in order to clarify the goal, we present here an ideal model Hamiltonian and show how the necessary unitary transformations can be performed. We can add that the Josephson junctions devices discussed in this review come rather close to this ideal model.

As has been stressed by DiVincenzo (1997, 2000) any physical system which is considered as a candidate for quantum computation, and similar for alternative applications of quantum state engineering, should satisfy the following criteria: (i) First of all, one needs well-defined two-state quantum systems (or quantum systems with a small number of states). This implies that higher states, present in most real systems, must not be excited during manipulations. (ii) One should be able to prepare the initial state of the qubits with sufficient accuracy. (iii) A long phase coherence time is needed, sufficient to allow for a large number (e.g., $\geq 10^4$) of coherent manipulations. (iv) Sufficient control over the qubit's Hamiltonian is required to perform the necessary unitary transformations, i.e., single-qubit and two-qubit logic operations (gates). For this purpose one should be able to control the fields at the sites of each qubit separately, and to couple qubits together in a controlled way, ideally with the possibility to switch the inter-qubit interactions on and off. In physics terms the two types of operations allow creating arbitrary superpositions and non-trivial coupled states, such as entangled states, respectively. (v) Finally, a quantum measurement is needed to read out the quantum information, either at the final stage or during the computation, e.g., for the purposes of error-correction.

We consider two-state quantum systems (e.g./ spins), or systems which under certain condition effectively reduce to two-state systems (charge in a box or flux in a SQUID near degeneracy points). Any single two-state quantum system can be represented as a spin-1/2 particle, and its Hamiltonian be written as $\mathcal{H}(t) = -\frac{1}{2}\boldsymbol{B}(t)\hat{\boldsymbol{\sigma}}$. Here $\sigma_{x,y,z}$ are Pauli matrices in the space of states $|\uparrow\rangle = \binom{1}{0}$ and $|\downarrow\rangle = \binom{0}{1}$, which form the basis states of a physical quantity (spin, charge, flux, ...) which is to be manipulated. The "spin" is coupled to an effective "magnetic field" $\boldsymbol{B}$. In an alternative notation used for two-state quantum systems the components B_z and $B_{x,y}$ correspond to an external bias and a tunneling amplitude, respectively. Full control of the quantum dynamics of the spin is possible if the magnetic field $\boldsymbol{B}(t)$ can be switched arbitrarily. In fact, arbitrary single-qubit operations can be performed already if two of the field components can be controlled, e.g.,

$$\mathcal{H}_{\rm ctrl}(t) = -\frac{1}{2}B_z(t)\hat{\sigma}_z - \frac{1}{2}B_x(t)\hat{\sigma}_x \ . \tag{A1}$$

If all three components of the magnetic field can be controlled the topological (Berry) phase of the system can be manipulated as well (Falci et al. 2000).

In order to manipulate a many-qubit system, e.g., to perform quantum computing, the magnetic field at the site of each spin has to be controlled separately. In addition, one needs two-qubit (unitary) operations which requires controlling the coupling energies between the qubits. For instance, a system with the following model Hamiltonian would be suitable:

$$\mathcal{H}_{\rm ctrl}(t) = -\frac{1}{2}\sum_{i=1}^{N}\boldsymbol{B}^i(t)\hat{\boldsymbol{\sigma}}^i + \sum_{i\neq j} J^{ij}_{ab}(t)\hat{\sigma}^i_a\hat{\sigma}^j_b \ , \tag{A2}$$

where a summation over spin indices $a, b = x, y, z$ is implied. In (A2) a general form of coupling is presented, but simpler forms, such as pure Ising zz-coupling, XY-, or Heisenberg coupling are sufficient.

The measurement device, when turned on, and residual interactions with the environment are accounted for by extra terms $\mathcal{H}_{\rm meas}(t)$ and $\mathcal{H}_{\rm res}$, respectively:

$$\mathcal{H} = \mathcal{H}_{\rm ctrl}(t) + \mathcal{H}_{\rm meas}(t) + \mathcal{H}_{\rm res} \ . \tag{A3}$$

During the manipulations the meter should be kept in the off-state, $\mathcal{H}_{\rm meas} = 0$. The residual interaction $\mathcal{H}_{\rm res}$ leads to dephasing and relaxation processes. It has to be weak in order to allow for a series of coherent manipulations.

A typical experiment involves preparation of an initial quantum state, switching the 'fields' $\boldsymbol{B}(t)$ and the coupling energies $J^{ij}_{ab}(t)$ to effect a specified unitary evolution of the wave function, and the measurement of the final state.

Preparation of the initial state

The initial state can be prepared by keeping the system at low temperatures so that it relaxes to the ground state. This is achieved by turning on a large value of $B_z \gg k_{\rm B}T$ for a sufficiently long time while $B_x(t) = B_y(t) = 0$. Then the residual interaction, $\mathcal{H}_{\rm res}$ relaxes each qubit to its ground state, $|\uparrow\rangle$. Switching $B_z(t)$ back to zero leaves the system in a well-defined pure quantum state. If $\mathcal{H} = 0$, there is no further time evolution.

Single-qubit operations

A single-bit operation on a given qubit can be performed, e.g., by turning on $B_x(t)$ for a time span τ. As a result of this operation the quantum state evolves according to the unitary transformation

$$U_x(\alpha) = \exp\left(\frac{iB_x\tau\hat{\sigma}_x}{2\hbar}\right) = \begin{pmatrix} \cos\frac{\alpha}{2} & i\sin\frac{\alpha}{2} \\ i\sin\frac{\alpha}{2} & \cos\frac{\alpha}{2} \end{pmatrix} \ , \tag{A4}$$

where $\alpha = B_x\tau/\hbar$. Depending on the time span τ, an $\alpha = \pi$- or an $\alpha = \pi/2$-rotation is performed, producing a spin flip (NOT-operation) or an equal-weight superposition of spin states. Switching on $B_z(t)$ for some time produces another needed single-bit operation: a phase shift between $|\uparrow\rangle$ and $|\downarrow\rangle$:

$$U_z(\beta) = \exp\left(\frac{iB_z\tau\hat{\sigma}_z}{2\hbar}\right) = \begin{pmatrix} e^{i\beta/2} & 0 \\ 0 & e^{-i\beta/2} \end{pmatrix} \ , \tag{A5}$$

where $\beta = B_z\tau/\hbar$. With a sequence of these x- and z-rotations any unitary transformation of the qubit state (single-qubit operation) can be performed. There is no need to turn on B_y.

Two-qubit operations

A two-bit operation on qubits i and j is induced by turning on the corresponding coupling $J^{ij}(t)$. For instance, for the XY-coupling, $J^{ij}_{ab}\hat{\sigma}_a\hat{\sigma}_b = J^{ij}(\hat{\sigma}_x\hat{\sigma}_x + \hat{\sigma}_y\hat{\sigma}_y)$, in the basis $|\uparrow_i\uparrow_j\rangle$, $|\uparrow_i\downarrow_j\rangle$, $|\downarrow_i\uparrow_j\rangle$, $|\downarrow_i\downarrow_j\rangle$ the result is described by the unitary operator

$$U^{ij}_{2\mathrm{b}}(\gamma) = \begin{pmatrix} 1 & 0 & 0 & 0 \\ 0 & \cos\gamma & i\sin\gamma & 0 \\ 0 & i\sin\gamma & \cos\gamma & 0 \\ 0 & 0 & 0 & 1 \end{pmatrix} , \tag{A6}$$

with $\gamma \equiv 2J^{ij}\tau/\hbar$. For $\gamma = \pi/2$ the operation leads to a swap of the states $|\uparrow_i\downarrow_j\rangle$ and $|\downarrow_i\uparrow_j\rangle$ (and multiplication by i), while for $\gamma = \pi/4$ it transforms the state $|\uparrow_i\downarrow_j\rangle$ into an entangled state $\frac{1}{\sqrt{2}}\left(|\uparrow_i\downarrow_j\rangle + i\,|\downarrow_i\uparrow_j\rangle\right)$.

We note that apart from the sudden switching of $B^i_{z,x}(t)$, $J^{ij}(t)$, discussed above for illustration, one can also use other techniques to implement single-bit or two-bit operations. For instance, one can induce Rabi oscillations between different states of a qubit or a qubit pair by ac resonance signals; or perform adiabatic manipulations of the qubits' Hamiltonian to exchange different eigenstates (with occupations remaining unchanged). We discuss some of these methods for particular physical systems in Sections II and III.

APPENDIX B: QUANTUM LOGIC GATES AND QUANTUM ALGORITHMS

In Appendix A and Sections II, III we showed how elementary quantum logic gates can be realized by simple manipulations of concrete physical systems. Details such as the application of a magnetic field pulse or the type of the two-qubit coupling depend on the specific model. On the other hand, quantum information theory discusses quantum computation in realization-independent terms. For instance, it is customary to build quantum algorithms out of specific, 'standard' single- and two-qubit gates, some of which will be discussed below. Hence, one needs to know how to express these standard gates in terms of the elementary operations specific for a given physical model. Furthermore, one may be interested in an optimized implementation, in terms of time, complexity of manipulations, or amount of additional dissipation. Here we give several examples of standard gates and quantum algorithms and cover optimization issues later.

Single- and two-qubit gates

The quantum generalization of the NOT gate,

$$\mathrm{NOT} = \begin{pmatrix} 0 & 1 \\ 1 & 0 \end{pmatrix} , \tag{B1}$$

permutes the basis vectors $|0\rangle \to |1\rangle$ and $|1\rangle \to |0\rangle$. It can be performed as the x-rotation (A4) with the time span corresponding to $\alpha = \pi$ (up to an unimportant overall phase factor): $U_x(\alpha = \pi) = i \cdot \mathrm{NOT}$. Unlike to classical computation, in quantum logic there exists a logic gate, called $\sqrt{\mathrm{NOT}}$, which when applied twice produces the NOT-gate:

$$\sqrt{\mathrm{NOT}} = \frac{1}{2}\begin{pmatrix} 1+i & -1+i \\ -1+i & 1+i \end{pmatrix} . \tag{B2}$$

This gate [17] is obtained by an x-rotation (A4) with $\alpha = \pi/2$, more precisely $U_x(\alpha = \pi/2) = i^{1/2} \cdot \sqrt{\mathrm{NOT}}$.

Another important, essentially quantum mechanical single-bit operation is the Hadamard gate:

$$-\boxed{\mathsf{H}}- = \mathsf{H} = \frac{1}{\sqrt{2}}\begin{pmatrix} 1 & 1 \\ 1 & -1 \end{pmatrix} . \tag{B3}$$

It transforms basis vectors into superpositions: $|0\rangle \to (|0\rangle + |1\rangle)/\sqrt{2}$, $|1\rangle \to (|0\rangle - |1\rangle)/\sqrt{2}$. This gate is of use to prepare a specific initial state: when applied to every qubit of the system in the ground state $|0\ldots0\rangle$, it provides an equally-weighted superposition of all basis states:

$$\mathsf{H} \otimes \ldots \otimes \mathsf{H}\,|0\ldots0\rangle = \frac{1}{2^{N/2}} \sum_{d_1,\ldots,d_N=0,1} |d_1 \ldots d_N\rangle . \tag{B4}$$

The terms in the sum can be viewed as binary representations of all integers from 0 up to $2^N - 1$. Thus the state (B4) is a superposition of all these integers. When used as input of a quantum algorithm, it represents 2^N classical inputs. Due to linearity of quantum time evolution they are processed simultaneously, and also the output is a superposition of 2^N classical results. This *quantum parallelism* is a fundamental property of quantum computation and is responsible for the exponential speed-up of certain quantum algorithms.

Among the two-qubit gates an important one is the exclusive-OR (XOR) or controlled-NOT (CNOT) gate:

$$\mathrm{CNOT} = \begin{pmatrix} 1 & 0 & 0 & 0 \\ 0 & 1 & 0 & 0 \\ 0 & 0 & 0 & 1 \\ 0 & 0 & 1 & 0 \end{pmatrix} . \tag{B5}$$

When applied to classical (basis) states it flips the second bit only if the first bit is 1. It was shown by Barenco et al. (1995) that the CNOT gate together with single-bit operations forms a universal set, sufficient for any quantum computation. In other words, any unitary transformation of a many-qubit system can be decomposed into single-bit gates and CNOT-gates. This explains the importance of CNOT in the quantum information-theoretical literature. However, it should be pointed out that *almost any* two-qubit gate (an exception is the classical SWAP-gate), when combined with single-bit operations, forms a universal set.

Let us also mention another useful two-bit gate, the controlled phase shift:

---

[17] $\sqrt{\mathrm{NOT}}$ is not uniquely defined: the matrices $i^{-n/2}U_x(\alpha = n\pi/2)$ with $n = 1, 3, 5, 7$ produce NOT, when squared.

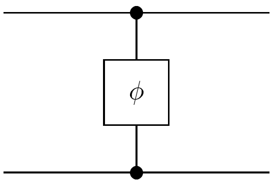

$$= R(\phi) = \begin{pmatrix} 1 & 0 & 0 & 0 \\ 0 & 1 & 0 & 0 \\ 0 & 0 & 1 & 0 \\ 0 & 0 & 0 & e^{i\phi} \end{pmatrix} . \tag{B6}$$

It shifts the phase of the state $|1\rangle$ of the second qubit when the first qubit is in the state $|1\rangle$. (We use an unconventional symbol for this operation, which stresses its symmetry with respect to the transposition of qubits.)

Quantum Fourier Transformation

As an example we discuss the quantum algorithm for a discrete Fourier transformation. N qubits allow us to represent the integers $j = 0, \ldots, 2^N - 1$ as basis states $|0\rangle, \ldots, |2^N - 1\rangle$. Starting from a superposition of these states with amplitudes c_j and applying the combination of controlled phase shifts and Hadamard gates shown in Fig. 21 one obtains an output:

$$\sum_{j=0}^{2^N-1} c_i \, |j\rangle \to \sum_{k=0}^{2^N-1} \tilde{c}_k \, |k\rangle \ , \tag{B7}$$

where the output amplitudes $\tilde{c}_k$ and input amplitudes c_j are related by the discrete Fourier transform:

$$\tilde{c}_k = \frac{1}{2^N} \sum_{j=0}^{2^N-1} \exp\left(\frac{2\pi i k j}{2^L}\right) c_j \, . \tag{B8}$$

While in classical computation the time needed for the Fourier transform grows exponentially with the number of bits N, the quantum algorithm in Fig. 21 takes $\propto N^2$ steps. The quantum Fourier transformation was developed by Shor (1994) and later improved by Coppersmith (1994) and Deutsch (see Ekert & Josza 1996). Its exponential speed-up compared to classical algorithms is crucial for the performance of Shor's (1994) algorithm for the factorization of large integers.

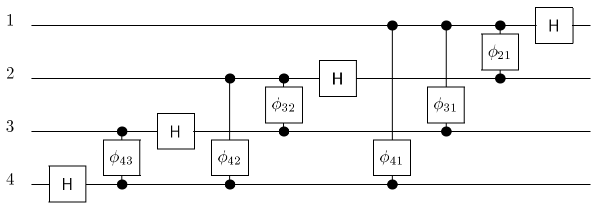

FIG. 21. A realization of the Fourier transformation for 4 qubits, i.e. 2^4 coefficients. The phase shifts are $\phi_{jk} = \pi/2^{j-k}$.

Quantum computation and optimization

The unitary transformations needed for quantum computation or any simple quantum manipulation should be realized in a particular physical system. For this purpose they should be decomposed into elementary unitary gates. This decomposition is not unique and should be optimized with respect to various parameters, for instance, the time, the number of steps, or the complexity of the manipulations involved. In some physical systems the manipulations involve additional dissipation (as compared to the idle state) which should be optimized as well. In this subsection we discuss how certain unitary logic gates can be realized in a spin system with model Hamiltonian (A2). The results are also useful for many other physical realizations of qubits (see Sections II, III) since many of them have similar Hamiltonians with similar control parameters.

First we consider the Hadamard gate (B3). It can be performed, up to an overall phase factor, as a sequence of elementary operations (A4) and (A5): $\mathsf{H} \propto U_x(\alpha = \pi/4) U_z(\beta = \pi/4) U_x(\alpha = \pi/4)$. However, it can also be performed faster by simultaneous switching of B_x and B_z:

$$\mathsf{H} \propto \exp\left(-i \frac{\pi}{2} \frac{\sigma_x + \sigma_z}{\sqrt{2}}\right) . \tag{B9}$$

The CNOT gate in the model system (A2) can be implemented by a combination of 2 two-qubit gates $U_{2\mathrm{b}}$ (A6) and several single-qubit gates (see also Imamoglu et al. 1999):

$$\begin{aligned} \mathrm{CNOT} \propto\, & U_x^2\left(\frac{\pi}{2}\right) U_z^2\left(-\frac{\pi}{2}\right) U_x^2\left(-\pi\right) U_{2\mathrm{b}}\left(-\frac{\pi}{2}\right) \times \\ & U_x^1\left(-\frac{\pi}{2}\right) U_{2\mathrm{b}}\left(\frac{\pi}{2}\right) U_z^1\left(-\frac{\pi}{2}\right) U_z^2\left(-\frac{\pi}{2}\right) . \end{aligned} \tag{B10}$$

Similarly, the controlled phase shift gate (B6) is produced by the sequence

$$\begin{aligned} R(\phi) \propto\, & U_x^2\left(-\frac{\pi}{2}\right) U_{2\mathrm{b}}\left(-\frac{\pi}{2}\right) U_x^1\left(-\frac{\phi}{2}\right) U_{2\mathrm{b}}\left(\frac{\pi}{2}\right) \times \\ & U_x^2\left(\frac{\pi}{2}\right) U_z^1\left(-\frac{\phi}{2}\right) U_z^2\left(-\frac{\phi}{2}\right) . \end{aligned} \tag{B11}$$

One can see from these examples that it takes quite a number of elementary gates to perform the CNOT or $R(\phi)$ and further optimization is desired. In many realizations two-qubit elementary gates are more costly (complicated or longer) than single-qubit gates. With this taken into account one can ask whether Eqs. (B10) and (B11) can be reduced to just one two-bit gate? An analysis of this problem (Makhlin 2000) shows that it is not possible if the two-bit elementary gate (A6), produced by the XY-coupling Hamiltonian, is used. The result is the same for the Heisenberg spin coupling, but the Ising-type coupling, $\propto \hat{\sigma}_z \hat{\sigma}_z$, allows to achieve $R(\phi)$ [and hence $\mathrm{CNOT} = \mathsf{H}^2 R(\pi) \mathsf{H}^2$] with only one two-bit operation: $R(\phi) \propto U_z^1(-\phi/2) U_z^2(-\phi/2) \exp(i\phi\sigma_z^1\sigma_z^2/4)$. The optimization of certain quantum logic circuits was also discussed in connection with qubits based on spins in quantum dots (Burkard et al. 1999).

APPENDIX C: CHARGING ENERGY OF A QUBIT COUPLED TO A SET

The charging energy of the system shown in Fig. 14 is a quadratic function of the charges n and N:

$$\begin{aligned}\mathcal{H}_{\rm C}(n,N,V_n,V_N) &= 4E_{\rm C,qb}n^2 + E_{\rm C,SET}N^2 \\ &+E_{\rm int}N(2n-1) + 2enV_n + eNV_N \ . \end{aligned} \tag{C1}$$

The form of the mixed term $\propto N(2n-1)$ is chosen for later convenience. The charging energy scales $E_{\rm C,qb}$, $E_{\rm C,SET}$ and $E_{\rm int}$ are set by the capacitances between all the islands. Elementary electrostatics shows that they can be written as

$$\begin{aligned} E_{\rm C,qb} &= e^2(C_{\rm g}^{\rm SET} + C_{\rm int} + 2C_{\rm T})/2A \approx e^2/2C_{\rm J} \ , \\ E_{\rm C,SET} &= e^2(C_{\rm g}^{\rm qb} + C_{\rm int} + C_{\rm J})/2A \approx e^2/(4C_{\rm T}) \ , \\ E_{\rm int} &= e^2 C_{\rm int}/A \approx e^2 C_{\rm int}/(2C_{\rm J}C_{\rm T}) \ . \end{aligned} \tag{C2}$$

Here we introduced

$$\begin{aligned} A &\equiv (C_{\rm g}^{\rm qb} + C_{\rm J})(C_{\rm g}^{\rm SET} + C_{\rm int} + 2C_{\rm T}) \\ &+ C_{\rm int}(C_{\rm g}^{\rm SET} + 2C_{\rm T}) \approx 2C_{\rm J}C_{\rm T} \ . \end{aligned} \tag{C3}$$

For simplicity we assumed that the two tunnel junctions of the SET have equal capacitances $C_{\rm T}$, and the approximate results refer to the limit $C_{\rm g}^{\rm qb}, C_{\rm int}, C_{\rm g}^{\rm SET} \ll C_{\rm T} \ll C_{\rm J}$, which we consider useful. The effective voltages V_n and V_N depend in general on the gate voltages $V_{\rm g}^{\rm qb}$, $V_{\rm g}^{\rm SET}$ and the transport voltages applied to the SET's electrodes. However, for a symmetric setup (equal junction capacitances) and symmetrically distributed transport bias (as shown in Fig. 14), V_n and V_N are controlled only by the two gate voltages:

$$\begin{aligned} V_N &= V_{\rm g}^{\rm SET}\frac{C_{\rm g}^{\rm SET}(C_{\rm g}^{\rm qb} + C_{\rm int} + C_{\rm J})}{A} \\ &+V_{\rm g}^{\rm qb}\frac{C_{\rm int}C_{\rm g}^{\rm qb}}{A} + \frac{E_{\rm int}}{e} \ , \\ V_n &= V_{\rm g}^{\rm SET}\frac{C_{\rm g}^{\rm SET}C_{\rm int}}{A} + V_{\rm g}^{\rm qb}\frac{(C_{\rm g}^{\rm SET} + C_{\rm int} + 2C_{\rm T})C_{\rm g}^{\rm qb}}{A} \ . \end{aligned} \tag{C4}$$

The total charging energy can thus, up to a nonessential constant, be presented as a sum of the contributions of the qubit (2.1), the SET (5.2), and the interaction term $E_{\rm int}N(2n-1)$ (cf. Eq.(5.5)). The effect of the SET is to renormalize the parameters of the qubit Hamiltonian (2.1): $E_{\rm C}$ and $n_{\rm g}$ should be substituted by $E_{\rm C,qb}$ and $n_{\rm g,qb} \equiv -eV_n/4E_{\rm C,qb}$.

APPENDIX D: DERIVATION OF THE MASTER EQUATION

We briefly review the rules for the evaluation of diagrams; for more details including the discussion of higher order diagrams we refer to Schoeller & Schön's (1994) paper. Typical diagrams, which are analyzed below, are displayed in Figs. 22 and 23. The horizontal lines, discussed in detail below, describe the time evolution of the system governed by the zeroth order Hamiltonian $\mathcal{H}_0$. The directed dashed lines stand for tunneling processes, in the example considered the tunneling takes place in the left junction. According to the rules, the dashed lines contribute the following factor to the self-energy Σ:

$$\alpha_{\rm L}\left(\frac{\pi k_{\rm B}T}{\hbar}\right)^2 \frac{\exp\left[\pm\frac{i}{\hbar}\mu_{\rm L}(t-t')\right]}{\sinh^2\left[\frac{\pi k_{\rm B}T}{\hbar}(t-t'\pm i\delta)\right]} \ , \tag{D1}$$

where $\alpha_{\rm L} \equiv h/(4\pi^2 e^2 R_{\rm T,L})$ is the dimensionless tunneling conductance, $\mu_{\rm L}$ is the electro-chemical potential of the left lead, and δ^{-1} is the high-frequency cut-off, which is at most of order of the Fermi energy. The sign of the infinitesimal term $i\delta$ depends on the direction of the dashed line in time. It is negative if the direction of the line with respect to the Keldysh contour coincides with its direction with respect to absolute time (from left to right), and positive otherwise. For example, the right part of Fig. 22 should carry a minus sign, while the left part carries a plus sign. Furthermore, the sign in front of $i\mu_{\rm L}(t-t')$ is negative (positive), if the line goes forward (backward) with respect to absolute time. Finally, the first order diagrams are multiplied by (-1) if the dashed line connects two points on different branches of the Keldysh contour.

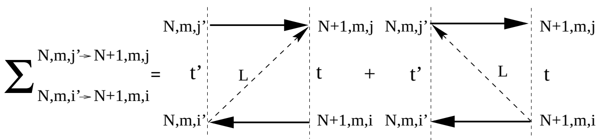

FIG. 22. Example of a self-energy diagram for an 'in'-rate.

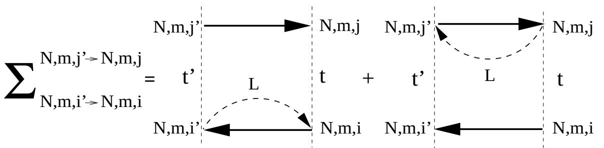

FIG. 23. Example of a self-energy diagram for an 'out'-rate.

The horizontal lines describe the time evolution of the system between tunneling processes. For an isolated central island they turn into exponential factors $e^{\pm\frac{i}{\hbar}E(t-t')}$, depending on the charging energy of the system. However, in the present case the island is coupled to the qubit, and we need to account for the nontrivial time evolution of the latter. For instance, the upper line in the left part of Fig. 22 corresponds to $\langle N,j|e^{-\frac{i}{\hbar}\mathcal{H}_0(t-t')}|N,j'\rangle$, while the lower line corresponds to $\langle N{+}1,i'|e^{\frac{i}{\hbar}\mathcal{H}_0(t-t')}|N{+}1,i\rangle$.

In the present problem we assume that the tunneling conductance of the SET is low compared to the quantum conductance. In this case lowest order perturbation theory in the single-electron tunneling, describing sequential tunneling processes, is sufficient. The diagrams for Σ can be split into two classes, depending on whether they provide expressions for off-diagonal ($N' \neq N$) or diagonal ($N' = N$) elements of Σ in N. In analogy to the scattering integrals in the Boltzmann equation these can be labeled 'in' and 'out' terms, in the sense that they describe the increase or decrease of a given element $\hat{\rho}_{j,N,m}^{i,N,m}$ of the density matrix due to transitions from or to other N-states. Examples for the 'in' and 'out' terms are shown in Figs. 22 and 23, respectively.

We now are ready to evaluate the rates in Figs. 22 and 23. For example, the 'in' tunneling process in the left junction is expressed as

$$\Sigma_{i',N,m\to i,N+1,m}^{j',N,m\to j,N+1,m}(\Delta t) = -\alpha_{\rm L}\left(\frac{\pi k_{\rm B}T}{\hbar}\right)^2 \times \left\{\frac{\exp\left[-\frac{i}{\hbar}(\tilde{E}_{N+1}^N + W_{N+1}^N)\Delta t\right]}{\sinh^2\left[\frac{\pi k_{\rm B}T}{\hbar}(\Delta t + i\delta)\right]} + \frac{\exp\left[-\frac{i}{\hbar}(\tilde{E}_N^{N+1} + W_N^{N+1})\Delta t\right]}{\sinh^2\left[\frac{\pi k_{\rm B}T}{\hbar}(\Delta t - i\delta)\right]}\right\}_{i'i}^{j'j}, \tag{D2}$$

where $\tilde{E}_{N_2}^{N_1} \equiv \left[E_{\rm C,SET}(N_1 - N_{\rm g,SET})^2 - \mu_{\rm L}\, N_1\right] - \left[E_{\rm C,SET}(N_2 - N_{\rm g,SET})^2 - \mu_{\rm L}\, N_2\right]$ is the Coulomb energy gain for the tunneling in the left junction in the absence of the qubit, and the operators

$$W_{N_2}^{N_1} = \mathcal{H}_0^{\rm T}(N_1) \otimes 1 - 1 \otimes \mathcal{H}_0(N_2)\ . \tag{D3}$$

provide corrections to the energy gain sensitive to the qubit's state. Here $\mathcal{H}_0(N)$ is the N-th block of the Hamiltonian $\mathcal{H}_{\rm ctrl} + \mathcal{H}_{\rm int}$ (note that $\mathcal{H}_{\rm ctrl}$ and $\mathcal{H}_{\rm int}$ are block-diagonal with respect to N). The indices j', j and i', i relate to the left and right side of the tensor product in (D3) correspondingly.

The form of the master equation (5.8) suggests the use of the Laplace transform, after which the last term in (5.8) becomes $\Sigma(s)\hat{\rho}(s)$. We Laplace transform (D2) in the regime $\hbar s, |W_{N+1}^N|, |W_N^{N+1}| \ll \tilde{E}_{N+1}^N$, i.e., we assume the density matrix $\hat{\rho}$ to change slowly on the time scale given by $\hbar/\tilde{E}_{N+1}^N$. This assumption should be verified later for self-consistency. The inequalities also mean that we choose the operation regime of the SET far enough from the Coulomb threshold. Therefore the tunneling is either energetically allowed for both states of the qubit or it is blocked for both of them. At low temperatures ($k_{\rm B}T \ll \tilde{E}_{N+1}^N$) and for $\tilde{E}_{N+1}^N\delta \ll \hbar$ we obtain

$$\Sigma_{N,m,i'\to N+1,m,i}^{N,m,j'\to N+1,m,j}(s) \approx \left\{\frac{\pi}{\hbar}\alpha_{\rm L}\Theta(\tilde{E}_{N+1}^N)\left[2\tilde{E}_{N+1}^N + (W_{N+1}^N - W_N^{N+1})\right] -\alpha_{\rm L} D(\tilde{E}_{N+1}^N)\left[2s + \frac{i}{\hbar}(W_{N+1}^N + W_N^{N+1})\right]\right\}_{i'i}^{j'j}, \tag{D4}$$

where $D(\tilde{E}_{N+1}^N) \approx 1 + \gamma + \ln(\tilde{E}_{N+1}^N\delta/\hbar)$ and $\gamma \approx 0.58$ is Euler's constant. The first term of (D4) is the standard Golden rule tunneling rate corresponding to the so-called orthodox theory of single-electron tunneling (Averin & Likharev 1991). The rate depends strongly on the charging energy difference, $\tilde{E}_{N+1}^N$, before and after the process, which in the present problem is modified according to the quantum state of the qubit (the W-terms). At finite temperatures the step-function is replaced by $\Theta(E) \to [1 - \exp(-E/k_{\rm B}T)]^{-1}$. We denote the full matrix of such rates $\check{\Gamma}$. As has already been mentioned, we concentrate on the regime when the leading tunneling process in the SET is the sequential tunneling, involving only two adjacent charge states, say, $N = 0$ and $N = 1$ (to avoid confusion with the states of the qubit we keep using the notation N and $N + 1$). Let us, for example, calculate a submatrix of $\check{\Gamma}$ which originates from the first term on the RHS of (D4) and corresponds to the tunneling process $N \to N + 1$, $m \to m$ in the left junction. This submatrix $\check{\Gamma}_L$ is a super-operator which acts on a 2×2-matrix $\hat{\rho}$ as

$$\hbar\check{\Gamma}_L\hat{\rho} = 2\pi\alpha_L\tilde{E}_{N+1}^N\hat{\rho} + \pi\alpha_L\ [\delta\mathcal{H}_{\rm int}, \hat{\rho}]_+\ , \tag{D5}$$

where $\delta\mathcal{H}_{\rm int} \equiv \mathcal{H}_0(N+1) - \mathcal{H}_0(N) = E_{\rm int}\sigma_z$.

The last, logarithmically diverging term of Eq. (D4) produces the commutator term in the RHS of the master equation (5.8). These terms turn out to be unimportant in the first order of the perturbation theory. Indeed, for the left junction we obtain the following contribution to the RHS of (5.8):

$$\alpha_{\rm L}\hat{D}_{\rm L}\left(\frac{d\hat{\rho}}{dt} - \frac{i}{\hbar}\left[\hat{\rho}, \bar{\mathcal{H}}_0\right]\right)\ , \tag{D6}$$

where $\bar{\mathcal{H}}_0 \equiv \frac{1}{2}(\mathcal{H}_0(N) + \mathcal{H}_0(N+1))$ and $\hat{D}_{\rm L}$ is a matrix in N and m spaces. The eigenvalues of the matrix $\hat{D}_{\rm L}$ are at most of order $D(\tilde{E}_{N+1}^N)$. Neglecting terms of order $\alpha_{\rm L}D(\tilde{E}_{N+1}^N)E_{\rm int}$ in Eq. (D6), we can replace $\bar{\mathcal{H}}_0$ by $\mathcal{H}_0$. Our analysis shows that these neglected "coherent-like" terms do not change the results as long as $\alpha_{\rm L}\,|\ln(\tilde{E}_{N+1}^N\delta/\hbar)| \ll 1$. A similar analysis can be carried out for the right tunnel junction of the SET.

Now we can transfer all the "coherent-like" terms into the LHS of the master equation,

$$\left(1 - \alpha_{\rm L}\hat{D}_{\rm L} - \alpha_{\rm R}\hat{D}_{\rm R}\right)\left\{\frac{d\hat{\rho}(t)}{dt} - \frac{i}{\hbar}[\hat{\rho}(t), \mathcal{H}_0]\right\} = \frac{1}{\hbar}\check{\Gamma}\hat{\rho}(t), \tag{D7}$$

and multiply Eq. (D7) from the left by $(1 - \alpha_{\rm L}\hat{D}_{\rm L} - \alpha_{\rm R}\hat{D}_{\rm R})^{-1} \approx (1 + \alpha_{\rm L}\hat{D}_{\rm L} + \alpha_{\rm R}\hat{D}_{\rm R})$ so that the corrections move back to the RHS. Since $\check{\Gamma}$ is itself linear in $\alpha_{\rm L}$ and $\alpha_{\rm R}$, the corrections are of second order in α (more accurately, they are small if $\alpha\,|\ln(\tilde{E}^N_{N+1}\delta/\hbar)| \ll 1$ for both junctions). Thus we drop the "coherent" corrections and arrive at the final form of the master equation:

$$\frac{d\hat{\rho}(t)}{dt} - \frac{i}{\hbar}[\hat{\rho}(t),\mathcal{H}_0] = \frac{1}{\hbar}\check{\Gamma}\hat{\rho}(t)\ . \tag{D8}$$

We have shown that under the assumption of sufficiently slow dynamics of the qubit and SET, $E_{\rm J}, B_z(V_{\rm g}), E_{\rm int}, \Gamma_{\rm L/R} \ll \tilde{E}^N_{N+1}, \tilde{E}^{N+1}_N$, the evolution of the system reduces to Markovian dynamics as described by the master equation (D8).

REFERENCES

Aharonov, D., 1998, in *Annual Reviews of Computational Physics*, edited by D. Stauffer, Vol. VI (World Scientific, Singapore).

Aleiner, I. L., N. S. Wingreen, and Y. Meir, 1997, "Dephasing and the orthogonality catastrophe in tunneling through a quantum dot: the "which path?" interferometer", Phys. Rev. Lett. **79**, 3740.

Ambegaokar, V., U. Eckern, and G. Schön, 1982, "Quantum dynamics of tunneling between superconductors", Phys. Rev. Lett. **48**, 1745.

Averin, D., 2000*a*, "Noise properties of the SET transistor in the co-tunneling regime", cond-mat/0010052.

Averin, D. V., 1998, "Adiabatic quantum computation with Cooper pairs", Solid State Commun. **105**, 659.

Averin, D. V., 2000*b*, "Continuous weak measurement of the macroscopic quantum coherent oscillations", cond-mat/0004364.

Averin, D. V., and K. K. Likharev, 1991, in *Mesoscopic Phenomena in Solids*, edited by B. L. Altshuler, P. A. Lee, and R. A. Webb (Elsevier, Amsterdam), p. 173.

Averin, D. V., and V. Y. Aleshkin, 1989, "Resonance tunneling of Cooper pairs in a system of two small Josephson junctions", JETP Lett. **50**, 367.

Barenco, A., 1996, "Quantum physics and computers", Contemp. Phys. **37**, 375.

Barenco, A., C. Bennett, R. Cleve, D. DiVincenzo, N. Margolus, P. Shor, T. Sleator, J. Smolin, and H. Weinfurter, 1995, "Elementary gates for quantum computation", Phys. Rev. A **52**, 3457.

Bennett, C., 1995, "Quantum information and computation", Physics Today **48**, 24.

Blais, A., and A. Zagoskin, 2000, "Operation of universal gates in a solid-state quantum computer based on clean Josephson junctions between *d*-wave superconductors", Phys. Rev. A **61**, 042308.

Blatter, G., V. B. Geshkenbein, and L. B. Ioffe, 1999, "Engineering superconducting phase qubits", cond-mat/9912163.

Bouchiat, V., 1997, Ph.D. Thesis, Université Paris VI.

Bouchiat, V., D. Vion, P. Joyez, D. Esteve, and M. H. Devoret, 1998, "Quantum coherence with a single Cooper pair", Physica Scripta **T76**, 165.

Braginsky, V. B., and F. Y. Khalili, 1992, *Quantum measurement* (Cambridge University Press, Cambridge).

Braunstein, S. & H.-K. Lo, eds. (2000), *Experimental proposals for quantum computation*, Fortschritte der Physik **48**, no. 9–11, pp. 765–1140.

Buisson, O., and F. W. J. Hekking, 2000, "Entangled states in a Josephson charge qubit coupled to a superconducting resonator", cond-mat/0008275.

Buks, E., R. Schuster, M. Heiblum, D. Mahalu, and V. Umansky, 1998, "Dephasing due to which path detector", Nature **391**, 871.

Burkard, G., D. Loss, D. DiVincenzo, and J. Smolin, 1999, "Physical optimization of quantum error correction circuits", Phys. Rev. B **60**, 11404.

Caldeira, A. O., and A. J. Leggett, 1983, "Quantum tunnelling in a dissipative system", Ann. Phys. (NY) **149**, 374.

Chang, I. L., 1998, in *Introduction to quantum computation and information*, edited by H.-K. Lo, S. Popescu, and T. Spiller (World Scientific, Singapore), p. 311.

Choi, M. S., R. Fazio, J. Siewert, and C. Bruder, 2000, "Coherent oscillations in a Cooper-pair box", preprint.

Cirac, J. I., and P. Zoller, 1995, "Quantum computations with cold trapped ions", Phys. Rev. Lett. **74**, 4091.

Clarke, J., A. N. Cleland, M. H. Devoret, D. Esteve, and J. M. Martinis, 1988, "Quantum mechanics of a macroscopic variable: the phase difference of a Josephson junction", Science **239**, 992.

Coppersmith, D., 1994, IBM, Research report 19642.

Cory, D., A. Fahmy, and T. Havel, 1997, "Ensemble quantum computing by NMR spectroscopy", Proc. Nat. Acad. Sci. of the U. S. **94**, 1634.

Cosmelli, C., P. Carelli, M. G. Castellano, F. Chiarello, R. Leoni, and G. Torrioli, 1998, in *Quantum Coherence and Decoherence – ISQM '98*, edited by Y. A. Ono, and K. Fujikawa (Elsevier, Amsterdam).

Cottet, A., A. Steinbach, P. Joyez, D. Vion, H. Pothier, D. Esteve, and M. E. Huber, 2000, "Superconducting electrometer for measuring the single Cooper pair box", preprint.

Devoret, M. H., and R. J. Schoelkopf, 2000, "Amplifying quantum signals with the single-electron transistor", Nature **406**, 1039.

Devoret, M. H., D. Esteve, H. Grabert, G. L. Ingold, and H. Pothier, 1990, "Effect of the electromagnetic environment on the Coulomb blockade in ultrasmall tunnel junctions", Phys. Rev. Lett. **64**, 1824.

DiVincenzo, D., 1995, "Quantum computation", Science **270**, 255.

DiVincenzo, D., 1997, in *Mesoscopic Electron Transport*, edited by L. Kouwenhoven, G. Schön, and L. Sohn, Vol. 345 of *NATO ASI Series E: Applied Sciences* (Kluwer Ac. Publ., Dordrecht), p. 657.

DiVincenzo, D., 2000, "The physical implementation of quantum computation", quant-ph/0002077, Fortschritte der Physik **48**, 771.

Ekert, A., and R. Josza, 1996, "Shor's quantum algorithm for factorizing numbers", Rev. Mod. Phys. **68**, 733.

Falci, G., R. Fazio, G. H. Palma, J. Siewert, and V. Vedral, 2000, "Detection of geometric phases in superconducting nanocircuits", Nature **407**, 355–358.

Fazio, R., G. M. Palma, and J. Siewert, 1999, "Fidelity and leakage of Josephson qubits", Phys. Rev. Lett. **83**, 5385.

Feigelman, M. V., V. B. Geshkenbein, L. B. Ioffe, and G. Blatter, 2000, "Andreev spectroscopy for superconducting phase qubits", J. Low Temp. Phys. **118**, 805.

Friedman, J. R., V. Patel, W. Chen, S. K. Tolpygo, and J. E. Lukens, 2000, "Detection of a Schroedinger's cat state in an rf-SQUID", Nature **406**, 43.

Gershenfeld, N., and I. Chuang, 1997, "Bulk spin resonance quantum computation", Science **275**, 350.

Goan, H. S., G. J. Milburn, H. M. Wiseman, and H. B. Sun, 2000, "Continuous quantum measurement of two coupled quantum dots using a quantum point contact: A quantum trajectory approach", cond-mat/0006333.

Görlich, R., M. Sassetti, and U. Weiss, 1989, "Low-temperature properties of biased two-level systems: effects of frequency-dependent damping", Europhys. Lett. **10**, 507.

Gurvitz, S. A., 1997, "Measurements with a noninvasive detector and dephasing mechanism", Phys. Rev. B **56**, 15215.

Gurvitz, S. A., and Y. S. Prager, 1996, "Microscopic derivation of rate equations for quantum transport", Phys. Rev. B **53**, 15932.

Hadley, P., E. Delvigne, E. H. Visscher, S. Lähteenmäki, and J. E. Mooij, 1998, "3e tunneling processes in a superconducting single-electron tunneling transistor", Phys. Rev. B **58**, 15317.

Harris, R. A., and L. Stodolsky, 1982, "Two state systems in media and Turing's paradox"', Phys. Lett. B **116**, 464.

Il'ichev, E., V. Zakosarenko, R. P. J. IJsselsteijn, H. E. Hoenig, V. Schultze, H. G. Meyer, M. Grajcar, and R. Hlubina, 1998, "Nonsinusoidal current-phase relationship of grain boundary Josephson junctions in high-T_c superconductors", Phys. Rev. Lett. **81**, 894.

Imamoglu, A., D. D. Awschalom, G. Burkard, D. P. DiVincenzo, D. Loss, M. Sherwin, and A. Small, 1999, "Quantum information processing using quantum dot spins and cavity QED", Phys. Rev. Lett. **83**, 4204.

Ioffe, L. B., V. B. Geshkenbein, M. V. Feigelman, A. L. Fauchére, and G. Blatter, 1999, "Quiet sds Josephson junctions for quantum computing", Nature **398**, 679.

Kane, B. E., 1998, "A silicon-based nuclear spin quantum computer", Nature **393**, 133.

Korotkov, A. N., 1999, "Continuous quantum measurement of a double dot", Phys. Rev. B **60**, 5737.

Korotkov, A. N., 2000*a*, "Output spectrum of a detector measuring quantum oscillations", cond-mat/0003225.

Korotkov, A. N., 2000*b*, "Selective quantum evolution of a qubit state due to continuous measurement", cond-mat/0008461.

Korotkov, A. N., and D. V. Averin, 2000, "Continuous weak measurement of quantum coherent oscillations", cond-mat/0002203.

Krupenin, V. A., D. E. Presnov, A. B. Zorin, and J. Niemeyer, 2000, "Aluminum single-electron transistors with islands isolated from the substrate", J. Low Temp. Phys. **118**, 287.

Lafarge, P., P. Joyez, D. Esteve, C. Urbina, and M. H. Devoret, 1993, "Measurement of the even-odd free-energy difference of an isolated superconductor", Phys. Rev. Lett. **70**, 994.

Leggett, A. J., 1987, in *Chance and Matter*, edited by J. Souletie, J. Vannimenus, and R. Stora (Elsevier, Amsterdam), p. 395.

Leggett, A. J., S. Chakravarty, A. T. Dorsey, M. P. A. Fisher, A. Garg, and W. Zwerger, 1987, "Dynamics of the dissipative two-state system", Rev. Mod. Phys. **59**, 1.

Levinson, Y., 1997, "Dephasing in a quantum dot due to coupling with a quantum point contact", Europhys. Lett **39**, 299.

Likharev, K. K., 1996, *Dynamics of Josephson junctions and circuits* (Gordon and Breach Publishers, Amsterdam).

Loss, D., and D. P. DiVincenzo, 1998, "Quantum computation with quantum dots", Phys. Rev. A **57**, 120.

Maassen van den Brink, A., 2000, "Quantum-efficient charge detection using a single-electron transistor", cond-mat/0009163.

Maassen van den Brink, A., G. Schön, and L. J. Geerligs, 1991, "Combined single electron and coherent Cooper pair tunneling in voltage-biased Josephson junctions", Phys. Rev. Lett. **67**, 3030.

Makhlin, Y., 2000, "Nonlocal properties of two-qubit gates and mixed states and optimization of quantum computations", quant-ph/0002045.

Makhlin, Y., G. Schön, and A. Shnirman, 1999, "Josephson-junction qubits with controlled couplings", Nature **386**, 305.

Makhlin, Y., G. Schön, and A. Shnirman, 2000*a*, "Josephson-junction qubits", Fortschritte der Physik **48**, 1043.

Makhlin, Y., G. Schön, and A. Shnirman, 2000*b*, in *Exploring the Quantum–Classical Frontier*, edited by J. R. Friedman, and S. Han (Nova Science Publishers, Commack, NY; cond-mat/9811029).

Makhlin, Y., G. Schön, and A. Shnirman, 2000*c*, "Nano-electronic realizations of quantum bits", J. Low Temp. Phys. **118**, 751.

Makhlin, Y., G. Schön, and A. Shnirman, 2000*d*, "Statistics and noise in a quantum measurement process", to be published in Phys. Rev. Lett.

Martinis, J. M., M. H. Devoret, and J. Clarke, 1987, "Experimental tests for the quantum behavior of a macroscopic degree of freedom: The phase difference across a Josephson junction", Phys. Rev. B **35**, 4682.

Monroe, C., D. M. Meekhof, B. E. King, W. M. Itano, and D. J. Wineland, 1995, "Demonstration of a fundamental quantum logic gate", Phys. Rev. Lett. **75**, 4714.

Mooij, J. E., T. P. Orlando, L. Levitov, L. Tian, C. H. van der Wal, and S. Lloyd, 1999, "Josephson persistent current qubit", Science **285**, 1036.

Nakamura, Y., C. D. Chen, and J. S. Tsai, 1997, "Spectroscopy of energy-level splitting between two macroscopic quantum states of charge coherently superposed by Josephson coupling", Phys. Rev. Lett. **79**, 2328.

Nakamura, Y., Y. A. Pashkin, and J. S. Tsai, 1999, "Coherent control of macroscopic quantum states in a single-Cooper-pair box", Nature **398**, 786.

Nakamura, Y., Y. A. Pashkin, and J. S. Tsai, 2000, in *Macroscopic Quantum Coherence and Quantum Computing* (Kluwer Ac. Publ., Dordrecht).

Nazarov, Y. V., 1989, "Anomalous current-voltage characteristics of tunnel junctions", Sov. Phys. JETP **68**, 561.

Nazarov, Y. V., 1993, "Quantum interference, tunnel junctions and resonant tunneling interferometer", Physica B **189**, 57.

Odintsov, A. A., 1988, "Effect of dissipation on the characteristics of small-area tunnel junctions: application of the polaron model", Sov. Phys. JETP **67**, 1265.

Orlando, T. P., J. E. Mooij, L. Tian, C. H. van der Wal, L. S. Levitov, S. Lloyd, and J. J. Mazo, 1999, "Superconducting persistent-current qubit", Phys. Rev. B **60**, 15398.

Panyukov, S. V., and A. D. Zaikin, 1988, "Quantum fluctuations and quantum dynamics of small Josephson junctions", J. Low. Temp. Phys. **73**, 1.

Pekola, J. P., J. J. Toppari, M. Aunola, M. T. Savolainen, and D. V. Averin, 1999, "Adiabatic transport of Cooper pairs in arrays of Josephson junctions", Phys. Rev. B **60**, R9931.

Preskill, J., 1998, in *Introduction to quantum computation and information*, edited by H.-K. Lo, S. Popescu, and T. Spiller (World Scientific, Singapore), p. 213.

Rouse, R., S. Han, and J. E. Lukens, 1995, "Observation of resonant tunneling between macroscopically distinct quantum levels", Phys. Rev. Lett. **75**, 1614.

Schoelkopf, R. J., P. Wahlgren, A. A. Kozhevnikov, P. Delsing, and D. E. Prober, 1998, "The radio-frequency single-electron transistor (rf-SET): a fast and ultrasensititve electrometer", Science **280**, 1238.

Schoeller, H., and G. Schön, 1994, "Mesoscopic quantum transport: resonant tunneling in the presence of strong Coulomb interaction", Phys. Rev. B **50**, 18436.

Schön, G., and A. D. Zaikin, 1990, "Quantum coherent effects, phase transitions, and the dissipative dynamics of ultra small tunnel junctions", Physics Reports **198**, 237.

Schön, G., and A. D. Zaikin, 1994, "Parity effects on electron tunneling through small superconducting islands", Europhys. Lett. **26**, 695.

Shnirman, A., and G. Schön, 1998, "Quantum measurements performed with a single-electron transistor", Phys. Rev. B **57**, 15400.

Shnirman, A., G. Schön, and Z. Hermon, 1997, "Quantum manipulations of small Josephson junctions", Phys. Rev. Lett. **79**, 2371.

Shor, P., 1994, in *Proceedings of the 35th Annual Symposium on the Foundations of Computer Science*, edited by S. Goldwasser, IEEE Computer Society (IEEE Comput. Soc. Press, Los Alamos, CA), p. 124.

Siewert, J., and G. Schön, 1996, "Charge transport in voltage-biased superconducting single-electron transistors", Phys. Rev. B **54**, 7421.

Silvestrini, P., V. G. Palmieri, B. Ruggiero, and M. Russo, 1997, "Observation of energy levels quantization in underdamped Josephson junctions above the classical-quantum regime crossover temperature", Phys. Rev. Lett. **79**, 3046.

Sprinzak, D., E. Buks, M. Heiblum, and H. Shtrikman, 1999, "Controlled dephasing via phase detection of electrons: demonstration of Bohr's complementarity principle", e-print cond-mat/9907162.

Steane, A., 1998, in *Introduction to quantum computation and information*, edited by H.-K. Lo, S. Popescu, and T. Spiller (World Scientific, Singapore), p. 184.

Stoof, T. H., and Y. V. Nazarov, 1996, "Time-dependent resonant tunneling via two discrete states", Phys. Rev. B **53**, 1050.

Tesche, C. D., 1990, "Can a noninvasive measurement of magnetic flux be performed with superconducting circuits?", Phys. Rev. Lett. **64**, 2358.

Tian, L., L. S. Levitov, C. H. van der Wal, J. E. Mooij, T. P. Orlando, S. Lloyd, C. J. P. M. Harmans, and J. J. Mazo, 2000, in *Quantum Mesoscopic Phenomena and Mesoscopic Devices in Microelectronics*, edited by I. Kulik, and R. Ellialtioglu, NATO-ASI Series E: Appl. Sci. (Kluwer Ac. Publ., Dordrecht; cond-mat/9910062).

Tinkham, M., 1996, *Introduction to Superconductivity*, 2nd edn (McGraw-Hill, New York).

Tuominen, M. T., J. M. Hergenrother, T. S. Tighe, and M. Tinkham, 1992, "Experimental evidence for parity-based 2e periodicity in a superconducting single-electron tunneling transistor", Phys. Rev. Lett. **69**, 1997.

Turchette, Q. A., C. J. Hood, W. Lange, H. Mabuchi, and H. J. Kimble, 1995, "Measurement of conditional phase shifts for quantum logic", Phys. Rev. Lett. **75**, 4710.

van der Wal, C. H., A. C. J. ter Haar, F. K. Wilhelm, R. N. Schouten, C. J. P. M. Harmans, T. P. Orlando, S. Lloyd, and J. E. Mooij, 2000, "Quantum superposition of macroscopic persistent-current states", to appear in Science.

von Neumann, J., 1955, *Mathematical Foundations of Quantum Mechanics* (Princeton Univ. Press, Princeton).

Voss, R. F., and R. A. Webb, 1981, "Macroscopic quantum tunneling in 1μm Nb Josephson junctions", Phys. Rev. Lett. **47**, 265.

Weiss, U., 1999, *Quantum dissipative systems*, 2nd edn (World Scientific, Singapore).

Weiss, U., and M. Wollensak, 1989, "Dynamics of the biased two-level system in metals", Phys. Rev. Lett **62**, 1663.

Zagoskin, A. M., 1999, "A scalable, tunable qubit, based on a clean dnd or grain boundary d-d junction", cond-mat/9903170.

Zurek, W. H., 1991, "Decoherence and the transition from quantum to classical", Physics Today **44 (10)**, 36.